# Unconventional Superconductivity in the Extended Attractive Hubbard Model

**Swagatam Nayak**

*A thesis submitted for the partial fulfillment of the degree of Doctor of Philosophy*


Department of Physical Sciences
Indian Institute of Science Education and Research Mohali
Knowledge city, Sector 81, SAS Nagar, Manauli PO, Mohali 140306, Punjab, India.

**December 2019**

# Dedication

*Dedicated to my grandparents, my parents and all the inquisitive minds out there!!!*

# Declaration

The work presented in this thesis has been carried out by me under the guidance of Dr. Sanjeev Kumar at the Indian Institute of Science Education and Research Mohali. This work has not been submitted in part or in full for a degree, a diploma, or a fellowship to any other university or institute. Whenever contributions of others are involved, every effort is made to indicate this clearly, with due acknowledgement of collaborative research and discussions. This thesis is a bonafide record of original work done by me and all sources listed within have been detailed in the bibliography.

Swagatam Nayak
(Candidate)

In my capacity as the supervisor of the candidate's thesis work, I certify that the above statements by the candidate are true to the best of my knowledge.

Dr. Sanjeev Kumar
(Supervisor)

# Acknowledgements

The journey of mine, as a PhD student, has been associated with so many human beings that it appears to be very difficult to put it into right words without failing to do justice to everyone's contribution. Still, I shall try my best expressing that. Let me begin with the person whom you might find behind the doors of '2F9', in the academic block I of IISER Mohali. Yes, he has been my supervisor and guide during my days as a PhD student. People call him by 'Sanjeev' or 'sir'. I stuck to the later alias from the beginning. The beginning reminds me of the good old days when I just joined IISERM as a PhD student. Surprisingly, I had no idea who 'Dr. Sanjeev Kumar' was until I chose to attend an 'advanced solid state physics' lecture by Dr. Sanjeev Kumar. Honestly, I enjoyed the way he taught all of us. I have always been fascinated by physics since 10th grade, and Sanjeev Kumar with his ' ever-humble' and enthusiastic approach inspired me so much that I had no choice but to join him. I would really like to mention that his contribution to my PhD is beyond description. The door to '2F9' has always been a welcome door, whenever I had doubts, wanted clarification, wanted to discuss possibilities or even share my failure to accomplish a goal. The struggle of defining a problem out of an idea, learning tools to solve it, getting results recognizing the obstacles, submitting a well-written manuscript, tackling questions by the referees, and ultimately publishing the work in a reputed journal in our field of work is not a cakewalk. Dr. Sanjeev Kumar, with his infinite patience and overwhelming positivity, literally taught me the path to push forward on that front. He put an enormous effort into rectifying the manuscripts and the thesis as well. In the world of academia, especially in our country, it takes a considerable amount of energy and patience before you get rewarded in some manner. At least that has been my experience. And I thank Dr. Kumar for still showing me how it is done, even today. I am grateful to him for his constant support, and his 'always-positive' attitude on various aspects during my whole PhD life, and also on the very last days of it. Thank you, sir!!!

I must thank the members of my doctoral committee, Dr. Abhishek Chaudhuri, Dr. Dipanjan Chakraborty, and Prof. Ramandeep S. Johal for their support and sincere suggestions from time to time. I am thankful to many of the faculty members of the department of physical science. I cannot thank Dr. Abhishek Chaudhuri enough for his constant, sincere pieces of advice and suggestions throughout my PhD tenure.

His ‘always smiling face’ and simplicity in addressing a research problem always motivated me. I am grateful to Dr. Dipanjan Chakraborty for all the friendly suggestions and the cheerful ‘coffee-discourses’ with him, which helped me a lot now and then. I especially thank Prof. Jasjeet Bagla for being a mentor to me in the early days during the coursework period. It was amusing doing a project with him. Even if he was not my supervisor, he was always there whenever I had any general queries. His positive outlook with a great smile motivated many of us. I frequented Dr. Rajeev Kapri’s office whenever I had any technical or any general queries, and he always welcomed me with his valuable suggestions from time to time. I thank him a lot for that. I also thank Dr. Yogesh Singh, Dr. Goutam Sheet, Dr. Kamal P. Singh, Dr. Harvinder Kaur Jassal, Dr. Mandip Singh, and Dr. Kavita Dorai for the fruitful interactions on different occasions.

Now it is time to thank my friends and colleagues. I especially thank Reema, Dheera, Ginny, Rajneesh, Satyam and Anshul for being there in my life. Reema opened a different world in front of me, which will never be forgotten. I cannot thank Dheera enough for always being there for me as a great sister and a great friend. I thank Ginny, Satyam and Rajneesh for being the closest friends who stood by me in my ups and downs on different occasions. I cannot thank them enough for their warm-hearted friendships, which helped me a lot at hard times. I especially thank Ayushi, Aman, Arnob, Abhinay, Deepak, Sudhanshu, Priyanka, Gokul, Ankit, Avinash, Pooja, Shubhendu, Gaurav, Abhishek, Nagesh and Bhisham for their amazing friendships. My experience as a PhD student had not been easier if these guys were not there with their constant presence to cheer me up. I also thank my friend-cum-philosopher Anshul for being there with me. Be it hiking together or the philosophical discourses we had, we enjoyed every bit of it to the fullest. I appreciate both Anshul and Chhavi for welcoming me for dinner and all the fun times we had. I thank my colleagues Kanika, Vivek, Preeti, Debmalya, George, Ritabrata, Shruti, Navdeep, Sandeep, Harpreet and Satnam for their support. I also thank Anirban, Ashwini, Manisha, Hema, Karishma, Kuldeep, Preetinder, Gopal, Bhupesh, Gopal bhaiya, Vikash, Navketan, Samridhi, Mandeep, Manpreet and Arun for their lively presence during my PhD days.

I thank my group members, Arnob, Ayushi, Deepak, Kanika and Abhinay for their support on different occasions. I thank Ravi, Ray, Lucy and Nirdosh for being such excellent hosts during my visit to Germany. I had an excellent stay there because of them. I especially thank Arnob, Deepak and Priyanka for helping me out at the time of thesis submission. I thank Anshul, Rajneesh, Arnob and Chaurasia for always being there so that I can bug them with computation related issues. I appreciate

every friend who was there during my PhD days. Finally, I thank all the members of my family for always being there for me in all the ups and downs. It is not possible for me to describe their contribution in words. So I would just say 'THANK YOU FOR BEING THERE'. I also thank all my teachers, from school days or college days, for inspiring me to pursue the quest of science. Thank you all!!

**Swagatam Nayak**

# List of Publications

- **Swagatam Nayak** and Sanjeev Kumar, **Exotic superconducting states in the extended attractive Hubbard model**
  2018 *J. Phys.: Condens. Matter* 30 135601

- Navketan Batra, **Swagatam Nayak**, and Sanjeev Kumar, **Topological transitions in a model for proximity-induced superconductivity**
  2019 *Phys. Rev. B* 100, 214517

- **Swagatam Nayak**, Navketan Batra and Sanjeev Kumar, **Broken-symmetry superconducting phases in Extended Attractive Hubbard Model.**
  *Manuscript in Preparation*

# List of acronyms

| | |
|---|---|
| BCS | Bardeen–Cooper–Schrieffer |
| BEC | Bose-Einstein condensate |
| BdG | Bogoliubov de-Gennes |
| OSP | opposite spin pairing |
| ESP | equal spin pairing |
| HFMF | Hartree-Fock-mean-field |
| OP | order parameter |
| SC | superconducting |
| TBM | tight-binding model |
| CDW | charge density wave |
| SDW | spin density wave |
| AHM | attractive Hubbard model |
| EHM | extended Hubbard model |
| EAHM | extended attractive Hubbard model |

# Abstract

This thesis work explores the possibility of finding exotic superconducting states in the extended attractive Hubbard model. The model is studied within a mean-field Bogoliubov-de-Gennes approach focusing on the nature of different superconducting order parameters that can be energetically stable in different regimes of the parameter space. In addition to pure singlet and pure triplet superconducting order, mixed parity states are also allowed within the mean-field decoupling approach followed in this work. In addition to $s$-wave and $d_{x^2-y^2}$-wave order, an exotic $p_x + ip_y$ superconducting state is found to exist. The influence of temperature and an external magnetic field is also studied. The transition between superconducting states with different order parameter symmetries is uncovered upon variations in temperature or external magnetic field. The details of the numerical methodology developed to investigate superconductivity in the extended attractive Hubbard model, and the characterization of the different superconducting states obtained in the study will be discussed.

# Contents

# List of Figures

# Chapter 1

# Introduction

## 1.1 Historical Perspective

Superconductivity has been one of the most significant discoveries of the last century. It all started the day Dutch physicist Heike Kamerling Onnes liquefied helium in his cryogenic laboratory at Leiden University in the Netherlands [1]. It was around 7:30 pm on 10th July 1908 when the helium thermometer reading got quite stable at 4 K and that miraculous moment created a cascade of events in Low-temperature physics in the last century. Onnes set up a cryogenic laboratory to test and modify theories on non-ideal gases, given by his friend Johannes Diderik van der Waals. It was a period when efforts had been going on for producing liquefied gases like oxygen, nitrogen, hydrogen, and helium, etc. on a large scale. Though efforts on liquefaction of oxygen, nitrogen, and hydrogen were quite successful, liquifying helium was still beyond anyone's reach before 10th July 1908. It was William Hampson and Carl Von Linde, who independently conceived the Hampson-Linde cycle in 1895, which was to be used for liquefaction of gases and was based on Joule-Thomson effect [2]. Onnes purchased a Linde machine for liquefaction of helium and was successful on that front. During that period, Scottish physicist James Dewar, known for his famous invention of the vacuum flask, was already carrying out his research on the electrical resistance of different materials at low temperatures. But to carry out experiments at really low temperatures required unparalleled cryogenic facilities and cryogenic gases with very low boiling temperature at atmospheric pressure. Onnes' decade long efforts made it possible to build a complex and perfect cryogenic facility which successfully liquefied helium. During that period, no other laboratory on earth could carry out research at such low temperatures as they did not have a perfect cryogenic facility that only the Leiden group had at that time. Onnes and his assistant Jacob Clay reinvestigated

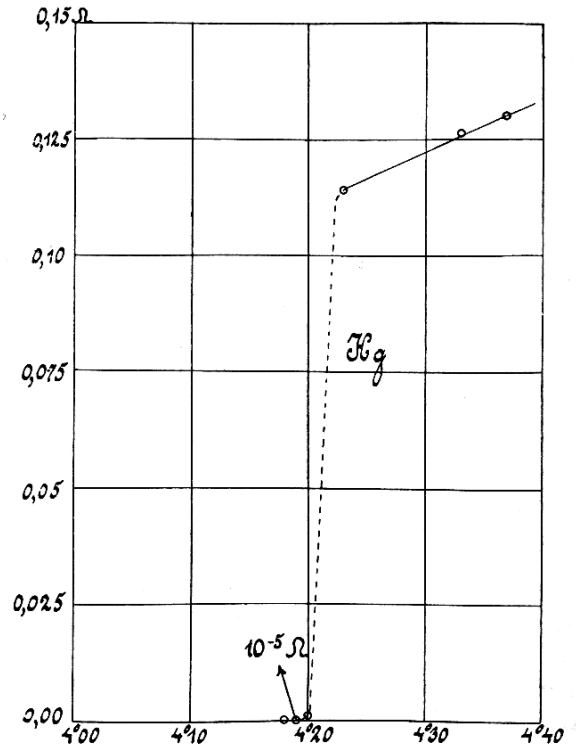


**Figure 1.1:** Historic plot of resistance (Ω) versus temperature (K) for mercury from the 26 October 1911 experiment shows the superconducting transition at 4.2 K. Within 0.01 K, the resistance jumps from unmeasurably small (less than $10^{-6}$ Ω) to 0.1 Ω.(From wikimedia commons)

some earlier experiments by Dewar on the reduction of resistance at low temperatures. Though thermometry was their primary interest, genuine scientific queries pushed them to look into the variation of resistance with the temperature of different metals like gold, platinum, and mercury, etc. After 10th July 1908, it took them almost three years to perfect a cryostat in which liquid helium was used as a cryogenic liquid. On 26th October of 1911 the first astonishing result came into existence: at 4.2 K resistance of mercury resistor dropped from 0.1Ω to $10^{-6}\Omega$ within an interval of 0.1 K (Fig.1.1). This was the first milestone in the field of superconductivity. Such a sudden jump in resistivity was a fact of a huge surprise. But Onnes perceived perfectly that what he found was indicative of a new state of matter, namely "supraconductivity", as he used to call it at the beginning. Extensive research on these materials by Onnes and his group was reported to the Royal Netherlands Academy of Arts and Sciences. After the seminal discovery of superconductivity in mercury Leiden group had a monopoly on experiments to find superconductivity in different materials. Leiden group already discovered superconductivity in lead ($T_c \equiv 6K$) and tin ($T_c \equiv 3.8K$). But the monopoly ended after first world war. Few years later

Walther Meissner and his group at PTR (Physikalisch-Technische Reichsanstalt) procured an expensive helium liquefier, capable of liquifying 10 liters of helium per hour. With the help of that liquefier, Meissner group successfully discovered superconductivity in three new elements: Thorium ($T_c$ of 1.4 K), Tantalum ($T_c$ of 4.4 K) and Niobium ($T_c$ of 9.2 K). The next surprise came from Walther Meissner and Robert Ochsenfeld in 1933, when they demonstrated the expulsion of an external magnetic field from the bulk of a superconductor [3]. This effect, which became popular as Meissner–Ochsenfeld effect afterwards, actually proved that superconductivity is a true thermodynamical macrostate of matter as it exhibits the property of a pure diamagnet. Since the discovery of superconductivity in mercury in 1911, there had not been much a major contribution from the theoretical community until 1935. In 1935 London brothers introduced London's equation making use of Maxwell's equations and intuitive approach to build a connection between superconducting current density $j_s$ and externally applied magnetic field $\mathbf{B}$ and gave a proper explanation of the complete expulsion of any magnetic field from the bulk of the superconductor, which is deeper than the penetration depth ($\lambda_L$) from the surface of the superconductor. Thus emerged the only free parameter of the theory, $\lambda_L$. Later many experiments were carried out testing the effect of magnetic field on different superconductors. It was found that the Meissner effect works only if the applied magnetic field is lower than some critical field, $H_c$. It was also found that not all superconductors expel magnetic field completely from the bulk. And it was observed that there were actually two types of superconductors: type-I and type-II. While type-I superconductors (such as aluminium, lead, mercury, etc.,) have a single critical field $H_c$, type-II superconductors (such as niobium, vanadium, technetium, etc.) have two critical fields, $H_{c_1}$ and $H_{c_2}$. In case of type-I superconductors beyond a critical field $H_c$ superconductivity is completely destroyed and so is its pure diamagnetism. While in the case of type-II superconductors, the external field is completely expelled from the bulk until the strength of the magnetic field becomes equal to $H_{c_1}$. Beyond $H_{c_1}$ the magnetic field starts to penetrate the bulk of the superconductor, thus creating a coexistence of superconducting and non-superconducting regions inside the bulk. But when the applied field exceeds a value $H_{c_2}$ superconductivity is completely destroyed in bulk and the material becomes entirely non-superconducting.

## 1.2 Superconductivity and its theories

Even after 20 years of the discovery scientists were not successful in finding a theoretical breakthrough in explaining the phenomenon of superconductivity. As it was a

period when the world had not gone through the breakthrough in quantum mechanics, theoretical physicists were busy trying to understand the perfect conductivity based on Drude theory of transport in metals. They were trying to understand how resistivity should behave at low temperatures based on the behaviour of scattering amplitude and mobility of electrons. But the perfect conductivity was not enough to get a clue of the underlying phenomenon. It was 1933 when Walther Meissner and his group discovered so-called "Meissner–Ochsenfeld effect", theoretical physicists got enough evidence to formulate different plausible theories. Though the most important theoretical breakthroughs were the phenomenological theory given by Lev Landau in 1950 and microscopic theory given by Bardeen, Cooper, and Schrieffer in 1957, it was London brothers, namely F. London and H. London, who successfully formulated electrodynamics of superconductors and explained the Meissner effect in the first place. It was after the discovery of Meissner effect scientists were convinced about superconductivity being a thermodynamical state of matter.

### 1.2.1 London theory of superconductors

In 1935, German physicist Fritz Wolfgang London and his brother Heinz London proposed a theory that describes electromagnetic properties of superconductors [4]. It is a phenomenological theory based on a two-fluid picture, which proposes a relation between the current and the electromagnetic fields in and around a superconductor. In a two-fluid picture it is assumed that in a superconducting state electrons form an equilibrium of two different types of fluid, namely the normal fluid and the superfluid. While the normal fluid carrys an ohmic current,

$$\mathbf{j}_n = \sigma_n \mathbf{E} \tag{1.1}$$

and governed by the Drude law,

$$\sigma_n = \frac{e^2 n_n \tau}{m}, \tag{1.2}$$

the superfluid is assumed to move in a frictionless state, leading to free acceleration of charges. Using Newton's equation of motion

$$m\dot{\mathbf{v}} = -e\mathbf{E} \tag{1.3}$$

with the supercurrent

$$\mathbf{j}_s = -en_s\mathbf{v}_s \tag{1.4}$$

we obtain the first London equation

$$\frac{\partial \mathbf{j}_s}{\partial t} = \frac{e^2 n_s}{m}\mathbf{E}. \tag{1.5}$$

Using the Maxwell equation and the first London equation, we arrive at the following equation:

$$\frac{\partial}{\partial t}\left(\frac{m}{n_s e^2}\boldsymbol{\nabla}\times\mathbf{j}_s + \frac{1}{c}\mathbf{B} = 0\right). \tag{1.6}$$

This perfectly describes the behaviour of a perfect conductor, but it fails to explain the Meissner effect. In order to describe Meissner effect, London proposed that the constant of integration must chosen to be zero, which gives us the second London equation,

$$\boldsymbol{\nabla}\times\mathbf{j}_s = -\frac{n_s e^2}{mc}\mathbf{B}. \tag{1.7}$$

Applying Maxwell equations further on the second London equation, we arrive at two important equations,

$$\nabla^2\mathbf{B} = \frac{4\pi\mu}{c^2\lambda_L}\mathbf{B} \quad \text{and} \quad \nabla^2\mathbf{j}_s = \frac{4\pi\mu}{c^2\lambda_L}\mathbf{j}_s \tag{1.8}$$

solutions to these equations explain the decay of the magnetic field and the persistent current in the bulk of the superconductors. Thus it explains the Meissner effect and gives us the free parameter $\lambda_L$, commonly known as the London penetration depth. Both the London equations can be rewritten as a single equation,

$$\mathbf{j}_s(\mathbf{r}) = \frac{n_s e^2}{mc}\mathbf{A}(\mathbf{r}) \tag{1.9}$$

where $\mathbf{A}$ is the electromagnetic vector potential. This raised concerns, as the current density depends on the electromagnetic vector potential, which is not even a physical variable. Furthermore, a gauge transformation of the vector potential, $\mathbf{A}(\mathbf{r}) \rightarrow \mathbf{A}(\mathbf{r}) + \boldsymbol{\nabla}\varphi(\mathbf{r})$ can change the supercurrent density. Thus London theory of conservation of current $\boldsymbol{\nabla}\cdot\mathbf{j}_s = 0$ causes a serious restriction on the choice of the vector potential, $\boldsymbol{\nabla}\cdot\mathbf{A} = 0$. London proposed that Eq.(1.9) is respected due to the rigidity of the collective

wave function $\Psi_s$ on a distance which is of the order of the London penetration depth. The rigidity of $\Psi_s$ was understood afterwards, in the BCS framework, as a result of the existence of a non-zero energy gap for excitations of BCS ground state.

### 1.2.2 Ginzburg Landau theory

Ginzburg and Landau start their remarkable paper of 1950 by stating that London's existing phenomenological theory, despite successfully describing several aspects of the electrodynamics of superconductors, cannot help determine the surface energy at the normal-superconducting phase interface. Moreover, they assert, his theory fails to describe the destruction of superconductivity by currents and magnetic fields. Ginzburg and Landau's starting key observation was that, in the absence of a a magnetic field, the transition into a superconducting state at the critical temperature $T_c$ is a phase transition of the second order. They postulated the existence of some order parameter in the theory of this transition analogous with other second-order phase transitions. They defined the order parameter $\Psi_s$ that is finite in a superconducting state and zero above $T_c$ and postulated that $\Psi_s$ plays the role of some "effective" wave function, a complex function to allow for supercurrent flow. It is important to remember, however, that $\Psi_s$ is not the true wave function of the electrons in the metal but rather some averaged quantity. In a nutshell the theory is based on minimization of the total free energy $\mathcal{F} = \int d\mathbf{r} F_s$, where

$$F_s = F_n + \alpha|\Psi_s|^2 + \frac{1}{2}|\Psi_s|^4 + \frac{1}{2m^*}\left|\left(-i\hbar\nabla - \frac{e^*\mathbf{A}}{c}\Psi_s\right)\right| + \frac{1}{8\pi}(\mathbf{B}(\mathbf{r}) - \mathbf{H}_a). \quad (1.10)$$

The minimization is carried out with respect to $\Psi_s$ and vector potential $\mathbf{A}$ (corresponding to the magnetic field $\mathbf{B} = \nabla \times \mathbf{A}$), choosing the London gauge.

GL theory provides us with two important characteristic length scales, namely the penetration depth ($\lambda_L$) and the coherence length ($\xi$). The ratio of the two lengths, the so-called Ginzburg-Landau parameter,

$$\kappa = \frac{\lambda}{\xi} \quad (1.11)$$

is temperature independent and is the fundamental characteristic of a superconducting material. Although we provide an essence of the GL theory, we do not intend to elaborate further, as we follow the BCS framework for most of our projects. Further details can be found in standard texts [5].

### 1.2.3 BCS Theory

*Cooper Instability* The first step in paving a path to formulate a microscopic theory of superconductivity was taken by Leon Cooper in 1956 when he showed that even a weak attractive interaction between two electrons on the Fermi sea of a degenerate Fermi gas can lead to a stable two-electron bound state causing Instability in Fermi sea [6]. Later this idea became popularly known as "Cooper Instability". The idea of "Cooper Instability" can be understood in different levels of complexity, starting from solving a simple two-body quantum problem in the presence of Fermi sea, to invoking Green's function method and Feynman diagrams to understand the scattering process leading to the effective attractive interaction. I would like to stay with the simplest approach to motivate the idea in the following section.

The ground state of a non-interacting Fermi gas of electrons in a potential well corresponds to the situation where all electronic states with wave vector $\mathbf{k}$ within the Fermi sphere ($E_F^0(T = 0K) = \hbar^2 k_F^2/2m$) are filled and all states with $E > E_F^0$ are unoccupied.

In a thought experiment we add to this system two electrons $(\mathbf{k}_1, E(\mathbf{k}_1))$ and $(\mathbf{k}_2, E(\mathbf{k}_2))$ in states just above $E_F^0$. The two electrons are made to experience a weak attractive interaction due to the exchange of phonons.

All other electrons in the Fermi sea are assumed to be non-interacting. But the presence of the background Fermi sea restrict the two electrons via Pauli exclusion principle, i.e. further occupation of states with $|\mathbf{k}| < k_F$ is not allowed. The two additional electrons exchange phonons continually, thus changing their wave vectors. However, momentum must be conserved:

$$\mathbf{k}_1 + \mathbf{k}_2 = \mathbf{k}_1' + \mathbf{k}_2' = \mathbf{K}. \tag{1.12}$$

The interaction in $\mathbf{k}$-space is restricted to a shell with an energy thickness of $\hbar\omega_D$ (with $\omega_D$ = Debye frequency) above $E_F^0$. It can be shown that the number of energy-reducing phonon exchange processes, i.e. the strength of the attractive interaction, is maximum for $\mathbf{K} = 0$. It is therefore sufficient in what follows to consider the case $\mathbf{k}_1 = -\mathbf{k}_2 = \mathbf{k}$, i.e. electron pairs with equal and opposite wave vectors. The associated two particle wave function $\psi(\mathbf{r}_1, \mathbf{r}_2)$ must obey the Schrödinger equation:

$$-\frac{\hbar^2}{2m}(\nabla_1^2+\nabla_2^2)\psi(\mathbf{r}_1,\mathbf{r}_2)+V(\mathbf{r}_1,\mathbf{r}_2)\psi(\mathbf{r}_1,\mathbf{r}_2)=E\psi(\mathbf{r}_1,\mathbf{r}_2)=(\varepsilon+2E_F^0)\psi(\mathbf{r}_1,\mathbf{r}_2) \tag{1.13}$$

$\varepsilon$ is the energy of the electron pair relative to the interaction-free state ($V=0$), in which each of the two electrons at the Fermi level would possess an eneryy $E_F^0=\frac{\hbar^2k_F^2}{2m}$. The two-particle function, in this case, consists of two plane waves

$$(\frac{1}{\sqrt{L^3}}e^{i\mathbf{k}_1\cdot\mathbf{r}_1})(\frac{1}{\sqrt{L^3}}e^{i\mathbf{k}_2\cdot\mathbf{r}_2})=\frac{1}{L^3}e^{i\mathbf{k}\cdot(\mathbf{r}_1-\mathbf{r}_2)} \tag{1.14}$$

We note that Eq.(1.14) implies that the two electrons have opposite spin. The most general representation of a two-particle state for the case of a non-vanishing interaction ($V\neq 0$) is given by the series

$$\psi(\mathbf{r}_1-\mathbf{r}_2)=\frac{1}{L^3}\sum_{\mathbf{k}}g(\mathbf{k})e^{i\mathbf{k}\cdot(\mathbf{r}_1-\mathbf{r}_2)}, \tag{1.15}$$

which depends only on the relative coordinate $\mathbf{r}=\mathbf{r}_1-\mathbf{r}_2$. The summation is confined to pairs with $\mathbf{k}=\mathbf{k}_1=-\mathbf{k}_2$, which, because the interaction is restricted to the region $\hbar\omega_D$, must obey the condition

$$E_F^0<\frac{\hbar^2k^2}{2m}<E_F^0+\hbar\omega_D \tag{1.16}$$

The quantity $|g(\mathbf{k})|^2$ is the probability of finding one electron in state $\mathbf{k}$ and the other in $-\mathbf{k}$, that is, the electron pair in $(\mathbf{k},-\mathbf{k})$. Due to the Pauli principle and the condition given in Eq.(1.16) we have

$$g(\mathbf{k})=0 \quad \text{for} \quad \begin{cases} k<k_F \\ k>\sqrt{2m(E_F^0+\hbar\omega_D)/\hbar^2} \end{cases} \tag{1.17}$$

Inserting Eq.(1.15) in Eq.(1.13), multiplying by $e^{-i\mathbf{k}'\cdot\mathbf{r}}$ and integrating over the normalization volume gives us

$$\frac{\hbar^2 k^2}{m} g(\mathbf{k}) + \frac{1}{L^3} \sum_{\mathbf{k}'} g(\mathbf{k}') V_{\mathbf{k}\mathbf{k}'} = (\varepsilon + 2E_F^0) g(\mathbf{k}) \tag{1.18}$$

The interaction matrix element

$$V_{\mathbf{k}\mathbf{k}'} = \int V(\mathbf{r}) e^{-i(\mathbf{k}-\mathbf{k}')\cdot\mathbf{r}} d\mathbf{r} \tag{1.19}$$

describes scattering of the electron pair from $(\mathbf{k}, -\mathbf{k})$ to $(\mathbf{k}', -\mathbf{k}')$ and vice versa. In the simplest model this matrix element $V_{\mathbf{k}\mathbf{k}'}$, is assumed to be independent of $\mathbf{k}$ and attractive, that is, $V_{\mathbf{k}\mathbf{k}'} < 0$:

$$V_{\mathbf{k}\mathbf{k}'} = \begin{cases} -V_0 (V_0 > 0) & \text{for} \quad E_F^0 < (\frac{\hbar^2 k^2}{2m}, \frac{\hbar^2 k'^2}{2m}) < E_F^0 + \hbar\omega_D \\ 0 & \text{otherwise} \end{cases} \tag{1.20}$$

It thus follows from Eq.(1.18) that

$$(-\frac{\hbar^2 k^2}{m} + \varepsilon + 2E_F^0) g(\mathbf{k}) = -A, \text{where} \tag{1.21}$$

$$A = \frac{V_0}{L^3} \sum_{\mathbf{k}'} g(\mathbf{k}') \tag{1.22}$$

is independent of $\mathbf{k}$.

After summing Eq.(1.21) over $\mathbf{k}$ and comparing with Eq.(1.22), consistency requires

$$1 = \frac{V_0}{L^3} \sum_{\mathbf{k}} \frac{1}{-\varepsilon + \hbar^2 k^2/m - 2E_F^0}. \tag{1.23}$$

We replace the sum over $\mathbf{k}$ by the integral

$$\frac{1}{L^3} \sum_{\mathbf{k}} \to \frac{1}{(2\pi)^3} \int d\mathbf{k} \tag{1.24}$$

and keep in mind that the sum, as well as the integral, extends only over the manifold of states of one spin type. We split the integral over the entire **k**-space into an integral over the Fermi sphere and the energy and obtain from Eq.(1.23)

$$1 = V_0 \frac{1}{(2\pi)^3} \int\int \frac{dS_E}{|\nabla_{\mathbf{k}} E(\mathbf{k})|} \frac{dE}{2E - \varepsilon - 2E_F^0} \quad \text{with} \quad E = \frac{\hbar^2 k^2}{2m} \tag{1.25}$$

Since the integral over the energy extends only over the narrow interval between $E_F^0$ and $E_F^0 + \hbar\omega_D$, the first part of the integral can be considered as a constant. This constant is the density of states for one spin type at the Fermi level, which we shall denote as $Z(E_F^0)$. By performing the integration, we obtain

$$1 = V_0 Z(E_F^0) \int_{E_F^0}^{E_F^0 + \hbar\omega_D} \frac{dE}{2E - \varepsilon - 2E_F^0} = \frac{1}{2} V_0 Z(E_F^0) ln \frac{\varepsilon - 2\hbar\omega_D}{\varepsilon}, \quad \text{i.e.}$$

$$\varepsilon = \frac{2\hbar\omega_D}{1 - exp[2/V_0 Z(E_F^0)]}. \tag{1.26}$$

For the case of weak interaction, $V_0 Z(E_F^0) \ll 1$, it follows that

$$\varepsilon \approx -2\hbar\omega_D e^{-2/V_0 Z(E_F^0)}. \tag{1.27}$$

Thus there exists a two-electron bound state, whose energy is lower than that of the fully occupied Fermi sea by an amount $\varepsilon = E - 2E_F^0 < 0$. The ground state of the non-interacting free electron gas becomes unstable when a little amount of attractive interaction between electrons is switched on.

*BCS GROUNDSATE* In the previous section, it should be noted that the energy reduction $\varepsilon$ is an outcome of a thought experiment, where the effect of attraction between two additional electrons is treated in the presence of Fermi sea. In reality, this instability leads to the formation of a high density of correlated electron pairs, so-called Cooper pairs, via which the system tries to achieve a new lower-energy ground state, namely superconducting state.

In general such a system of many Cooper pairs can be described by the following effective Hamiltonian:

$$H = \sum_{\mathbf{k}\sigma} \varepsilon_{\mathbf{k}} c^\dagger_{\mathbf{k}\sigma} c_{\mathbf{k}\sigma} + \frac{1}{N} \sum_{\mathbf{k}\mathbf{k}'} V_{\mathbf{k}\mathbf{k}'} c^\dagger_{\mathbf{k}\uparrow} c^\dagger_{-\mathbf{k}\downarrow} c_{-\mathbf{k}'\downarrow} c_{\mathbf{k}'\uparrow} \tag{1.28}$$

Here, $c^\dagger_{\mathbf{k}\sigma}$ creates an electron with momentum $\mathbf{k}$ and spin projection $\sigma$. We have included the chemical potential via the definition, $\varepsilon_{\mathbf{k}} = \epsilon_{\mathbf{k}} - \mu$. The second term describes the destruction of a Cooper pair (two electrons with opposite momenta and spin) and the subsequent creation of another Cooper pair. $V_{\mathbf{k}\mathbf{k}'}$ is the strength of the interaction, which is expected to generate an effective, attractive interaction between the electrons.

Bardeen, Cooper, and Schrieffer (BCS) proposed an ansatz for the ground state of the above Hamiltonian. It is based on the idea that electrons from the states $|\mathbf{k},\uparrow\rangle$ and $|-\mathbf{k},\downarrow\rangle$ form so-called Cooper pairs and that the ground state is a superposition of states built up of such pairs.

The ansatz reads

$$|\psi_{BCS}\rangle = \prod_{\mathbf{k}} (u_{\mathbf{k}} + v_{\mathbf{k}} c^\dagger_{\mathbf{k}\uparrow} c^\dagger_{-\mathbf{k}\downarrow})|0\rangle \tag{1.29}$$

Now the idea is to minimize $\langle\psi_{BCS}|H|\psi_{BCS}\rangle$ with respect to the $u_{\mathbf{k}}$ and $v_{\mathbf{k}}$.

Following a standard parametrization of $u_{\mathbf{k}}$ and $v_{\mathbf{k}}$ in terms of $\varepsilon_{\mathbf{k}}$ and $\Delta_{\mathbf{k}}$, and then using a proper normalization, the idea of above minimization leads to the following equation:

$$\Delta_{\mathbf{k}} = -\frac{1}{N}\sum_{\mathbf{k}'} V_{\mathbf{k}\mathbf{k}'} \frac{\Delta_{\mathbf{k}'}}{2\sqrt{\varepsilon^2_{\mathbf{k}'} + \Delta^2_{\mathbf{k}'}}}, \tag{1.30}$$

popularly known as BCS gap equation. Solving this self-consistent gap equation we can obtain the original variational parameters in terms of $\Delta_{\mathbf{k}}$:

$$\begin{aligned} u_{\mathbf{k}} &= \frac{1}{2}\left(1 + \frac{\varepsilon_{\mathbf{k}}}{\sqrt{\varepsilon^2_{\mathbf{k}} + \Delta^2_{\mathbf{k}}}}\right) \\ v_{\mathbf{k}} &= \frac{1}{2}\left(1 - \frac{\varepsilon_{\mathbf{k}}}{\sqrt{\varepsilon^2_{\mathbf{k}} + \Delta^2_{\mathbf{k}}}}\right) \\ u_{\mathbf{k}} v_{\mathbf{k}} &= \frac{\Delta_{\mathbf{k}}}{2\sqrt{\varepsilon^2_{\mathbf{k}} + \Delta^2_{\mathbf{k}}}} \end{aligned} \tag{1.31}$$

Now choosing the right form of interaction $V_{\mathbf{k}\mathbf{k}'}$ and solving the above equation, we can exactly calculate the BCS ground state energy and the corresponding BCS wavefunction.

Instead of solving the Hamiltonian in Eq.(1.28) using a variational approach following the BCS ansatz, we can also find the solution following a mean-field approach. Following a standard Hartree-Fock mean-field decoupling in pairing channel the Hamiltonian in Eq.(1.28) takes the following form:

$$H_{MF} = \sum_{\mathbf{k}\sigma} \varepsilon_{\mathbf{k}} c^{\dagger}_{\mathbf{k}\sigma} c_{\mathbf{k}\sigma} - \sum_{\mathbf{k}} \left( \Delta_{\mathbf{k}} c^{\dagger}_{\mathbf{k}\uparrow} c^{\dagger}_{-\mathbf{k}\downarrow} + H.c. \right) + \sum_{\mathbf{k}} |\Delta^2_{\mathbf{k}}| \tag{1.32}$$

Now this Hamiltonian in Eq.(1.32) can be solved via the so called Bogoliubov transformation [7],

$$\begin{aligned} c_{\mathbf{k}\uparrow} &= u^{*}_{\mathbf{k}} \gamma_{\mathbf{k}\uparrow} + v_{\mathbf{k}} \gamma^{\dagger}_{-\mathbf{k}\downarrow} \\ c^{\dagger}_{-\mathbf{k}\downarrow} &= u_{\mathbf{k}} \gamma^{\dagger}_{-\mathbf{k}\downarrow} - v^{*}_{\mathbf{k}} \gamma_{\mathbf{k}\uparrow} \end{aligned} \tag{1.33}$$

Therefore, the effective Hamiltonian becomes

$$H_{MF} = \sum_{\mathbf{k}\sigma} E_{\mathbf{k}} \gamma^{\dagger}_{\mathbf{k}\sigma} \gamma_{\mathbf{k}\sigma} + E_0 \tag{1.34}$$

in terms of Bogoliubov-quasiparticle operators ($\gamma^{\dagger}_{\mathbf{k}\sigma}$).

The BCS ground state wavefunction, corresponds to the vacuum of these Bogoliubov-quasiparticles:

$$\gamma_{\mathbf{k}\sigma} |\psi_{BCS}\rangle = 0 \tag{1.35}$$

It is interesting to note that the parameters $u_{\mathbf{k}}$ and $v_{\mathbf{k}}$ in both the formalism turns out to be the same. Thus BCS ground state can be formed using Eq.(1.35) after solving for the corresponding $u_{\mathbf{k}}$ and $v_{\mathbf{k}}$.

In this section, we tried to describe the basic essence of the original variational BCS theory and the generalized BCS theory in terms of Bogoliubov excitations. Detailed calculations can be found in standard texts [7, 8]. In our projects, we followed the general Bogoliubov-de Gennes framework of excitations to find solutions in the effective lattice model we used.

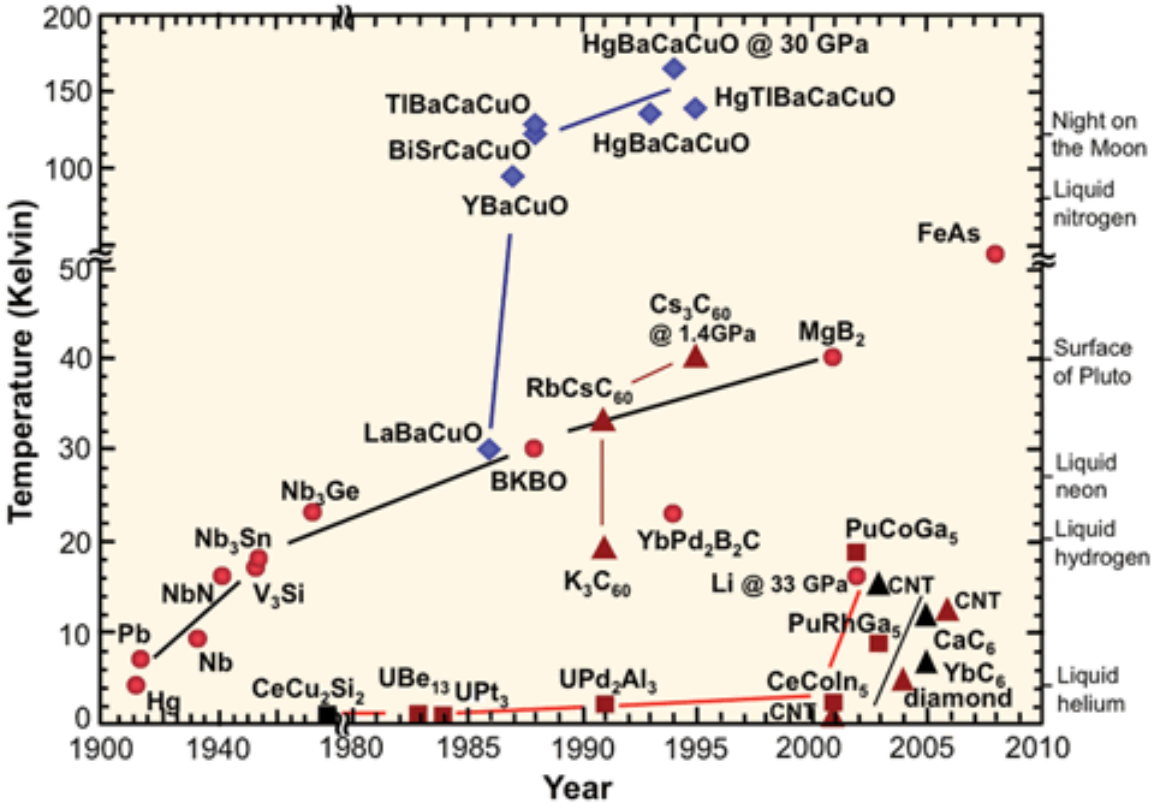


**Figure 1.2:** Timeline of discovery of different superconductors. Image courtesy of U.S. DOE Office of Basic Energy Sciences

## 1.3 Unconventional Superconductivity

Since the discovery of the first superconductor by Kamerling Onnes, many materials have been found to be superconducting. Fig.(1.2) provides us a very useful timeline for the discoveries of different superconductors. While the line connecting the solid red circles represents the group of conventional superconductors, rest of the lines connecting blue diamond-shaped markers or the dark red squares represent unconventional superconductors. While the line connecting the blue diamonds represents the family of unconventional high-$T_c$ cuprate superconductors, the line joining the dark red squares represents the family of unconventional heavy-fermion superconductors. On the one hand, the superconductors can be classified based on their magnetic properties, their critical temperatures, their constituent materials, etc. On the other hand, from a theorist's point of view, we can definitely classify superconductors under two broad categories, namely, conventional and unconventional superconductors. The general consensus is that the superconductors which can be described in the framework of conventional BCS-Eliashberg-Migdal theory of superconductivity [9], based on electron-phonon interaction, are called *conventional superconductors*. On the other

hand, the superconductors which cannot be described by the conventional theory, are called *unconventional superconductors*. Unconventional superconductors cannot be explained by the conventional theory, broadly, because of two reasons. Either they have high critical temperatures or some of their properties point towards a different pairing mechanism. Heavy fermion superconductors are the first class of superconductors which were identified as unconventional superconductors [10]. In 1979, Frank Steglich found superconductivity below $T_c \approx 0.5K$ in $CeCu_2Si_2$, which was a heavy-fermion superconductor [11]. In the same year, Klaus Bechgaard's group discovered superconductivity in an organic salt named $(TMTSF)_2PF_2$ with critical temperature 1.1 K. The next discovery of unconventional superconductor came from Bednorz and Muller when they found superconductivity in a layered perovskite cuprate, namely $La_{2-x}Ba_xCuO_4$ [12]. It has a critical temperature of the order of 35 K. In the following years many other unconventional cuprate superconductors were found (See Fig.(1.2)).

**Unconventional pairing mechanism and pairing symmetry** Discoveries of different classes of unconventional superconductors in the last decades motivated physicists to look for unconventional pairing mechanisms and unconventional pairing symmetries [13–15]. After the success of the conventional pairing mechanism, driven by electron-phonon interaction, there had been many efforts to find new pairing mechanisms. Magnetism-driven pairing mechanisms had been studied extensively. Spin-fluctuation in different systems has been claimed as a strong candidate for unconventional pairing mechanism. While the search for unconventional pairing mechanism has not been an easy path, understanding unconventional pairing symmetries of the order parameter has been of utmost importance since it certainly gives us a clue about the possible pairing mechanisms. Popular experiments like NMR, Angle-resolved photo-emission spectroscopy (ARPES), Microwave resonator penetration depth measurements, Josephson interferometry experiments, etc. can confirm the $k$-dependence of the energy gap and reveal the existence of any nodal structure. Motivated by these ideas, we intend to study unconventional pairing symmetries of the superconducting order parameter under the framework of a lattice Hamiltonian like extended attractive Hubbard Hamiltonian.

## 1.4 Extended Attractive Hubbard Model

After the scientific community encountered discoveries of different classes unconventional superconductors during the 70s and 80s, there was a strong urge amongst theorists to find a quantum mechanical model Hamiltonian that will explain various

aspects of unconventional superconductivity. Hubbard model was found to be such a model during that period, which qualified as a strong candidate to explain superconductivity. Initially conceived by British physicist John Hubbard in 1963 [16], the Hubbard model has been one of the legendary models to describe strongly correlated electronic behaviour. It's worth mentioning that Swiss-American physicist Martin Gutzwiller [17] and Japanese physicist Junjiro Kanamori [18] also conceived the same model independently in the same year. Conceptualizing research on the Hubbard model was not confined to the year it was designed first. In the following years, Hubbard successfully published five more research articles on the Hubbard model as an improvement to the original model [19–22], while Gutzwiller and Kanamori also extracted different physics from the same model. Though originally Hubbard model was conceived to explain the behaviour of strongly correlated electrons and itinerant ferromagnetism in transition metals, over the years, it opened many doors of research in multiple directions. Superconductivity was one of those directions. The whole physics community was engulfed in the excitement of discovery of cuprates, the class of unconventional high-$T_c$ superconductors. Still, certainly, there were not many effective Hamiltonians which can explain different aspects of these newly found superconducting materials. Hubbard model gave hope in that direction. Before we slide into the facts why we choose Extended Hubbard Model (EHM) we would like to shed some lights on the Hubbard model itself, to create a premise for understanding the reason to choose such effective Hamiltonians to study superconducting order parameter.

### 1.4.1 Hubbard Model

The Hubbard model can be thought of as an extension to the famous tight-binding model. So it looks like:

$$\mathcal{H}_{Hubbard} = -t \sum_{\langle ij \rangle, \sigma} [c^{\dagger}_{i\sigma} c_{j\sigma} + H.c.] + U \sum_{i} \hat{n}_{i\uparrow} \hat{n}_{i\downarrow} \tag{1.36}$$

Where, $c^{\dagger}_{i\sigma}(c_{i\sigma})$ creates (annihilates) an electron in the Wannier state $\phi(\mathbf{r} - \mathbf{R}_i)$ with spin projection $\sigma$, $i$ being the lattice site index. $\langle ij \rangle$ represents nearest neighbor sites $i$ and $j$ in the lattice. $\hat{n}_{i\uparrow}$ and $\hat{n}_{i\downarrow}$ are the corresponding number operators for $\uparrow$ and $\downarrow$ spin projections respectively.

While the first term in $\mathcal{H}_{Hubbard}$ denotes the kinetic energy of the electrons:

$$\mathcal{H}_{band} = -t \sum_{\langle ij \rangle, \sigma} [c^{\dagger}_{i\sigma} c_{j\sigma} + H.c.] \tag{1.37}$$

the second term represents the Coulomb repulsion between electrons with opposite spin projections on the same orbital,

$$\mathcal{H}_U = U \sum_i \hat{n}_{i\uparrow} \hat{n}_{i\downarrow} \tag{1.38}$$

We can define the interaction strength in $\mathcal{H}_U$, i.e. Hubbard-$U$, in the following manner:

$$U = \int d\mathbf{r}_1 \int d\mathbf{r}_2 |\phi(\mathbf{r}_1 - \mathbf{R}_i)|^2 \frac{e^2}{|\mathbf{r}_1 - \mathbf{r}_2|} |\phi(\mathbf{r}_2 - \mathbf{R}_i)|^2 \tag{1.39}$$

Looking at the definition of Hubbard-$U$, it is quite clear that we are talking about repulsive-$U$ Hubbard model. As long as superconductivity is concerned both repulsive-$U$ and attractive-$U$ Hubbard models play important roles in describing different regime of correlated phenomena [23, 24]. As our focus would be on negative-$U$ Hubbard model, we should clarify that negative-$U$ Hubbard model can arise from two different aspects. Firstly, negative-$U$ Hubbard model can be derived from the original repulsive-$U$ Hubbard model, in some particular cases, following a straightforward canonical particle-hole transformation [25]. Secondly, negative-$U$ Hubbard model can be used as an effective model, describing a net effective electron-electron attraction-mechanism, the details of the mechanism being not mentioned. Such effective Hamiltonians give us crucial insight into the interplay of different correlated phases of matter. In the afore-mentioned spirit, we choose negative-$U$ Hubbard model, which is a natural model for superconductivity, where BCS theory can be applied in the form of mean-field theory.

### 1.4.2 Extended Hubbard Model

In principle, we do not confine ourselves to the Hubbard model, as the effect of Coulomb repulsion is restricted to the region of individual sites only. We choose Extended Hubbard Model (EHM) as our base model and we should have a preliminary idea where such a model comes from. So we would like to motivate the origin of EHM

based on the idea of Coulomb repulsion. We can conveniently write Coulomb repulsion term in Wannier basis as follows:

$$\mathcal{H}_{Coulomb} = \frac{1}{2} \sum_{\substack{\mathbf{g}_1,\mathbf{g}_2,\mathbf{g}_3,\mathbf{g}_4 \\ \sigma_1,\sigma_2}} c^\dagger_{\mathbf{g}_1\sigma_1} c^\dagger_{\mathbf{g}_2\sigma_2} \mathcal{V}(\mathbf{g}_1,\mathbf{g}_2,\mathbf{g}_3,\mathbf{g}_4) c_{\mathbf{g}_4\sigma_2} c_{\mathbf{g}_3\sigma_1} \tag{1.40}$$

where $\mathbf{g}_1, \mathbf{g}_2, \mathbf{g}_3, \mathbf{g}_4$ are lattice sites, and the matrix elements are expressed in terms of Wannier states $\phi(\mathbf{r} - \mathbf{g})$ as:

$$\mathcal{V}(\mathbf{g}_1,\mathbf{g}_2,\mathbf{g}_3,\mathbf{g}_4) = \int d\mathbf{r}_1 \int d\mathbf{r}_2 \phi^*(\mathbf{r}_1 - \mathbf{g}_1)\phi^*(\mathbf{r}_2 - \mathbf{g}_2) \frac{e^2}{|\mathbf{r}_1 - \mathbf{r}_2|} \phi(\mathbf{r}_1 - \mathbf{g}_3)\phi(\mathbf{r}_2 - \mathbf{g}_4) \tag{1.41}$$

It is reasonable to confine ourselves to on-site and nearest neighbor contributions. While the largest matrix element is the Hubbard-$U \equiv \mathcal{V}(i,i,i,i)$, $V \equiv \mathcal{V}(i,j,i,j)$ gives the strength of Coulomb interaction at nearest neighbor distance. And the corresponding density-density interaction term is:

$$\mathcal{H}_V = V \sum_{\substack{\langle ij \rangle \\ \sigma_1,\sigma_2}} \hat{n}_{i\sigma_1} \hat{n}_{j\sigma_2} \tag{1.42}$$

which is exactly the term we use with negative-$V$, along with negative-$U$ Hubbard term, in our model.

### 1.4.3 Motivation

Both the Hubbard model and Extended Hubbard model are fascinating models to study correlated electron systems. While exact solutions for both the models in two or more dimensions are still beyond reach, the emergent physics due to the consideration of electron-electron correlation in these models is extremely fascinating in its own right. Thus it's crucial to understand the essence of these models. Before the arrival of these models, the tight-binding model (TBM) was good enough to explain the behaviour of many metals and insulators. But TBM, which is basically a band theory based on non-interacting electron picture, failed to explain certain metal-insulator transitions. It was understood that band theory based on non-interacting electron picture was not enough to describe such behaviour of metals or insulators. According to band theory, a half-filled band cannot describe an insulator; it has to be metallic.

In reality, it was not the case for many insulators, namely Mott-insulators. It was British physicists Nevill Mott, Rudolf Peierls, and John Hubbard, whose work suggested that taking electron-electron correlation into consideration can explain such insulating behaviour and doping can cause a metal-insulator transition in such materials. Hubbard model at half-filling successfully reproduced such metal-insulator transition, namely the Mott-Hubbard transition. $d$-wave pairing superconductivity is well-known in cuprate superconductors, and it's well explained by $t$-$J$ model, which is just another adaptation of the Hubbard model. While $U$-term is known to capture on-site superconducting pairing correlation (such as $s$-wave pairing) and spin density wave solutions (SDW), $V$-term is a natural candidate to generate inter-site superconducting pairing correlation (such as $d_{x^2-y^2}$-wave pairing) and charge density wave (CDW) solutions. There have been many studies indicative of unconventional superconductivity being an emergent phase, from spin or charge-ordered phases, due to strong electron-electron correlations. For decades, the Hubbard model and Extended Hubbard model has been one of the favourite tools to describe such correlated effects, especially in the field of unconventional superconductivity.

## 1.5 Focus of the Thesis

### 1.5.1 Superconducting Order Parameter Symmetry

Understanding the order parameter symmetry of a superconductor is a key step towards achieving a comprehensive understanding of the mechanism leading to superconductivity [26]. This serves as the central motivation for the present thesis. The thesis explores the possibility of stabilizing unconventional order parameter symmetries for the superconducting order using a generic square-lattice model of on-site and inter-site attractive interactions. The Bogoliubov-de Gennes mean-field approach is used to analyze the model. The vital point of the exploration is that no order parameter symmetry is imposed on the superconducting solution, and the energetics dictates the stability of different SC phases.

### 1.5.2 Outline of 1st Problem

It is a well-known and fact that an effective attraction between electrons is a key ingredient to generate superconducting (SC) order [6, 27, 28]. Thus it is a common practice to invoke effective models with attractive interaction to investigate properties of superconductors [29, 30]. Attractive Hubbard model (AHM) [31, 32] is a natural

candidate to study such SC states. On-site AHM has been extensively studied and it is known to stabilize the most symmetric $s$-wave SC phase [29, 33, 34]. Including a nearest-neighbour (nn) attractive interaction spontaneously supports the nodal $d$-wave SC solutions [35]. In many scenarios, it is suggested that the induced effective attraction between electrons is not enough to overcome on-site Coulomb repulsion, but it can overcome nn repulsion. Such scenarios are investigated using an effective extended Hubbard model (EHM) with on-site repulsion and nn attraction terms. Such a model is useful in studying $d$-wave SC orders occurring in the vicinity of antiferromagnetic (AFM) state, specifically in case of cuprates [36–39]. Another plausible direction is to consider the case where the effective attraction is strong enough to overcome both the on-site and nn repulsions, leading to extended attractive Hubbard model (EAHM). Surprisingly, this model has not been explored much for the possibility of unconventional, particularly the mixed OP symmetry, SC solutions. The possibility of mixed symmetry superconductivity, although not reported in any experiment yet, has not been ruled out [40]. Therefore, understanding and characterizing unconventional mixed-symmetry SC states remain a problem of critical importance.

We address this problem in our first project, considering an EAHM on a square lattice. In this model, we have two independent mechanisms, one favouring on-site pairing and the other favouring inter-site pairing, competing with each other. Motivated by the fact that unconventional SC order gets stabilized in the vicinity of AFM state, we safely neglect the inter-site attractive interaction between electrons with the same spin projections ($\uparrow\uparrow$ and $\downarrow\downarrow$ spins). In fact, in the absence of any magnetic or exchange field, it is natural to assume that equal-spin interactions will not be favoured energetically. Next, we perform a general Hartree-Fock mean-field (HFMF) decoupling in "pairing channel" [41], to consider possible SC orders. Also, motivated by the fact that the long-range Coulomb interaction will not allow for charge-inhomogeneities in the system, we look for homogeneous density SC solutions. Thus, invoking translational invariance, we transform our Hamiltonian into a Hartree-Fock-BCS (HFBCS) mean-field Hamiltonian in Fourier space. SC pairing correlations terms, e.g. $\Delta^{+}_{i\gamma} = \langle c_{i+\gamma\downarrow} c_{i\uparrow} \rangle$, $\Delta^{-}_{i\gamma} = \langle c_{i\downarrow} c_{i+\gamma\uparrow} \rangle$, are treated as mean fields [41], to be calculated self-consistently, diagonalizing the mean field Hamiltonian. We emphasize on the fact that, unlike most studies of SC orders in literature, we do not put any restriction on these pairing correlations. And that gives us freedom to explore the competition of all possible mixed-parity SC states at the mean-field level. We use standard definitions of SC order parameter (OP) symmetries [13–15, 26, 42], e.g. $s$, extended-$s$, $d$, and $p$-wave OPs, in terms of the set of mean field pairing correlations,

denoted by the set $\{\Delta\}$.

In this project, we carried out explicit minimization of the energy over the variational space of the set $\{\Delta\}$. To reduce the number of variational parameters, we study the energy variation of relative angles between different SC OPs. In most of the cases, we found the relative phase angle between any such OPs is either 0 or $\pi/2$. We summarize our results in terms of a $n$-$(U/t)$ and a $n$-$(V/t)$ phase diagrams, $U$, $V$, $n$, and $t$ being the on-site attractive interaction, inter-site attractive interaction, electron density per site and electron-hopping amplitude, respectively.

Most notably, we find a chiral $p_x + ip_y$ order being stabilized in the mid-density region. The $d_{x^2-y^2} + p_x$ is particularly stable over a large density regime. This is intriguing as a number of experiments on cuprates report on the possibility of a secondary unconventional OP in addition to the dominant order $d_{x^2-y^2}$. Moreover, for smaller values of $V$ we also find a pure $d_{x^2-y^2}$ order in the low-doping regime. Two of the unconventional phases, the $d_{x^2-y^2} + p_x$ order and the chiral $p_x + \mathrm{i}p_y$ state, exist over a wide parameter regime. Both these orderings also support non-trivial edge-state dispersions. We also discuss the finite-temperature behaviour and show that for certain densities, the system undergoes multiple transitions before reaching a normal state at high temperature. This work is published in Journal of Physics: Condensed Matter [41].

### 1.5.3 Outline of 2nd Problem

One of the limitations of the study performed as a part of the first project is that only $S_z = 0$ component of triplet was allowed as we restricted ourselves to nearest-neighbour superconducting correlations with opposite spin pairing (OSP) states only. It can be argued that the degeneracy of the triplet states in the absence of magnetic fields ensures that crucial physics was not missed out as a result of the approximation used. However, if the effect of the external magnetic field via Zeeman coupling is to be investigated, then one must allow for the equal spin pairing (ESP) states to be present in the analysis [43]. This is the second project undertaken as a part of this thesis.

In this project, we retain the interactions between same spins on the neighbouring sites and present a more complete analysis of the competition among various superconducting order parameters. We perform a general Hartree-Fock mean-field decoupling in pairing channel on the initial Hamiltonian to get an effective mean-field Hamiltonian, where the effective, attractive interaction between an electron pair

is mediated via a set of self-consistent mean fields. We incorporate the possibility of ESP states by choosing appropriate HFMF decoupling of the initial Hamiltonian. As we focus on finding homogeneous superconducting phases, we invoke the translational symmetry of the underlying system and work with the mean-field Hamiltonian in the Fourier space. The resulting Hamiltonian depends on parameters: $U$, the attractive on-site potential, $V$, the inter-site attractive potential, and $\mu$, the chemical potential. Variations with applied magnetic field $\mathbf{B}$ and temperature $T$ are also studied. We use iterative self-consistency method with variational initial-configuration as the major tool to solve for the mean-field variables for a given parameter set. To include the possibility of both OSP and ESP states, we write our effective $k$-space mean-field Hamiltonian matrix using four-component Nambu spinors and diagonalize the Hamiltonian matrix using standard BdG canonical transformations. In this formulation, $\hat{\Delta}_{\mathbf{k}}$, a $2 \times 2$ matrix known as the superconducting gap function, characterizes the superconducting order parameter. $\hat{\Delta}_{\mathbf{k}}$ incorporates all possible superconducting pairing correlations that can be derived from the effective mean-field Hamiltonian. To be precise, it also contains information regarding the orbital and spin part of the Cooper pair wavefunction. In our unrestricted approach, in addition to the pure singlet and pure triplet pairing states, mixed parity superconducting states are also retained.

In the presence of a magnetic field, we find that ESP states are favoured energetically. To characterize the singlet and triplet pairing states of our system, we follow the conventional $\mathbf{d}$-vector formalism by Balian and Werthamer [44]. Applying a change of basis in spin space we transform $\hat{\Delta}_{\mathbf{k}}$ in a manner that the information about the spin state of $\hat{\Delta}_{\mathbf{k}}$ is retrieved from an anti-symmetric complex scalar function $d_0(\mathbf{k})$ and a three-component symmetric complex vector function $\mathbf{d}(\mathbf{k})$. We use magnitudes of $d_0(\mathbf{k})$ and $\mathbf{d}(\mathbf{k})$ averaged over the Brillouin zone to be the order parameters for singlet ($\Delta_{SP}$) and triplet ($\Delta_{TP}$) pairing states respectively.

To understand the behaviour of the newly included pairing correlations related to ESP states, we study the variation of energy with the relative phase angle between such pairing correlations. We find that the system gains energy when the relative phase angle between $x$ and $y$ pairing correlations corresponding to either $\uparrow$ or $\downarrow$ spin projection assumes a value of $\pi/2$. But we find no such relation between spin $\uparrow$ and spin $\downarrow$ pairing correlations along $x$ (or $y$) direction. We also study the variation of energy corresponding to $\uparrow\uparrow$, $\downarrow\downarrow$, and $\uparrow\downarrow$ states with increasing hopping amplitude $t$ and *in-plane* magnetic field $\mathbf{B}$. While energetics provides us with information regarding the relative behaviour of ESP and OSP pairing correlations, a self-consistent approach is used for a complete exploration of the different possibilities of stabilizing ESP

or OSP states. We find the existence of singlet, triplet, and exotic mixed parity states in different regimes of the parameter space of the model Hamiltonian. In the absence of an external magnetic field, pure triplet occupies the mid-density region, and mixed-parity states are found near half-filling. While the presence of a magnetic field suppresses the OSP-states, a pure-triplet state occupies a larger region in the parameter space. We also study the behaviour of these unconventional states at finite temperature and discover temperature-driven transitions involving the change in symmetry of the superconducting order parameters. The manuscript reporting all these findings is currently under preparation.

### 1.5.4 Summary

In summary, this thesis presents the results of an extensive numerical study of the extended attractive Hubbard model on a square lattice. Following an unrestricted Hartree-Fock mean-field approach, we allow for the possibility of different broken-symmetry superconducting phases and find unconventional superconducting phases being stable in different regimes of parameter space. We also study possibilities of phase transitions driven by external magnetic field and temperature. Motivated by properties of unconventional superconductors discovered in the past few decades, we explored EAHM as an effective model for unconventional superconductors. This work also motivated an MS thesis that focused on topological transitions driven by the proximity effect. This work has recently been accepted for publication in Physical Review B [45].

# Chapter 2

# Model and Methodology

As motivated in the previous chapter, the attractive Hubbard model and its extended versions are the elementary lattice models that can describe the physics associated with superconductivity. In this chapter, we describe extended attractive Hubbard model in detail and discuss the methodology required to explore different superconducting order parameters that can emerge from such a lattice Hamiltonian.

## 2.1 Extended Attractive Hubbard Model

In real space, the Hamiltonian corresponding to the Extended Attractive Hubbard Model (EAHM) on a two-dimensional square lattice can be written as,

$$\mathcal{H} = \mathcal{H}_{kin} + \mathcal{H}_{\mu} + \mathcal{H}_{int}^{onsite} + \mathcal{H}_{int}^{nn} + \mathcal{H}_{\mathbf{B}}, \tag{2.1}$$

where, $\mathcal{H}_{kin}$ is the kinetic energy of the electrons, $\mathcal{H}_{\mu}$ is the chemical potential term, $\mathcal{H}_{int}^{onsite}$ is the on-site attractive interaction and $\mathcal{H}_{int}^{nn}$ is the nearest-neighbor (nn) attractive interaction. $\mathcal{H}_{\mathbf{B}}$ describes the Zeeman coupling of electrons to an external magnetic field $\mathbf{B}$. The corresponding operator terms, written in the second quantization notation are,

$$
\begin{aligned}
\mathcal{H}_{kin} &= -t \sum_{\langle ij \rangle, \sigma} c^{\dagger}_{i\sigma} c_{j\sigma} + H.c. \\
\mathcal{H}_{\mu} &= -\mu \sum_{i\sigma} n_{i\sigma} = -\mu \sum_{i\sigma} c^{\dagger}_{i\sigma} c_{i\sigma} \\
\mathcal{H}^{onsite}_{int} &= -U \sum_{i} n_{i\uparrow} n_{i\downarrow} = -U \sum_{i} c^{\dagger}_{i\uparrow} c_{i\uparrow} c^{\dagger}_{i\downarrow} c_{i\downarrow} \\
\mathcal{H}^{nn}_{int} &= -V \sum_{\langle ij \rangle} n_i n_j = -V \sum_{\substack{\langle ij \rangle \\ \sigma, \sigma'}} c^{\dagger}_{i\sigma} c_{i\sigma} c^{\dagger}_{j\sigma'} c_{j\sigma'} \\
\mathcal{H}_{\mathbf{B}} &= -B_z \sum_{i} (n_{i\uparrow} - n_{i\downarrow}) = -B_z \sum_{i} (c^{\dagger}_{i\sigma\uparrow} c_{i\sigma\uparrow} - c^{\dagger}_{i\sigma\uparrow} c_{i\sigma\uparrow}).
\end{aligned}
\tag{2.2}
$$

In the above, $c^{\dagger}_{i\sigma}(c_{i\sigma})$ creates (annihilates) an electron at $i$-th site of the lattice. $\langle ij \rangle$ represents nearest-neighbor sites of the lattice. $n_{i\sigma}$ is the electron occupation number operator at $i$-th site for $\sigma$ spin-projection. The total electron occupation number at $i$-th site is defined via $n_i = n_{i\uparrow} + n_{i\downarrow}$. $U$ is the onsite attractive interaction strength, whereas $V$ is the inter-site attractive interaction strength. $B_z$ is the $z$- component of the magnetic field. $t$ is the nearest-neighbor hopping amplitude. $\mu$ is the chemical potential, as the system is defined in a grand canonical ensemble.

## 2.2 Mean-Field Decoupling in Pairing Channel

Both the interaction terms, the on-site one and the inter-site one, are represented by two-body operator terms in $2^{\text{nd}}$ quantization formalism. To reduce the complexity of these terms, we consider the path of mean-field treatment, where the many-body interaction effects are mimicked via the interaction of a single-electron system with a mean-field created by the aggregated effect of rest of the electrons, present in the system. Mathematically speaking, such a two-body operator term $\hat{X}\hat{Y}$ can be written as

$$
\begin{aligned}
\hat{X}\hat{Y} &= \big\{\langle \hat{X} \rangle + (\hat{X} - \langle \hat{X} \rangle)\big\}\big\{\langle \hat{Y} \rangle + (\hat{Y} - \langle \hat{Y} \rangle)\big\} \\
&= \langle \hat{X} \rangle \langle \hat{Y} \rangle + \langle \hat{X} \rangle (\hat{Y} - \langle \hat{Y} \rangle) + \langle \hat{Y} \rangle (\hat{X} - \langle \hat{X} \rangle) \\
&\quad + (\hat{X} - \langle \hat{X} \rangle)(\hat{Y} - \langle \hat{Y} \rangle) \\
&\approx \hat{X} \langle \hat{Y} \rangle + \hat{Y} \langle \hat{X} \rangle - \langle \hat{X} \rangle \langle \hat{Y} \rangle,
\end{aligned}
\tag{2.3}
$$

where we have neglected the deviation in the $2^{\text{nd}}$ order. In practice, we can apply

this idea of mean-field decoupling to the interaction terms of the Hamiltonian using different channels, such as density channel or pairing channel etc. Where density channel decoupling leads to mean-fields of the form $\langle c^\dagger c\rangle$, pairing channel decoupling leads to mean-fields of the form $\langle c^\dagger c^\dagger\rangle$. As we are specifically interested in superconducting solutions, we carefully choose "pairing channel" decoupling for our system. After mean-field decoupling in the particle-particle channel (or pairing channel), the on-site interacting two-particle operator terms becomes:

$$\begin{aligned}
H_{int}^{onsite} &= -U\sum_i n_{i\uparrow}n_{i\downarrow} \\
&= -U\sum_i (c_{i\uparrow}^\dagger c_{i\uparrow} c_{i\downarrow}^\dagger c_{i\downarrow}) \\
&= -U\sum_i c_{i\uparrow}^\dagger c_{i\downarrow}^\dagger c_{i\downarrow} c_{i\uparrow} \quad \textbf{Using Fermionic Anticommutation Property} \\
&\approx -U\sum_i \Big[\langle c_{i\downarrow}c_{i\uparrow}\rangle c_{i\uparrow}^\dagger c_{i\downarrow}^\dagger + H.c. - \langle c_{i\uparrow}^\dagger c_{i\downarrow}^\dagger\rangle\langle c_{i\downarrow}c_{i\uparrow}\rangle\Big] \quad \textbf{Mean-Field Decoupling} \\
&= -U\sum_i \Big[\Delta_i c_{i\uparrow}^\dagger c_{i\downarrow}^\dagger + H.c. - |\Delta_i|^2\Big] \quad \text{where, } \Delta_i = \langle c_{i\downarrow}c_{i\uparrow}\rangle
\end{aligned} \tag{2.4}$$

Expanding the inter-site interaction term we obtain:

$$\begin{aligned}
H_{nn}^{int} &= -V\sum_{\langle ij\rangle} n_i n_j = -V\sum_{i,\delta} n_i n_{i+\delta} \\
&= -V\sum_{i,\delta}(n_{i\uparrow}+n_{i\downarrow})(n_{i+\delta\uparrow}+n_{i+\delta\downarrow}) \\
&= -V\sum_{i,\delta}\Big(\overbrace{n_{i\uparrow}n_{i+\delta\uparrow}}^{A} + \overbrace{n_{i\downarrow}n_{i+\delta\downarrow}}^{B} + \overbrace{n_{i\uparrow}n_{i+\delta\downarrow}}^{C} + \overbrace{n_{i\downarrow}n_{i+\delta\uparrow}}^{D}\Big),
\end{aligned} \tag{2.5}$$

where $\delta$ is an index, which denotes unit vectors along the direction of two nearest neighbors, namely $\boldsymbol{\delta} = +\hat{x}$ and $\boldsymbol{\delta} = +\hat{y}$. Note that we have grouped terms as $A$,$B$,$C$, and $D$ for the ease of reference. Now terms $A$ and $B$ lead to the possibility of triplet solution with $S_z = \pm 1$, while terms $C$ and $D$ lead to singlet and triplet solution with $S_z = 0$.

**Singlet and Triplet with $S_z = 0$:** Let's start with term $C$:

$$
\begin{aligned}
&- V \sum_{i,\delta} n_{i\uparrow} n_{i+\delta\downarrow} \\
&= -V \sum_{i,\delta} c^{\dagger}_{i\uparrow} c_{i\uparrow} c^{\dagger}_{i+\delta\downarrow} c_{i+\delta\downarrow} \\
&= -V \sum_{i,\delta} c^{\dagger}_{i\uparrow} c^{\dagger}_{i+\delta\downarrow} c_{i+\delta\downarrow} c_{i\uparrow} \quad \textbf{Using Anti-commutation} \\
&= -V \sum_{i,\delta} \langle c_{i+\delta\downarrow} c_{i\uparrow} \rangle c^{\dagger}_{i\uparrow} c^{\dagger}_{i+\delta\downarrow} + H.c. + V \sum_{i,\delta} |\langle c_{i+\delta\downarrow} c_{i\uparrow} \rangle|^2 \\
&= -V \sum_{i,\delta} \Delta^{+}_{i\delta} \;\; c^{\dagger}_{i\uparrow} c^{\dagger}_{i+\delta\downarrow} + H.c. + V \sum_{i,\delta} |\Delta^{+}_{i\delta}|^2
\end{aligned} \tag{2.6}
$$

Similarly for term $D$:

$$
\begin{aligned}
&V \sum_{i,\delta} n_{i\downarrow} n_{i+\delta\uparrow} \\
&= -V \sum_{i,\delta} c^{\dagger}_{i\downarrow} c_{i\downarrow} c^{\dagger}_{i+\delta\uparrow} c_{i+\delta\uparrow} \\
&= -V \sum_{i,\delta} c^{\dagger}_{i+\delta\uparrow} c^{\dagger}_{i\downarrow} c_{i\downarrow} c_{i+\delta\uparrow} \quad \textbf{Using Anti-commutation} \\
&= -V \sum_{i,\delta} \langle c_{i\downarrow} c_{i+\delta\uparrow} \rangle c^{\dagger}_{i+\delta\uparrow} c^{\dagger}_{i\downarrow} + H.c. + V \sum_{i,\delta} |\langle c_{i\downarrow} c_{i+\delta\uparrow} \rangle|^2 \\
&= -V \sum_{i,\delta} \Delta^{-}_{i\delta} \;\; c^{\dagger}_{i+\delta\uparrow} c^{\dagger}_{i\downarrow} + H.c. + V \sum_{i,\delta} |\Delta^{-}_{i\delta}|^2
\end{aligned} \tag{2.7}
$$

**Triplet with $S_z = \pm 1$** Term $A$ goes like:

$$
\begin{aligned}
&- V \sum_{i,\delta} n_{i\uparrow} n_{i+\delta\uparrow} \\
&= -V \sum_{i,\delta} c^{\dagger}_{i\uparrow} c_{i\uparrow} c^{\dagger}_{i+\delta\uparrow} c_{i+\delta\uparrow} \\
&= -V \sum_{i,\delta} c^{\dagger}_{i\uparrow} c^{\dagger}_{i+\delta\uparrow} c_{i+\delta\uparrow} c_{i\uparrow} \quad \textbf{Using Anti-Commutation} \\
&= -V \sum_{i,\delta} \langle c_{i+\delta\uparrow} c_{i\uparrow} \rangle c^{\dagger}_{i\uparrow} c^{\dagger}_{i+\delta\uparrow} + H.c. + V \sum_{i,\delta} |\langle c_{i+\delta\uparrow} c_{i\uparrow} \rangle|^2 \\
&= -V \sum_{i,\delta} \Delta^{\uparrow}_{i\delta} \;\; c^{\dagger}_{i\uparrow} c^{\dagger}_{i+\delta\uparrow} + H.c. + V \sum_{i,\delta} |\Delta^{\uparrow}_{i\delta}|^2
\end{aligned} \tag{2.8}
$$

Similarly, term $B$ goes like:

$$
\begin{aligned}
& -V \sum_{i,\delta} n_{i\downarrow} n_{i+\delta\downarrow} \\
&= -V \sum_{i,\delta} c^{\dagger}_{i\downarrow} c_{i\downarrow} c^{\dagger}_{i+\delta\downarrow} c_{i+\delta\downarrow} \\
&= -V \sum_{i,\delta} c^{\dagger}_{i\downarrow} c^{\dagger}_{i+\delta\downarrow} c_{i+\delta\downarrow} c_{i\downarrow} \quad \textbf{Using Anti-Commutation} \\
&= -V \sum_{i,\delta} \langle c_{i+\delta\downarrow} c_{i\downarrow} \rangle c^{\dagger}_{i\downarrow} c^{\dagger}_{i+\delta\downarrow} + H.c. + V \sum_{i,\delta} |\langle c_{i+\delta\downarrow} c_{i\downarrow} \rangle|^2 \\
&= -V \sum_{i,\delta} \Delta^{\downarrow}_{i\delta} \;\; c^{\dagger}_{i\downarrow} c^{\dagger}_{i+\delta\downarrow} + H.c. + V \sum_{i,\delta} |\Delta^{\downarrow}_{i\delta}|^2
\end{aligned} \tag{2.9}
$$

**Effective Mean-Field Hamiltonian in Real Space**:
So the effective mean-field hamiltonian in real space becomes:

$$
\begin{aligned}
\mathcal{H}_{MF} = & -t \sum_{\langle ij \rangle, \sigma} \left[ c^{\dagger}_{i\sigma} c_{j\sigma} + H.c. \right] - \mu \sum_{i\sigma} c^{\dagger}_{i\sigma} c_{i\sigma} \\
& - B_z \sum_{i} (c^{\dagger}_{i\uparrow} c_{i\uparrow} - c^{\dagger}_{i\downarrow} c_{i\downarrow}) \\
& - U \sum_{i} \left[ \Delta_i c^{\dagger}_{i\uparrow} c^{\dagger}_{i\downarrow} + H.c. - |\Delta_i|^2 \right] \\
& - V \sum_{i,\delta} \left[ \Delta^{+}_{i\delta} c^{\dagger}_{i\uparrow} c^{\dagger}_{i+\delta\downarrow} + H.c. - |\Delta^{+}_{i\delta}|^2 \right] \\
& - V \sum_{i,\delta} \left[ \Delta^{-}_{i\delta} c^{\dagger}_{i+\delta\uparrow} c^{\dagger}_{i\downarrow} + H.c. - |\Delta^{-}_{i\delta}|^2 \right] \\
& - V \sum_{i,\delta} \left[ \Delta^{\uparrow}_{i\delta} c^{\dagger}_{i\uparrow} c^{\dagger}_{i+\delta\uparrow} + H.c. - |\Delta^{\uparrow}_{i\delta}|^2 \right] \\
& - V \sum_{i,\delta} \left[ \Delta^{\downarrow}_{i\delta} c^{\dagger}_{i\downarrow} c^{\dagger}_{i+\delta\downarrow} + H.c. - |\Delta^{\downarrow}_{i\delta}|^2 \right]
\end{aligned} \tag{2.10}
$$

## 2.3 Effective Hamiltonian in Momentum Space

Observing the effective mean-field Hamiltonian in real space (Eq.2.10) it's apparent that the effective Hamiltonian is a function of

- a set of parameters: t, $\mu$, $U$, $V$, $B_z$, and
- a set of complex variables (pairing correlations): $\Delta_i$, $\Delta^{+}_{i\delta}$, $\Delta^{-}_{i\delta}$, $\Delta^{\uparrow}_{i\delta}$, and $\Delta^{\downarrow}_{i\delta}$.

In our projects, we treat a clean system on a square lattice. Thus we exclude the possibility of inhomogeneity in our solutions, i.e., we expect our superconducting solutions to respect translational symmetry of the underlying lattice. This particular choice of translational symmetry makes Bloch basis to be more suitable candidate to describe the effective Hamiltonian. Thus we apply the following transformation from Wannier basis to bloch basis:

$$c_{i\sigma} = \frac{1}{\sqrt{N_s}} \sum_{\mathbf{k}} e^{-i\mathbf{k}\cdot\mathbf{r}_i} c_{\mathbf{k}\sigma} \quad \text{and} \quad c^\dagger_{i\sigma} = \frac{1}{\sqrt{N_s}} \sum_{\mathbf{k}} e^{i\mathbf{k}\cdot\mathbf{r}_i} c^\dagger_{\mathbf{k}\sigma} \tag{2.11}$$

In Bloch basis, the effective mean-field Hamiltonian looks like:

$$\begin{aligned}
\mathcal{H}_{MF} = &\sum_{\mathbf{k}} \left[ \epsilon^{\uparrow}(\mathbf{k}) c^\dagger_{\mathbf{k}\uparrow} c_{\mathbf{k}\uparrow} + \epsilon^{\downarrow}(\mathbf{k}) c^\dagger_{\mathbf{k}\downarrow} c_{\mathbf{k}\downarrow} \right] \\
&+ \sum_{\mathbf{k}} \left[ \Delta^{\uparrow\downarrow}(\mathbf{k}) c^\dagger_{\mathbf{k}\uparrow} c^\dagger_{-\mathbf{k}\downarrow} + H.c. \right] \\
&+ \sum_{\mathbf{k}} \left[ \Delta^{\uparrow\uparrow}(\mathbf{k}) c^\dagger_{\mathbf{k}\uparrow} c^\dagger_{-\mathbf{k}\uparrow} + H.c. \right] \\
&+ \sum_{\mathbf{k}} \left[ \Delta^{\downarrow\downarrow}(\mathbf{k}) c^\dagger_{\mathbf{k}\downarrow} c^\dagger_{-\mathbf{k}\downarrow} + H.c. \right] \\
&+ N_s U |\Delta|^2 \\
&+ N_s V \sum_{\delta} \left[ |\Delta^+_\delta|^2 + |\Delta^-_\delta|^2 + |\Delta^{\uparrow}_\delta|^2 + |\Delta^{\downarrow}_\delta|^2 \right]
\end{aligned} \tag{2.12}$$

Where,

$$\begin{aligned}
\epsilon^{\uparrow}(\mathbf{k}) &= -2t(\cos(k_x) + \cos(k_y)) - \mu - B_z \\
\epsilon^{\downarrow}(\mathbf{k}) &= -2t(\cos(k_x) + \cos(k_y)) - \mu + B_z \\
\Delta^{\uparrow\downarrow}(\mathbf{k}) &= -U\Delta - V \sum_{\delta} \left[ \Delta^+_\delta e^{-i(\mathbf{k}\cdot\boldsymbol{\delta})} + \Delta^-_\delta e^{i(\mathbf{k}\cdot\boldsymbol{\delta})} \right] \\
\Delta^{\uparrow\uparrow}(\mathbf{k}) &= -V \sum_{\delta} \Delta^{\uparrow}_\delta e^{-i(\mathbf{k}\cdot\boldsymbol{\delta})} \\
\Delta^{\downarrow\downarrow}(\mathbf{k}) &= -V \sum_{\delta} \Delta^{\downarrow}_\delta e^{-i(\mathbf{k}\cdot\boldsymbol{\delta})}
\end{aligned} \tag{2.13}$$

As mentioned earlier, in Fourier space, translational invariance leads to spatial homogeneity of the set of variables, namely superconducting pairing correlations. So the set of variables: $\{\Delta_i, \Delta^{\uparrow}_{i\delta}, \Delta^{\downarrow}_{i\delta}, \Delta^{+}_{i\delta}$ and $\Delta^{-}_{i\delta}\}$ becomes independent of site index

$i$ and our new set of variables becomes: $\{\Delta, \Delta_\delta^\uparrow, \Delta_\delta^\downarrow, \Delta_\delta^+$ and $\Delta_\delta^-\}$. In this effective Hamiltonian, $\epsilon^\uparrow(\mathbf{k})$ describes the kinetic energy of $\uparrow$-spin electrons with respect to an effective chemical potential $\mu_{\text{eff}}^\uparrow = \mu + B_z$. Similarly $\epsilon^\downarrow(\mathbf{k})$ describes the kinetic energy of $\downarrow$-spin electrons with respect to an effective chemical potential $\mu_{\text{eff}}^\downarrow = \mu - B_z$. It's evident that the presence of a magnetic field breaks the spin-degeneracy in the system via Zeeman coupling. It's worth mentioning that we work in the regime where magnetic field couples only with spin-degree of freedom. Orbital degree of freedom remains completely unperturbed by the presence of magnetic field, which leaves us with the freedom to ignore the inclusion of Peierls substitution. In the above mentioned Hamiltonian (Eq.2.12) $\Delta^{\uparrow\uparrow}(\mathbf{k})$ and $\Delta^{\downarrow\downarrow}(\mathbf{k})$ represent superconducting correlations corresponding to equal spin pairing (ESP) states, while $\Delta^{\uparrow\downarrow}(\mathbf{k})$ represents superconducting correlations corresponding to opposite spin pairing (OSP) states. While the on-site attraction strength $U$ controls OSP states only, which is evident from the definitions of these pairing correlations (Eq.2.13), inter-site attraction $V$ controls both OSP and ESP states. This very fact suggests that $V$ is meant to play an important role in stabilizing non-trivial superconducting orders with variety of pairing symmetries.

## 2.4 Solving the Hamiltonian

To understand the nature of the superconducting solutions emerging from the effective Hamiltonian in Eq.(2.12) we need to diagonalize the Hamiltonian and study its eigenspectrum. It is apparent from the Eq.(2.12) that the effective Hamiltonian is not diagonal in Bloch basis. Presence of pairing terms like $c_{\mathbf{k}\uparrow}^\dagger c_{-\mathbf{k}\downarrow}^\dagger$ have the following important consequences:

1. Particle number is not conserved in the ground state of the Hamiltonian, and

2. Bloch states are not eigenstates of such Hamiltonian.

Thus we follow Bogoliubov–de Gennes approach to diagonalize such Hamiltonian [7]. In the following sections (Section 2.4.1-2.4.2) we address this problem.

### 2.4.1 Bogoliubov-de Gennes Method

As we focus on finding the eigenspectrum of the Hamiltonian in Eq.(2.12), we ignore the extra classical energy terms in the Hamiltonian. Such Hamiltonian, also known as BdG Hamiltonian, takes the form:

$$\begin{aligned}\mathcal{H}_{BdG} = &\sum_{\mathbf{k}} \left[\epsilon^{\uparrow}(\mathbf{k}) c^{\dagger}_{\mathbf{k}\uparrow} c_{\mathbf{k}\uparrow} + \epsilon^{\downarrow}(\mathbf{k}) c^{\dagger}_{\mathbf{k}\downarrow} c_{\mathbf{k}\downarrow}\right] \\ &+ \sum_{\mathbf{k}} \left[\Delta^{\uparrow\downarrow}(\mathbf{k}) c^{\dagger}_{\mathbf{k}\uparrow} c^{\dagger}_{-\mathbf{k}\downarrow} + H.c.\right] \\ &+ \sum_{\mathbf{k}} \left[\Delta^{\uparrow\uparrow}(\mathbf{k}) c^{\dagger}_{\mathbf{k}\uparrow} c^{\dagger}_{-\mathbf{k}\uparrow} + H.c.\right] \\ &+ \sum_{\mathbf{k}} \left[\Delta^{\downarrow\downarrow}(\mathbf{k}) c^{\dagger}_{\mathbf{k}\downarrow} c^{\dagger}_{-\mathbf{k}\downarrow} + H.c.\right]. \end{aligned} \tag{2.14}$$

We use Bogoliubov-Valatin transformation, which was independently developed in 1958 by Nikolay Bogolyubov and John George Valatin for finding solutions of BCS theory in a homogeneous system [8, 46], to diagonalize the Hamiltonian in Eq.(2.14). The canonical transformation looks like:

$$\begin{aligned} c_{\mathbf{k}\uparrow} &= \sum_{n} u^{n}_{\mathbf{k}\uparrow} \gamma_{\mathbf{k}n} + (v^{n}_{\mathbf{k}\uparrow})^{*} \gamma^{\dagger}_{-\mathbf{k}n} \\ c_{\mathbf{k}\downarrow} &= \sum_{n} u^{n}_{\mathbf{k}\downarrow} \gamma_{\mathbf{k}n} + (v^{n}_{\mathbf{k}\downarrow})^{*} \gamma^{\dagger}_{-\mathbf{k}n} \end{aligned} \tag{2.15}$$

Where $\gamma^{\dagger}_{\mathbf{k}n}$ ($\gamma_{\mathbf{k}n}$) creates (annihilates) so called "Bogoliubov quasi-particles", $\mathbf{k}$ and $n$ being the indices associated with momentum $\mathbf{k}$ and pseudospin of the quasi-particle. Coefficients $u^{n}_{\mathbf{k}\sigma}$ and $v^{n}_{\mathbf{k}\sigma}$ connects to electron-like and hole-like (quasi-holes) quasi-particles respectively. In the quasi-particle (quasi-hole) picture the Hamiltonian in Eq.(2.14) must be diagonalized:

$$\mathcal{H}_{BdG} = \sum_{\mathbf{k}n} E_{\mathbf{k}n} \gamma^{\dagger}_{\mathbf{k}n} \gamma_{\mathbf{k}n} + E_G. \tag{2.16}$$

$E_G$ is the ground state energy of the system, $\gamma^{\dagger}$ being the creation operator corresponding to the excitations above the ground state.
Invoking the following identities between anticommutator and commutator of any three quantum-mechanical operators $A$, $B$, and $C$:

$$[A, BC] = \{A, B\}C - B\{A, C\} \tag{2.17}$$

we can derive the following identities, if we calculate the commutators of $c_{\mathbf{k}\uparrow}$, $c^{\dagger}_{-\mathbf{k}\downarrow}$,

$c_{\mathbf{k}\downarrow}$, and $c^{\dagger}_{-\mathbf{k}\uparrow}$ with $\mathcal{H}$:

$$
\begin{aligned}
[c_{\mathbf{k}\uparrow}, \mathcal{H}_{BdG}] &= \epsilon^{\uparrow}(\mathbf{k})c_{\mathbf{k}\uparrow} + \Delta^{\uparrow\downarrow}(\mathbf{k})c^{\dagger}_{-\mathbf{k}\downarrow} + 0 \times c_{\mathbf{k}\downarrow} + \Delta_s^{\uparrow\uparrow}(\mathbf{k})c^{\dagger}_{-\mathbf{k}\uparrow} \\
[c^{\dagger}_{-\mathbf{k}\downarrow}, \mathcal{H}_{BdG}] &= (\Delta^{\uparrow\downarrow}(\mathbf{k}))^{*}c_{\mathbf{k}\uparrow} - \epsilon^{\downarrow}(-\mathbf{k})c^{\dagger}_{-\mathbf{k}\downarrow} + (\Delta_s^{\downarrow\downarrow}(\mathbf{k}))^{*}c_{\mathbf{k}\downarrow} + 0 \times c^{\dagger}_{-\mathbf{k}\uparrow} \\
[c_{\mathbf{k}\downarrow}, \mathcal{H}_{BdG}] &= 0 \times c_{\mathbf{k}\uparrow} + \Delta_s^{\downarrow\downarrow}(\mathbf{k})c^{\dagger}_{-\mathbf{k}\downarrow} + \epsilon^{\downarrow}(\mathbf{k})c_{\mathbf{k}\downarrow} - \Delta^{\uparrow\downarrow}(-\mathbf{k})c^{\dagger}_{-\mathbf{k}\uparrow} \\
[c^{\dagger}_{-\mathbf{k}\uparrow}, \mathcal{H}_{BdG}] &= (\Delta_s^{\uparrow\uparrow}(\mathbf{k}))^{*}c_{\mathbf{k}\uparrow} + 0 \times c^{\dagger}_{-\mathbf{k}\downarrow} - (\Delta^{\uparrow\downarrow}(-\mathbf{k}))^{*}c_{\mathbf{k}\downarrow} - \epsilon^{\uparrow}(-\mathbf{k})c^{\dagger}_{-\mathbf{k}\uparrow}
\end{aligned}
\tag{2.18}
$$

Where, $\Delta_s^{\uparrow\uparrow}(\mathbf{k}) = (\Delta^{\uparrow\uparrow}(\mathbf{k}) - \Delta^{\uparrow\uparrow}(-\mathbf{k}))$ and $\Delta_s^{\downarrow\downarrow}(\mathbf{k}) = (\Delta^{\downarrow\downarrow}(\mathbf{k}) - \Delta^{\downarrow\downarrow}(-\mathbf{k}))$. While calculating the first commutator in Eq.(2.18), if we look closely, we notice how $c_{\mathbf{k}\uparrow}$ is coupled with the operators $c^{\dagger}_{-\mathbf{k}\downarrow}$ and $c^{\dagger}_{-\mathbf{k}\uparrow}$. This coupling, natuarally occuring due to the form of the Hamiltonian itself, is used a guide to calculate the other commutators. Applying Eq.(2.15) in Eq.(2.18) and collecting Coefficients of $\gamma_{\mathbf{k}n}$ we get the following equation:

$$
\overbrace{\begin{bmatrix}
\epsilon^{\uparrow}(\mathbf{k}) & \Delta^{\uparrow\downarrow}(\mathbf{k}) & 0 & \Delta_s^{\uparrow\uparrow}(\mathbf{k}) \\
(\Delta^{\uparrow\downarrow}(\mathbf{k}))^{*} & -\epsilon^{\downarrow}(-\mathbf{k}) & (\Delta_s^{\downarrow\downarrow}(\mathbf{k}))^{*} & 0 \\
0 & \Delta_s^{\downarrow\downarrow}(\mathbf{k}) & \epsilon^{\downarrow}(\mathbf{k}) & -\Delta^{\uparrow\downarrow}(-\mathbf{k}) \\
(\Delta_s^{\uparrow\uparrow}(\mathbf{k}))^{*} & 0 & -(\Delta^{\uparrow\downarrow}(-\mathbf{k}))^{*} & -\epsilon^{\uparrow}(-\mathbf{k})
\end{bmatrix}}^{\mathbf{M}_{BdG}(\mathbf{k})}
\overbrace{\begin{bmatrix} u^n_{\mathbf{k}\uparrow} \\ v^n_{-\mathbf{k}\downarrow} \\ u^n_{\mathbf{k}\downarrow} \\ v^n_{-\mathbf{k}\uparrow} \end{bmatrix}}^{\varphi_{\mathbf{k}n}}
= E_{\mathbf{k}n}
\begin{bmatrix} u^n_{\mathbf{k}\uparrow} \\ v^n_{-\mathbf{k}\downarrow} \\ u^n_{\mathbf{k}\downarrow} \\ v^n_{-\mathbf{k}\uparrow} \end{bmatrix}
\tag{2.19}
$$

On the other hand, if we collect coefficients of $\gamma^{\dagger}_{-\mathbf{k}n}$ after applying Eq.(2.15) in Eq.(2.18) and make a parity transformation $\mathbf{k} \to -\mathbf{k}$, we get the following equation:

$$\overbrace{\begin{bmatrix} \epsilon^{\uparrow}(-\mathbf{k}) & \Delta^{\uparrow\downarrow}(-\mathbf{k}) & 0 & \Delta_s^{\uparrow\uparrow}(-\mathbf{k}) \\ (\Delta^{\uparrow\downarrow}(-\mathbf{k}))^* & -\epsilon^{\downarrow}(\mathbf{k}) & (\Delta_s^{\downarrow\downarrow}(-\mathbf{k}))^* & 0 \\ 0 & \Delta_s^{\downarrow\downarrow}(-\mathbf{k}) & \epsilon^{\downarrow}(-\mathbf{k}) & -\Delta^{\uparrow\downarrow}(\mathbf{k}) \\ (\Delta_s^{\uparrow\uparrow}(-\mathbf{k}))^* & 0 & -(\Delta^{\uparrow\downarrow}(\mathbf{k}))^* & -\epsilon^{\uparrow}(\mathbf{k}) \end{bmatrix}}^{\mathbf{M}_{BdG}(-\mathbf{k})} \overbrace{\begin{bmatrix} (v^n_{-\mathbf{k}\uparrow})^* \\ (u^n_{\mathbf{k}\downarrow})^* \\ (v^n_{-\mathbf{k}\downarrow})^* \\ (u^n_{\mathbf{k}\uparrow})^* \end{bmatrix}}^{\phi_{\mathbf{k}n}} = -E_{\mathbf{k}n} \begin{bmatrix} (v^n_{-\mathbf{k}\uparrow})^* \\ (u^n_{\mathbf{k}\downarrow})^* \\ (v^n_{-\mathbf{k}\downarrow})^* \\ (u^n_{\mathbf{k}\uparrow})^* \end{bmatrix} \tag{2.20}$$

Comparing Eq.(2.19) with Eq.(2.20) we observe that if $\varphi_{\mathbf{k}n}$ is an eigenstate of the matrix $\mathbf{M}_{BdG}(\mathbf{k})$ with an eigenvalue $E_{\mathbf{k}n}$, there must exist a state $\phi_{\mathbf{k}n}$, which is also an eigenstate of $\mathbf{M}_{BdG}(-\mathbf{k})$ with an eigenvalue $-E_{\mathbf{k}n}$. It's easy to test it numerically diagonalizing both the matrices $\mathbf{M}_{BdG}(\mathbf{k})$ and $\mathbf{M}_{BdG}(-\mathbf{k})$. We found that eigenvalues of these two matrices are connected. Negative counterparts of two positive eigenvalues of $\mathbf{M}_{BdG}(\mathbf{k})$ can be found as eigenvalues of $\mathbf{M}_{BdG}(-\mathbf{k})$ and vice versa. This actually gives us the idea of how the very design of BdG Hamiltonian (Eq.2.14) imposes a particle-hole symmetry in the space of quasi-particles. Quasi-particles with energies E,-E are not actually two different states. Rather it represents a single quantum state, which is a coherent superposition of electron-like and hole-like states. This idea will also be evident in the next section.

### 2.4.2 BdG with Nambu spinors

Rather than treating the Hamiltonian in Eq.(2.14) in the typical BdG-equations approach, we can use Nambu spinors to describe the same Hamiltonian. Our mean field Hamiltonian $\mathcal{H}_{BdG}$ (Eq.2.14) can be written in terms of Nambu spinors $\mathbf{\Psi_k}$ as:

$$\mathcal{H}_{BdG} = \sum_{\mathbf{k}} \mathbf{\Psi}^{\dagger}_{\mathbf{k}} \mathcal{M}_{BdG}(\mathbf{k}) \mathbf{\Psi_k} \tag{2.21}$$

Where, Nambu spinor $\mathbf{\Psi_k}$ is a column vector of the following form: $\mathbf{\Psi_k} = (c_{\mathbf{k}\uparrow} \quad c^{\dagger}_{-\mathbf{k}\downarrow} \quad c_{\mathbf{k}\downarrow} \quad c^{\dagger}_{-\mathbf{k}\uparrow})$ and $\mathcal{M}_{BdG}(\mathbf{k})$ is a $4 \times 4$ Hamiltonian matrix of the following form:

$$\mathcal{M}_{BdG}(\mathbf{k}) = \begin{pmatrix} \epsilon^{\uparrow}(\mathbf{k}) & \Delta^{\uparrow\downarrow}(\mathbf{k}) & 0 & \Delta_s^{\uparrow\uparrow}(\mathbf{k}) \\ (\Delta^{\uparrow\downarrow}(\mathbf{k}))^* & -\epsilon^{\downarrow}(-\mathbf{k}) & (\Delta_s^{\downarrow\downarrow}(\mathbf{k}))^* & 0 \\ 0 & \Delta_s^{\downarrow\downarrow}(\mathbf{k}) & \epsilon^{\downarrow}(\mathbf{k}) & -(\Delta^{\uparrow\downarrow}(-\mathbf{k})) \\ (\Delta_s^{\uparrow\uparrow}(\mathbf{k}))^* & 0 & -(\Delta^{\uparrow\downarrow}(-\mathbf{k}))^* & -\epsilon^{\uparrow}(-\mathbf{k}) \end{pmatrix} \tag{2.22}$$

$\mathcal{M}_{BdG}(\mathbf{k})$ is known as the mean-field Bogoliubov-de Gennes Hamiltonian matrix. It is to be noted that while forming the BdG matrix we doubled the available degrees of freedom offered in $\mathcal{H}_{BdG}$. This particular point is not apparent while dealing with BdG-equations in the previous section. While writing down the BdG Hamiltonian $\mathcal{H}_{BdG}$ in terms of Nambu spinors, we perform a particle-hole transformation ($c_\sigma^\dagger \rightarrow c_\sigma$; $c_\sigma \rightarrow c_\sigma^\dagger$) to each spin-sectors and effectively make two copies of the Hamiltonian, one corresponding to the particle sector and the other corresponding to the hole sector. This redundant degree of freedom is needed to incorporate Bogoliubov excitations. So-called "Bogoliubov quasi-particles" are actually a superposition of electron-like and hole-like states, as mentioned earlier. One should take note of the fact that while calculating different expectation values, after having diagonalized this Hamiltonian, this redundant degree of freedom is ignored.

## 2.5 Energy Minimization and Self-consistency

Having solved the BdG Hamiltonian matrix $\mathcal{M}_{BdG}$, we calculate different pairing correlations $\{\Delta, \Delta_\delta^\uparrow, \Delta_\delta^\downarrow, \Delta_\delta^+$ and $\Delta_\delta^-\}$ in terms of the eigenspectrum of the diagonalized BdG Hamiltonian. In our projects we use two approaches to find superconducting solutions:

1. Brute-force energy minimization with respect to $\{\Delta, \Delta_\delta^\uparrow, \Delta_\delta^\downarrow, \Delta_\delta^+$ and $\Delta_\delta^-\}$
2. Calculating the set $\{\Delta, \Delta_\delta^\uparrow, \Delta_\delta^\downarrow, \Delta_\delta^+$ and $\Delta_\delta^-\}$ in a self-consistent manner by diagonalizing $\mathcal{H}_{BdG}$ repetitively and using the set $\{\Delta, \Delta_\delta^\uparrow, \Delta_\delta^\downarrow, \Delta_\delta^+$ and $\Delta_\delta^-\}$ as a feedback to the corresponding matrix $\mathcal{M}_{BdG}$.

In the first method, we perform a pair-wise energy minimization with respect to the relative phase angle between each member of the set $\{\Delta, \Delta_\delta^\uparrow, \Delta_\delta^\downarrow, \Delta_\delta^+$ and $\Delta_\delta^-\}$. Then we assume that the phase relations among these members still hold in general, which

leads to a huge reduction of the size of the parameter space. Then we perform a brute-force energy minimization with respect to that reduced parameter space to find the minimum energy superconducting solutions.

In the second method we treat the set $\{\Delta, \Delta_\delta^\uparrow, \Delta_\delta^\downarrow, \Delta_\delta^+$ and $\Delta_\delta^-\}$ as a group of mean-field variables, which are calculated self-consistently by diagonalizing the BdG Hamiltonian $\mathcal{H}_{BdG}$ repetitively. To be more perfect, we use a variational self-consistency approach, where we start the self-consistent iteration from different initial point in the parameter space and ultimately choose the converged solution with minimum energy. More importantly, we have verified for selected points in the parameter space that the two methods described above lead to identical superconducting solutions.

# Chapter 3

# Unconventional superconducting phases from opposite spin pairing

We show that the extended attractive Hubbard model on a square lattice allows for a variety of superconducting phases, including exotic mixed-symmetry phases with $d_{x^2-y^2} + \mathrm{i}[s + s^*]$ and $d_{x^2-y^2} + p_x$ symmetries, and a novel $p_x + \mathrm{i}p_y$ state. The calculations are performed within the Hartree-Fock Bardeen-Cooper-Schrieffer (HF-BCS) framework. The ground states of the mean-field Hamiltonian are obtained via a minimization scheme that relaxes the symmetry constraints on the superconducting solutions, hence allowing for a mixing of $s$-, $p$- and $d$-wave order parameters. The results are obtained within the assumption of uniform-density states. Our results show that extended attractive Hubbard model can serve as an effective model for investigating properties of exotic superconductors.

## 3.1 Introduction

Identifying the symmetry of the superconducting (SC) order parameter (OP) is an important step towards understanding the properties of a SC state [47]. The OP symmetry can also provide crucial insights regarding possible pairing mechanisms. Indeed, the appearance of a non-$s$-wave component in the OP symmetry is taken as an indication of unconventional pairing mechanism. Non-trivial OP symmetries have been experimentally identified in many SC materials. Cuprates provide a famous example where the OP symmetry is known to be of $d$-wave type with a possible mixing of a secondary $s$-wave or $p$-wave component in some materials [48–54]. Recent ARPES experiments also show the evolution of the OP from a node less form to the nodal $d$-wave form [55]. An exotic chiral $p$-wave OP has been put forward as a

strong candidate for the SC state in $Sr_2RuO_4$ [56–59]. Spin triplet SC order has also been inferred from Knight-shift experiments on Bechgaard salts, $TMTSF_2PF_6$ and $TMTSF_2ClO_4$ [60–64]. A direct observation of a parity-breaking transition in an attractive cold-atom system has been reported recently [65]. The possibility of mixed parity superconductivity, although not reported in any experiment yet, has not been ruled out [66–68]. Therefore, understanding and characterizing unconventional mixed-symmetry SC states remains a problem of critical importance.

It is well accepted that an effective attraction between electrons is a prerequisite for generating SC order. Therefore, effective models with attractive interactions are commonly employed for investigating properties of SC states [69–72]. The simplest choice among such models is the attractive Hubbard model (AHM) which has been extensively studied using a variety of numerical and semi-analytical methods [71, 73–79]. The on-site AHM allows for the conventional $s$-wave superconductivity. Including a nearest-neighbour (nn) attractive term readily supports a $d$-wave SC solution [69, 80–82]. It has been asserted that in some cases the induced attraction between electrons is not large enough to overcome the on-site Coulombic repulsion. However it can overcome the nn repulsion, and therefore an effective model with on-site repulsion and nn attraction may be realized [69, 83, 84]. Indeed, this is a popular model for studying the competition between antiferromagnetism and d-wave superconductivity in the context of cuprates [69, 85–87]. Another realistic possibility is that the induced attraction overcomes both the on-site and nn repulsive interactions, leading to an EAHM. Surprisingly, this model has not been explored much for the possibility of unconventional, particularly the mixed OP symmetry, SC solutions [87, 88].

In this work, we unveil the exciting possibility of the existence of unconventional mixed symmetry SC states in an EAHM on a square lattice. A justifiable approximation on the nn attractive interaction followed by a general decoupling scheme together with an explicit minimization procedure allows us to construct comprehensive phase diagrams for the model. Superconducting phases with mixed OPs dominate the phase diagram. We present simple energetic arguments for the stability of mixed OP phases. Two of the unconventional phases, the $d_{x^2-y^2} + p_x$ order and the chiral $p_x + ip_y$ state, exist over a wide parameter regime. Both these orderings also support non-trivial edge-state dispersions. While the two OP symmetries mentioned above are directly relevant to some cuprates and $Sr_2RuO_4$, respectively, our results have a general implication that the EAHM can be a universal effective model for studying unconventional superconductivity. We also discuss the finite-temperature behavior and show that for certain densities the system undergoes multiple transitions before reaching a normal state at high temperature.

## 3.2 Model and Method

### 3.2.1 Extended Attractive Hubbard Hamiltonian

We begin with the EAHM defined on a 2D square lattice. The model is described by the Hamiltonian,

$$\begin{aligned} H &= -t\sum_{\langle ij\rangle,\sigma}[c^{\dagger}_{i\sigma}c_{j\sigma}+H.c.]-\mu\sum_{i\sigma}c^{\dagger}_{i\sigma}c_{i\sigma} \\ &\quad -U\sum_{i}n_{i\uparrow}n_{i\downarrow}-V\sum_{\langle ij\rangle}n_{i}n_{j}. \end{aligned} \tag{3.1}$$

Here $c_{i\sigma}(c^{\dagger}_{i\sigma})$ annihilates (creates) an electron at site $i$ with spin $\sigma$, $\langle ij\rangle$ implies that sites $i$ and $j$ are nearest neighbours. $\mu$ is the chemical potential, $n_{i\sigma}=c^{\dagger}_{i\sigma}c_{i\sigma}$ is the electron number operator at site $i$ and spin-projection $\sigma$, and $n_i = n_{i\uparrow}+n_{i\downarrow}$. $U$ and $V$ denote the strengths of on-site and nearest neighbour attractive interactions, respectively. Using $t = 1$ as the basic energy scale, and restricting ourselves to zero temperatures ($T = 0$), we are left with three independent parameters in the Hamiltonian, *viz.*, $U$, $V$ and $\mu$.

Before we proceed with the study of the Hamiltonian Eq. (3.1), it is important to motivate the physical relevance of the EAHM as an effective lattice model. A possible realization of such a model via a competition of bare Coulomb repulsion and phonon-mediated effective attraction was already mentioned in the previous section. In general, the EAHM represents a physical situation where two independent mechanisms, one favouring on-site pairing and other favouring inter-site pairing, are simultaneously active [88]. These mechanisms then compete for superconducting order with different OP symmetries. A microscopic model for such a situation will depend of the specific details of the system. Nevertheless, the EAHM can serve as an elementary model to study such a competition among different SC states. Furthermore, it has been shown that a model with on-site repulsion and inter-site Ising type antiferromagnetic exchange can be mapped onto an on-site attractive model [89]. The existence of such mappings between attractive and repulsive models also makes it worthwhile to investigate the ordered states arising in purely attractive models. A promising avenue for realization of such models is ultracold Fermionic atoms in optical lattices [90–94]. The standard Hubbard model with both repulsive and attractive interactions has indeed been realized in these systems. Yet another possibility, which has so far been demonstrated for repulsive models, is the use of artificial crystals

where semiconducting quantum dots can be patterned to form a two dimensional lattice [95].

We analyze the Hamiltonian in Eq. (3.1) by making a mean-field approximation for the interaction term [96]. In the inter-site attractive term we ignore the same-spin attraction parts $n_{i\uparrow}n_{j\uparrow}$ and $n_{i\downarrow}n_{j\downarrow}$. This can be qualitatively justified for systems where superconductivity emerges in the vicinity of antiferromagnetism. The antiferromagnetic tendency ensures that electrons with opposite spin orientations are more likely to reside on neighbouring sites as compared to those with same spin orientation.

### 3.2.2 General Decoupling in the Pairing Channel

We now discuss how a general decoupling of the nearest-neighbour (nn) attractive interaction allows for possible mixed order parameter solutions. The interaction term is given by,

$$H_{\text{int}} = -U \sum_i n_{i\uparrow}n_{i\downarrow} - V \sum_{\langle ij \rangle} n_i n_j. \tag{3.2}$$

The Hartree-Fock decoupling in the pairing channel of the first term in Eq. (3.2) is straightforward, and leads to the replacement $n_{i\uparrow}n_{i\downarrow} \longrightarrow [\langle c_{i\downarrow}c_{i\uparrow}\rangle c^\dagger_{i\uparrow}c^\dagger_{i\downarrow} + \langle c^\dagger_{i\uparrow}c^\dagger_{i\downarrow}\rangle c_{i\downarrow}c_{i\uparrow} - \langle c_{i\downarrow}c_{i\uparrow}\rangle\langle c^\dagger_{i\uparrow}c^\dagger_{i\downarrow}\rangle]$. The second term in Eq. (3.2) can be written as,

$$H^{nn}_{\text{int}} = -V \sum_{i,\gamma=+\hat{\mathbf{x}},+\hat{\mathbf{y}}} (n_{i\uparrow} + n_{i\downarrow})(n_{i+\gamma\uparrow} + n_{i+\gamma\downarrow}). \tag{3.3}$$

In the above, $\gamma$ denotes the unit vectors $+\hat{\mathbf{x}}$ and $+\hat{\mathbf{y}}$ on the square lattice. Expanding further, we obtain four terms corresponding to each $i, i+\gamma$ bond. These are $n_{i\uparrow}n_{i+\gamma\uparrow}$, $n_{i\downarrow}n_{i+\gamma\downarrow}$, $n_{i\uparrow}n_{i+\gamma\downarrow}$ and $n_{i\downarrow}n_{i+\gamma\uparrow}$. As mentioned earlier, we assume that electrons with identical spin orientations are less likely to reside on nn sites, and taking an approximation we drop the $\uparrow\uparrow$ and $\downarrow\downarrow$ interaction terms. Rearranging the order of $c$ operators, we can write the remaining terms as,

$$H^{nn}_{\text{int}} \approx -V \sum_{i,\gamma=+\hat{\mathbf{x}},+\hat{\mathbf{y}}} [c^\dagger_{i\uparrow}c^\dagger_{i+\gamma\downarrow}c_{i+\gamma\downarrow}c_{i\uparrow} + c^\dagger_{i+\gamma\uparrow}c^\dagger_{i\downarrow}c_{i\downarrow}c_{i+\gamma\uparrow}] \tag{3.4}$$

Implementing the mean-field decoupling in the pairing channel for the on-site and

the nn interaction term, we obtain the mean-field Hamiltonian,

$$\begin{aligned} H_{\rm MF} &= -t\sum_{\langle ij\rangle,\sigma}\left[c^{\dagger}_{i\sigma}c_{j\sigma}+H.c.\right]-U\sum_{i}\left[\Delta_i c^{\dagger}_{i\uparrow}c^{\dagger}_{i\downarrow}+H.c.\right] \\ &\quad -V\sum_{i\gamma}\left[\Delta^{+}_{i,\gamma}c^{\dagger}_{i\uparrow}c^{\dagger}_{i+\gamma\downarrow}+\Delta^{-}_{i,\gamma}c^{\dagger}_{i-\gamma\downarrow}c^{\dagger}_{i\uparrow}+H.c.\right] \\ &\quad +U\sum_{i}|\Delta_i|^2+V\sum_{i,\gamma}\left[|\Delta^{+}_{i,\gamma}|^2+|\Delta^{-}_{i,\gamma}|^2\right]. \end{aligned} \tag{3.5}$$

Note that in order to retain the generality of the decoupling we have introduced two different pair expectation values for a given nn pair of sites. These expectation values, $\Delta^{+}_{i,\gamma}=\langle c_{i+\gamma\downarrow}c_{i\uparrow}\rangle$ and $\Delta^{-}_{i+\gamma,\gamma}=\langle c_{i\downarrow}c_{i+\gamma\uparrow}\rangle$ need not be equal, in principle. Indeed, if we assume that the pair satisfies antisymmetry under spin exchange, then $\Delta^{+}_{i,\gamma}=\Delta^{-}_{i+\gamma,\gamma}$, and if the pair satisfies antisymmetry under site-index exchange then $\Delta^{+}_{i,\gamma}=-\Delta^{-}_{i+\gamma,\gamma}$. In most studies a singlet condition on the pairing correlations is imposed and therefore the possibility of odd parity pairing in this model is left out. Here, we do not impose this symmetry constraint on our pairing correlations.

Motivated by the fact that large-scale charge inhomogeneities will not be allowed by long range Coulomb interactions in any real material, we search for uniform density solutions. Therefore, we focus on the SC phases that respect the translational symmetry of the Hamiltonian, and assume the above quantum expectation values to be independent of lattice sites, $\Delta_i\equiv\Delta_0$, $\Delta^{+}_{i,x/y}\equiv\Delta^{+}_{x/y}$ and $\Delta^{-}_{i,x/y}\equiv\Delta^{-}_{x/y}$, leading to five complex-valued mean-field parameters. Given that the model is purely attractive, possibility of magnetic ordering is ruled out [89, 97]. The charge ordering may be present at special filling fractions such as half-filling. Furthermore, while on-site attraction leads to charge ordering at half filling, the inter-site attraction destabilizes such charge modulated order. Therefore, we have not considered the competition between charge- and spin-ordering and superconductivity. The competition between superconductivity and charge ordering has been discussed in the extended model with on-site attraction and inter-site repulsion [89, 97]. Among the different possibilities for SC order, we have considered those OPs that are spatially uniform, therefore, possibilities such as pair density wave or finite momentum pairing have not been considered. Going over to the Fourier space by using, $c_{i\sigma}=N_s^{-1/2}\sum_{\mathbf{k}}e^{-i\mathbf{k}\cdot\mathbf{r}_i}c_{\mathbf{k}\sigma}$ and $c^{\dagger}_{i\sigma}=N_s^{-1/2}\sum_{\mathbf{k}}e^{i\mathbf{k}\cdot\mathbf{r}_i}c^{\dagger}_{\mathbf{k}\sigma}$, $N_s$ being the number of sites, the Hamiltonian can be reduced to a $2\times2$ matrix form. The resulting HF-BCS Hamiltonian in the Nambu spinor notation is,

$$
\begin{aligned}
H_{\mathrm{MF}} &= \sum_{\mathbf{k}} \begin{bmatrix} c^{\dagger}_{\mathbf{k}\uparrow} & c_{-\mathbf{k}\downarrow} \end{bmatrix} \begin{bmatrix} h_{11}(\mathbf{k}) & h_{12}(\mathbf{k}) \\ h_{21}(\mathbf{k}) & h_{22}(\mathbf{k}) \end{bmatrix} \begin{bmatrix} c_{\mathbf{k}\uparrow} \\ c^{\dagger}_{-\mathbf{k}\downarrow} \end{bmatrix} + \\
& N_s \left\{ U|\Delta_0|^2 + V(|\Delta_x^+|^2 + |\Delta_x^-|^2 + |\Delta_y^+|^2 + |\Delta_y^-|^2) \right\}.
\end{aligned} \tag{3.6}
$$

The matrix elements in the above equation are explicitly given by,

$$
\begin{aligned}
h_{11}(\mathbf{k}) &= -2t(\cos k_x + \cos k_y) - \mu = -h_{22}(\mathbf{k}) \\
h_{12}(\mathbf{k}) &= -U\Delta_0 - V(\Delta_x^+ e^{-\mathrm{i}k_x} + \Delta_x^- e^{\mathrm{i}k_x} \\
&\quad + \Delta_y^+ e^{-\mathrm{i}k_y} + \Delta_y^- e^{\mathrm{i}k_y}) = h_{21}^*(\mathbf{k}).
\end{aligned} \tag{3.7}
$$

For a given set $\{\Delta\} \equiv \{\Delta_0, \Delta_x^+, \Delta_x^-, \Delta_y^+, \Delta_y^-\}$, we can diagonalize the electronic part of the Hamiltonian Eq. (3.6) via the Bogoliubov transformations,

$$
\begin{bmatrix} c_{\mathbf{k}\uparrow} \\ c^{\dagger}_{-\mathbf{k}\downarrow} \end{bmatrix} = \begin{bmatrix} u_{\mathbf{k}} & -v^*_{\mathbf{k}} \\ v_{\mathbf{k}} & u^*_{\mathbf{k}} \end{bmatrix} \begin{bmatrix} \gamma_{\mathbf{k}0} \\ \gamma^{\dagger}_{-\mathbf{k}1} \end{bmatrix}, \tag{3.8}
$$

where $u_{\mathbf{k}}$ and $v_{\mathbf{k}}$ are complex numbers satisfying $|u_{\mathbf{k}}|^2 + |v_{\mathbf{k}}|^2 = 1$ for all $\mathbf{k}$, and $\gamma$, $\gamma^{\dagger}$ are the annihilation and creation operators for Bogoliubov quasiparticles. The resulting quasiparticle dispersion is given by,

$$
\begin{aligned}
E_{\mathbf{k}} &= \sqrt{(-2t(\cos k_x + \cos k_y) - \mu)^2 + \Delta_g^2}, \\
\Delta_g^2 &= |-U\Delta_0 - V(\Delta_x^+ e^{-\mathrm{i}k_x} + \Delta_x^- e^{\mathrm{i}k_x} \\
&\quad + \Delta_y^+ e^{-\mathrm{i}k_y} + \Delta_y^- e^{\mathrm{i}k_y})|^2
\end{aligned} \tag{3.9}
$$

Using the above quasiparticle spectrum along with the purely classical terms in the mean-field Hamiltonian Eq. (3.6), we can compute the total energy $E$ of a general SC state specified by set $\{\Delta\}$. This is achieved by constructing HF-BCS states as the vacuum of Bogoliubov quasiparticle for the given set $\{\Delta\}$. Therefore, the problem now reduces to minimizing the total energy of such HF-BCS states w.r.t. the set $\{\Delta\}$ of pairing correlations. We want to emphasize here that in most previous studies a particular form of the SC OP is assumed *a priori* [88]. In contrast, we allow for different combinations of spatially uniform OPs.

### 3.2.3 Minimization scheme

To put our results in proper context, we observe the following relations between the pair expectation values defined in the previous section (section 3.2.2) and the commonly used SC OPs.

$$\begin{aligned}
\Delta_s &= \Delta_0 \\
\Delta_{s^*} &= (\Delta_x^+ + \Delta_x^- + \Delta_y^+ + \Delta_y^-)/4 \\
\Delta_{d_{x^2-y^2}} &= (\Delta_x^+ + \Delta_x^- - \Delta_y^+ - \Delta_y^-)/4 \\
\Delta_{p_x} &= (\Delta_x^+ - \Delta_x^-)/2 \\
\Delta_{p_y} &= (\Delta_y^+ - \Delta_y^-)/2.
\end{aligned} \tag{3.10}$$

The $s$-, $p$- and $d$-wave OPs defined above have their usual meaning. $\Delta_{s^*}$ denotes the OP for the extended $s$-wave order which arises due to inter-site attraction [98]. It is easy to see that the form-factors that enter the $\mathbf{k}$-space matrix acquire their typical pure-singlet or pure-triplet form in the limiting cases. Note that a general set $\{\Delta\}$ may break symmetries of the Hamiltonian Eq. (3.1). Such broken-symmetry states are indeed allowed at the mean-field level, and therefore to retain the generality of the discussion within the mean-field approach we have included such broken symmetry states in our variational set $\{\Delta\}$. In addition to the magnitude of the OPs in the minimum energy state, we also need to determine the relative phase angles between different OPs in the mixed states. Therefore, we carry out variational calculations for energy as a function of relative phase angle between different OPs. We illustrate the details in Fig. 3.1 (a) where we assume the magnitudes of the order parameters $\Delta_s$ and $\Delta_{s^*}$ to be finite, keeping all other OPs equal to zero, and compute the total energy with varying relative phase angle $\Phi$. Variation of $E/N_s$ as a function of $\Phi$ for the state described by OP $\Delta_s + e^{\mathrm{i}\Phi}\Delta_{s^*}$ is shown in Fig. 3.1 (a). This allows us to determine the value of the phase angle corresponding to the minimum energy. This is defined as $\Phi_{min}$ for the pair of OPs selected. The variation in $\Phi_{min}$ with chemical potential is shown in the inset in Fig. 3.1 (b). Similarly, we are able to find $\Phi_{min}$ for other choices of OP pairs.

The results are summarized in Fig. 3.1 (b) where we plot the variation in $\Phi_{min}$ for a different pairs of OPs as a function of chemical potential $\mu$. For $s$-wave and $d_{x^2-y^2}$-wave order, we find that $\Phi = \pm\pi/2$ leads to the minimum energy for any value of chemical potential $\mu$ (see Fig. 3.1 (b)). Similarly, the relative phase angle between $p_x$ and $p_y$ order parameters, when both of them are assumed finite in magnitude, is

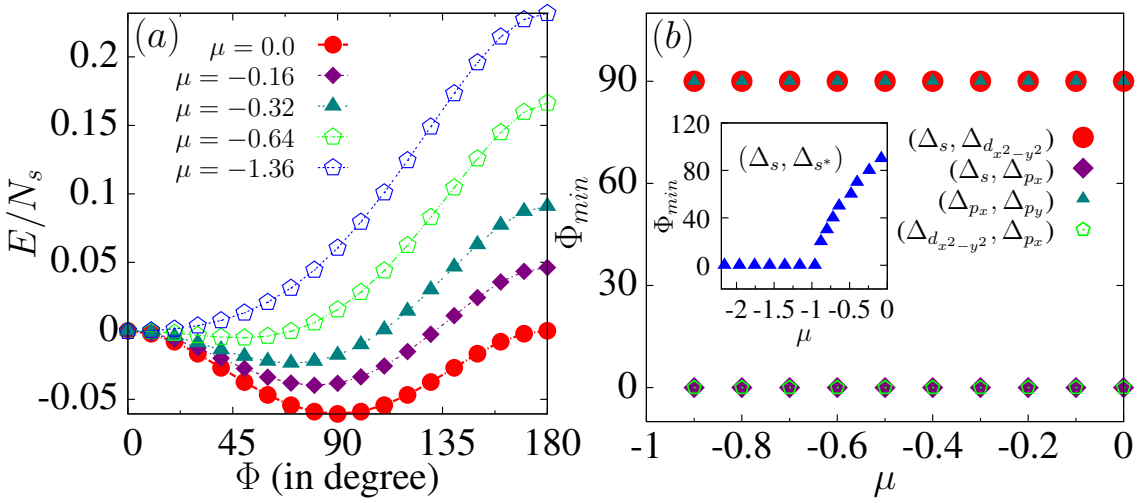


**Figure 3.1:** (Colour online) $(a)$ Variation of energy per site with change in relative phase angle $\Phi$ between OPs $\Delta_s$ and $\Delta_{s^*}$ for different values of $\mu$. Angle corresponding to the minimum energy is defined as $\Phi_{min}$. Panel $(b)$ shows $\Phi_{min}$ for different OP pairs, indicated by legends, as a function of chemical potential. Inset in (b) shows variations in $\Phi_{min}$ with chemical potential for OP pair $\Delta_s$ and $\Delta_{s^*}$.

$\pm\pi/2$. The relative angle $\Phi_{min}$ vanishes for $s$ and $d_{x^2-y^2}$, and $s$ and $p_x$ OP pairs. These results do not depend on the choice of $\mu$ values.

The relative angle between $s$-wave and $s^*$-wave order parameters shows an interesting behavior. $\Phi_{min}$ is found to evolve with change in $\mu$. For $\mu = 0$, corresponding to the half-filled band, $\Phi_{min} = \pi/2$. It decreases monotonically and becomes zero near $\mu = -1$, which corresponds to $n \approx 0.7$ (see inset in Fig. 3.1 (b)). However, we will see that $s$ and $s^*$ OPs are found to be finite only in the low density regime. Therefore, we can safely assume the relative phase between these two OPs to be zero. For most range of parameters, the relative phase angle between different OP pairs is either 0 or $\pi/2$. The above analysis helps us in reducing the number of variational parameters used in the minimization scheme by assigning fixed values to these relative phases. This allows us to perform explicit minimization by discretizing the parameter space of five real valued variables corresponding to the magnitudes of $s$-, $s^*$-, $p_x$-, $p_y$- and $d$-wave OPs.

## 3.3 Results and Discussions

### 3.3.1 Order parameters and phase diagram

We focus our discussion on the variations in $U/t$ and $\mu$ for a fixed value of $V/t = 4$. Direct minimization is carried out by varying different real-valued OPs and relative phase factors among them. The density dependence of SC OPs corresponding to minimum total energy are plotted in Fig. 3.2($a$)-($d$). For small $U$, the high-density regime is dominated by $d_{x^2-y^2}$ and $p_x$ OPs. Both $p_x$ and $p_y$ are finite in the intermediate density range. At further lower densities OPs with $p_x$, $s$ and $s^*$ (also called extended-$s$) symmetries are finite. Eventually, the low-density regime supports $s$ and $s^*$ OPs (see Fig. 3.2($a$)-($b$)). For larger values of on-site attraction, $\Delta_{p_x}$ and $\Delta_{p_y}$ remain zero, and instead $\Delta_{s^*}$ and $\Delta_{d_{x^2-y^2}}$ together with $s$-wave OP become finite (see Fig. 3.2($c$)). Finally, in the limit of large $U$, $s$ and extended-$s$ OPs dominates. We simultaneously track the values of relative phase angles between these OPs in the minimum energy state, allowing us to describe the specific combination of the mixed SC OPs. The step-like behavior in the density dependence of OPs is a consequence of the discretization of the parameter space and should not be misunderstood as a finite-size effect. For $V = 4$ and $U = 2$, the OPs are allowed to vary with an increment of 0.01 (0.02) for $p_x$ and $p_y$ ($s$, $s^*$ and $d_{x^2-y^2}$). We have ensured that the step-size used for a given choice of Hamiltonian parameters does not effect the observed trends. We will further discuss finite-size effects in section III C.

We summarize the results in the form of a $n-U$ phase diagram in Fig. 3.3. Most notably, a chiral $p_x + \mathrm{i}p_y$ order is present in the density range $0.35 < n < 0.55$ in the limit of weaker on-site attraction. Within this interaction regime, $p_x$ order also mixes with $d_{x^2-y^2}$ and extended $s$-wave order for different electronic densities. The possibility of chiral $p$-wave order in the extended repulsive Hubbard model has been pointed out within fluctuation exchange approximation [99,100]. The $d_{x^2-y^2}+p_x$ order is particularly stable over a large density regime. This is intriguing as a number of experiments on cuprates report on the possibility of a secondary unconventional OP in addition to the dominant $d_{x^2-y^2}$ order. The secondary OP is proposed to be either $s$-wave or $p$-wave. Interestingly, phases with $d_{x^2-y^2}+\mathrm{i}[s+s^*]$ and $d_{x^2-y^2}+p_x$ OPs reside next to each other in the density regime $0.6 < n < 1$. Moreover, for smaller values of $V$ we also find a pure $d_{x^2-y^2}$ order in the low-doping regime. This will be discussed later in section III D.. From the angular dependence of the gap function it is easy to see that some of the OPs break the rotational symmetry of the lattice (see Fig. 3.3($b$)-($e$)). Such spontaneously-broken-symmetry states are allowed in our explicit minimization

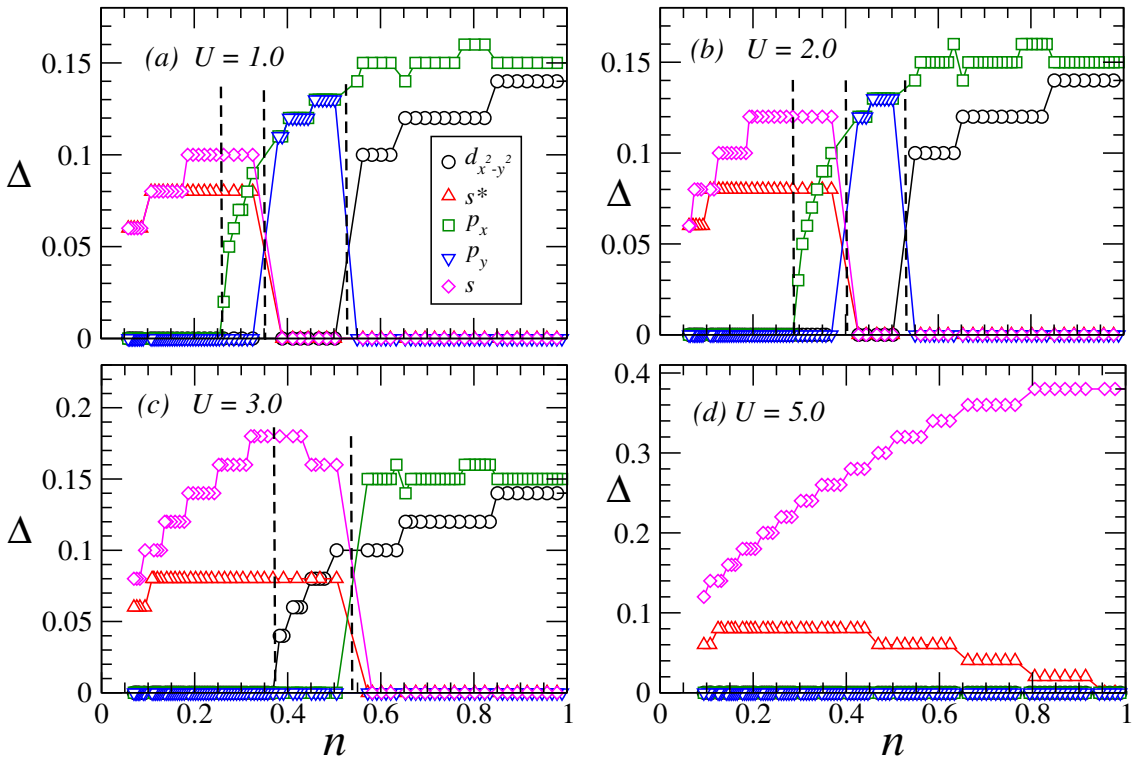


**Figure 3.2:** (Colour online) $(a)$-$(d)$ The values of various OPs corresponding to the minimum energy states as a function of average electronic density $n$. Results for representative values of $U$ are shown. The dashed vertical lines in each plot mark the boundary between qualitatively distinct phases. The results are obtained for $V = 4t$. In the minimization procedure the OP values are discretized in units of 0.01 (0.02) for $p_x$ and $p_y$ ($s$, $s^*$ and $d_{x^2-y^2}$).

approach. Note further that the inversion symmetry is also spontaneously broken by the mean-field solutions that allow for a mixing of singlet and triplet symmetries. The mean-field Hamiltonian (3.6) can also be solved via the standard self-consistent approach [96]. We have checked that various SC states discussed above are also the self-consistent states. At the mean-field level it is easy to motivate the stability of the SC states discussed here, against possible charge- and spin-ordering. Inter-site attraction, $V$, favour equal charge on neighbouring sites. Given that the SC states are all charge homogeneous, they will be preferred over any charge modulated state. Similarly, attractive interactions energetically disfavour magnetic moment formation and therefore magnetic ordering is not expected to be present in the phase diagram. We also note that allowing for same-spin pairing interactions can lead to spin-triplet SC states with $S_z = \pm 1$. Such states, However, require population imbalance between $\uparrow$ and $\downarrow$ electrons and are likely candidates only in the presence of external magnetic field. Furthermore, charge ordering, as compared to superconductivity, is strongly suppressed by quenched disorder which is always present in real materials [101]. It

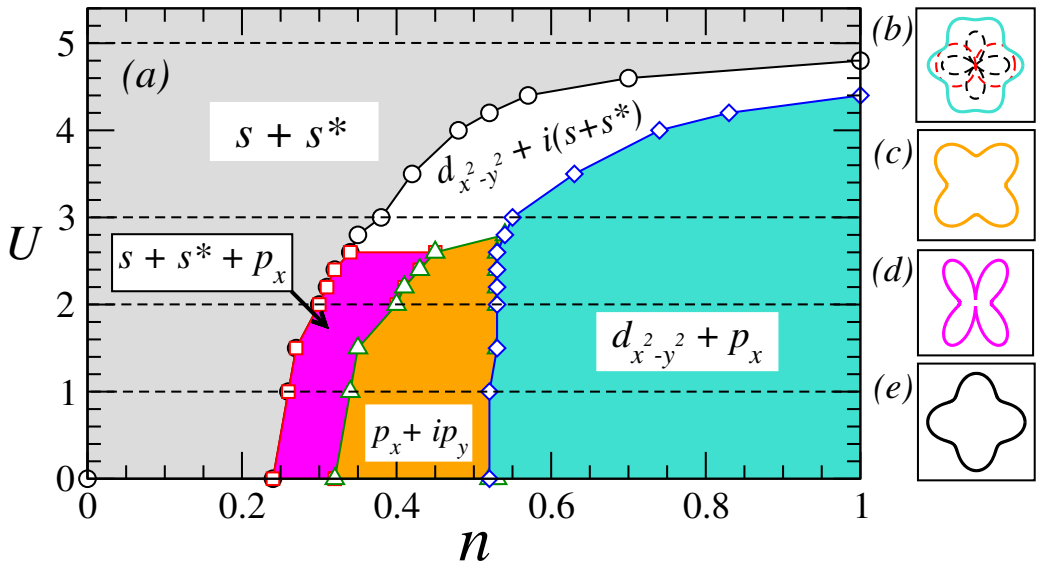


**Figure 3.3:** (Colour online) (*a*) Phase diagram in the $U$-$n$ parameter space for inter-site attraction strength $V = 4t$. The results are obtained via brute-force minimization of total energy using a 16×16 **k**-point grid for different combinations of OPs described in text. The phase diagram is constructed from the data similar to that presented in Fig. 3.2. The dashed horizontal lines are the cuts corresponding to the data shown in Fig. 3.2. The angular dependence of the magnitude of the OP for, (*b*) $d_{x^2-y^2}+p_x$, (*c*) $p_x+\mathrm{i}p_y$, (*d*) $s+s^*+p_x$ and (*e*) $d_{x^2-y^2}+\mathrm{i}[s+s^*]$ symmetries. Dashed lines in (*b*) correspond to pure-$d_{x^2-y^2}$ and pure $p_x$ OP symmetries.

is important to add that while we discuss the presence of $d_{x^2-y^2}$ symmetry of the OP in the present model, we do not claim the EAHM to be a microscopic model for cuprates. Indeed, the presence of strong on-site repulsions in cuprates suggest that $t-J-U$ model is a better candidate for a microscopic model [102–105]. The effect of antiferromagnetic exchange term in a model with inter-site pairing has been discussed by R. Micnas and coworkers [106]. They conclude that the inter-site exchange term favours extended-$s$ or $d$-wave pairing over the $p$-wave. It is also worth noting that the density-density part of the interaction term in the $t-J$ model is of attractive type.

### 3.3.2 Bulk and edge-state spectra

We now investigate further some of the mixed OP SC phases discussed above. We begin with the calculation of tunneling density of states (TDOS) in different phases. Normalized TDOS is defined as,

$$N(\omega) = 1/N_s \sum_{\mathbf{k}} \left[ |u_{\mathbf{k}}|^2 \delta(\omega - E_{\mathbf{k}}) + |v_{\mathbf{k}}|^2 \delta(\omega + E_{\mathbf{k}}) \right], \tag{3.11}$$

where $E_{\mathbf{k}}$ is the energy dispersion for Bogoliubov quasiparticles and $u_{\mathbf{k}}$ measures electron-like amplitude in the quasiparticle state labeled by wave vector $\mathbf{k}$. TDOS can be directly probed by tunneling experiments and therefore characterization of different mixed OP states in terms of TDOS is desirable [107, 108].

Mixing of a $p_x$ component in the $d_{x^2-y^2}$ superconductivity completely modifies the TDOS structure and opens a clean gap much like that present in the simple $s$-wave superconductors (see Fig. 3.4 ($a$)). Indeed, the nodes present in the $d_{x^2-y^2}$ gap function are removed by the presence of $\mathrm{i}\Delta_{p_x} \sin k_x$ term. Multiple coherence peaks in the TDOS are also clearly observed. In fact, it is easy to see why a mixing of $p$-wave component is energetically favoured. The system gains energy by pushing the eigenenergies further away from the chemical potential by opening a clean gap. The chiral $p$-wave order and the mixed $s + s^* + p_x$ orders also support a clean gap in the TDOS (see Fig. 3.4 ($b$)). The $s + s^*$ ordering shows the expected TDOS with the coherence peaks residing right at the gap edge. In the $d_{x^2-y^2} + \mathrm{i}[s + s^*]$ state the features corresponding to $s$-wave and $d$-wave ordering are present at larger value of electronic density (see Fig. 3.4 ($d$)). For the smaller density, the $d$-wave component reduces and the TDOS appears $s$-wave-like. The occurrence of a $d + \mathrm{i}s$ phase in extended Hubbard model has also been reported previously [82]. Recent ARPES data on cuprates is consistent with the presence of a secondary OP that opens a gap at the nodal points of the pure $d$-wave OP [109].

We further investigate the nature of various phases in terms of their edge-state spectra. To this end, we perform calculations on a $20 \times 200$ stripe by imposing periodic boundary conditions only along the $y$ direction and plotting the spectra as a function of $k_y$. Two of the new phases obtained from our calculations turn out to be trivial as no edge states are found to appear inside the SC gap (see Fig. 3.5($c$)-($d$)). The chiral $p$-wave superconductor shows the expected non-trivial behaviour wherein counter-propagating edge states appear in the gap (see Fig. 3.5($b$)) [110]. An intriguing situation occurs for $d_{x^2-y^2} + p_x$ superconductor where pairs of states are present on each edge (see Fig. 3.5($a$)). While the topology of the bulk band will remain trivial in this case as the states traverse back to their respective original band, the presence of such mid-gap states will have observable consequences. Indeed, if such a situation can be realized in a real material, then the surface spectroscopy with voltage bias smaller than the gap value will have contributions from the edge states. This is in contrast to the situation where such states are absent, and only Andreev reflection contributions are observed in tunnelling.

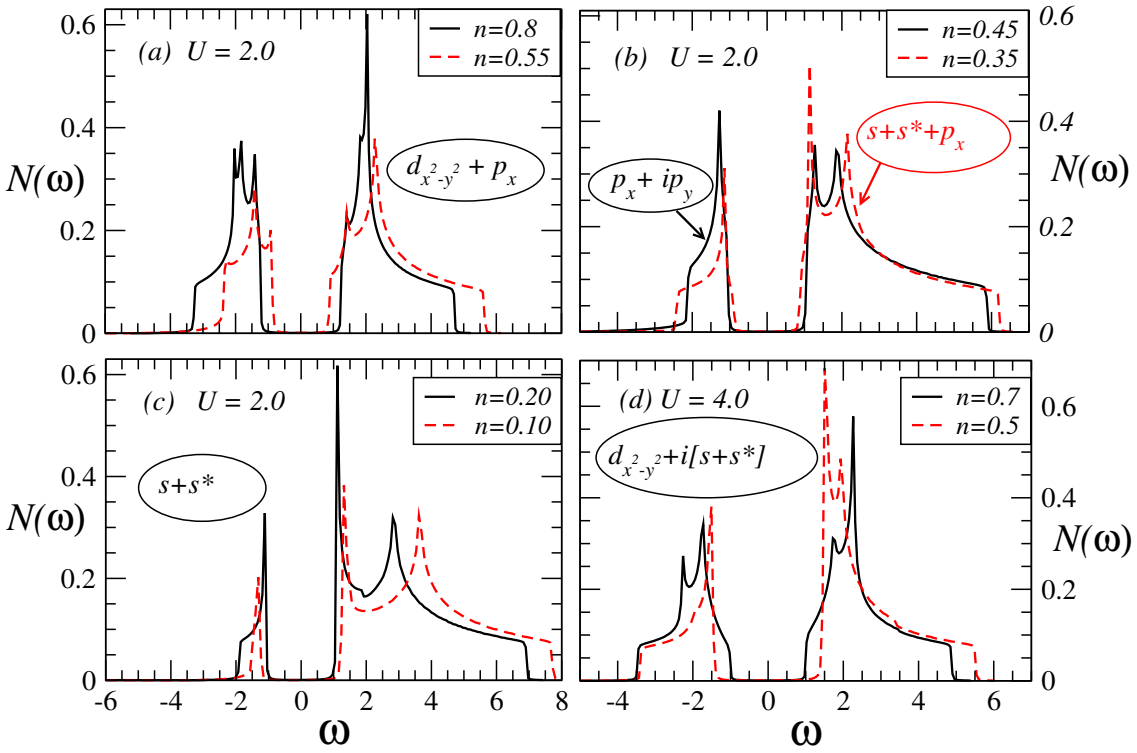


**Figure 3.4:** (Colour online) $(a)$-$(d)$ Density of states for electrons in different phases at different values of average electronic density. These calculations are performed on $600 \times 600$ **k**-point grid. A Lorentzian broadening of $0.01t$ is used.

### 3.3.3 Finite-size effects and $V - n$ phase diagram

Although the detailed discussion for the phase diagram has been presented for $V = 4t$, it is important to discuss the dependence of results on the specific choice of the inter-site interaction strength. Before we present results for smaller values of $V$, it is instructive to discuss the role of lattice sizes used for calculations. In Fig. 3.6 we show the dependence of OPs on number of lattice sites, $N_s$, for different values of $V$. Since explicit minimization on larger lattices is time consuming, we have made use of the self-consistent approach for obtaining data on larger lattices. Starting with some initial values of OP set $\{\Delta\}$, we can calculate different pair correlations using the set of equations,

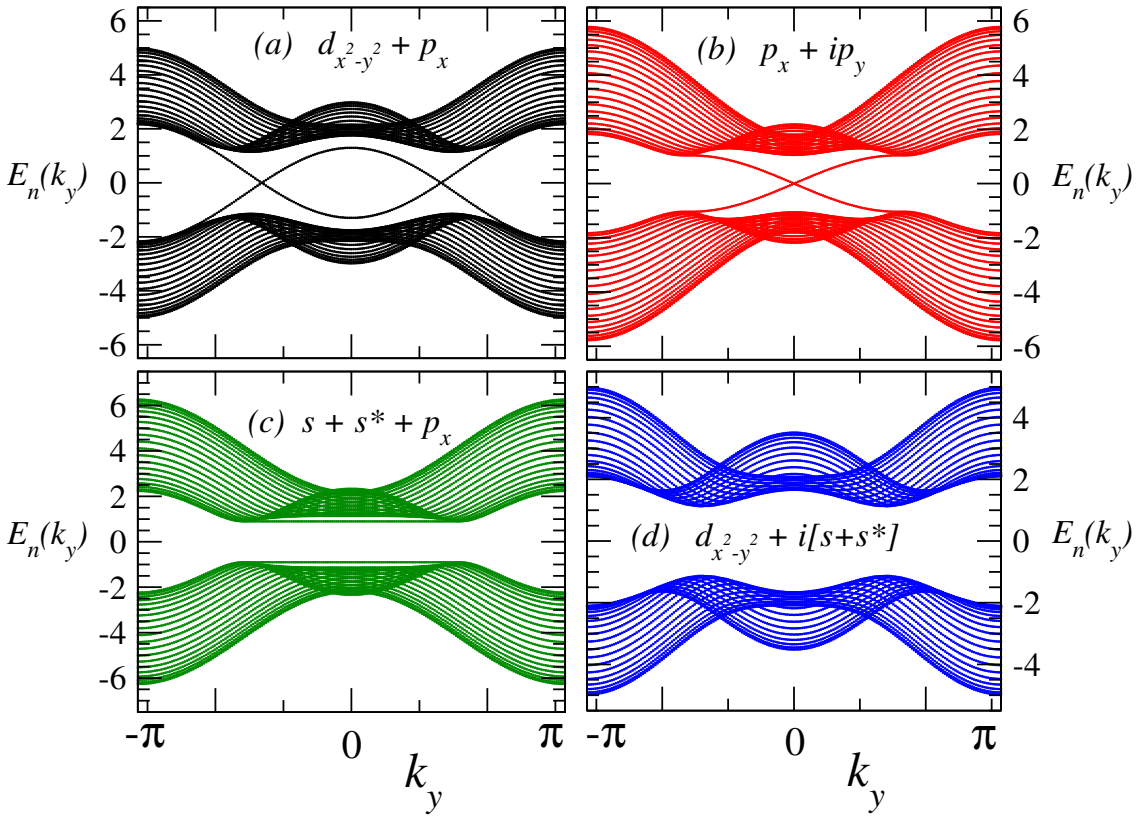


**Figure 3.5:** (Colour online) $(a)$-$(d)$ Bogoliubov quasiparticle dispersions for different SC states obtained by using open (periodic) boundary condition along $x$ $(y)$ direction. Edge states disperse across the SC gap for, $(a)$ $p_x + \mathrm{i}p_y$ and for $(b)$ $d_{x^2-y^2} + p_x$ OP symmetries.

$$
\begin{aligned}
\Delta_0 &= 1/N_s \sum_{\mathbf{k}} u_k v_k^* (2f(E_{\mathbf{k}}) - 1) \\
\Delta_x^+ &= 1/N_s \sum_{\mathbf{k}} e^{\mathrm{i}k_x}\ u_k v_k^* (2f(E_{\mathbf{k}}) - 1) \\
\Delta_x^- &= 1/N_s \sum_{\mathbf{k}} e^{-\mathrm{i}k_x}\ u_k v_k^* (2f(E_{\mathbf{k}}) - 1) \\
\Delta_y^+ &= 1/N_s \sum_{\mathbf{k}} e^{\mathrm{i}k_y}\ u_k v_k^* (2f(E_{\mathbf{k}}) - 1) \\
\Delta_y^- &= 1/N_s \sum_{\mathbf{k}} e^{-\mathrm{i}k_y}\ u_k v_k^* (2f(E_{\mathbf{k}}) - 1).
\end{aligned}
\tag{3.12}
$$

In the above, $E_{\mathbf{k}}$ are the eigenvalues, $f(E_{\mathbf{k}})$ denotes the Fermi function and $u_{\mathbf{k}}$, $v_{\mathbf{k}}$ are the coefficients that appear in the Bogoliubov transformation Eq. (3.8). We then repeat this procedure of diagonalizing the Hamiltonian for a given set $\{\Delta\}$ and recalculating the set $\{\Delta\}$ using Eq. (3.12) until the parameters converge within

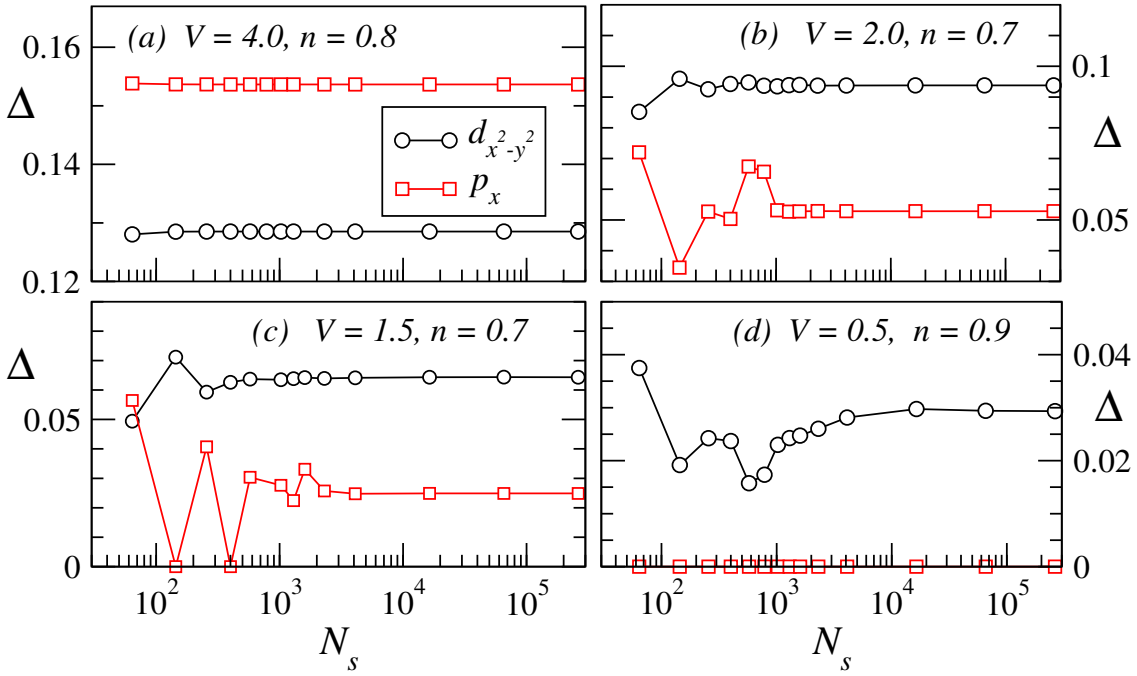


**Figure 3.6:** (Colour online) Variation of $\Delta_{d_{x^2-y^2}}$ and $\Delta_{p_x}$ with number of lattice sites $N_s$ for $(a)$ $V = 4.0$, $(b)$ $V = 2.0$, $(c)$ $V = 1.5$ and $(d)$ $V = 0.5$. All the results are for $U = 0$. Note the logarithmic scale on x-axis. The electronic density values are specified in the plots.

an accuracy limit of $10^{-6}$. We have preferred explicit minimization over the above self-consistent approach for the reason that in a multivariable parameter space self-consistent solutions may lead to metastable states. However, the availability of results from explicit minimization guides our choice of initial set $\{\Delta\}$ and hence the self-consistency approach can then be used to obtain results on much larger lattices.

For $V = 4$ the results obtained on $N_s = 16^2$ are representative of thermodynamic-limit behaviour (see Fig. 3.6 $(a)$). For smaller values of $V$, one needs to perform calculations on progressively larger lattices in order to obtain reliable results. For example, for $V = 0.5$ one needs to use $N_s \approx 100^2$ (see Fig. 3.6 $(d)$). This restricts the use of our explicit minimization procedure to $V \geq 1.5$. To illustrate further the point about finite size effects, we obtain results for $V = 1.5$ using $N_s = 32^2$. As one can anticipate by looking at Fig. 3.6 $(c)$, $N_s = 32^2$ should lead to results representative of the thermodynamic limit. Nevertheless, fluctuations are expected to be present. We indeed find that while the overall trends for the OPs are well behaved, considerable fluctuations in the $n$-dependence are present (see Fig. 3.7). Comparing the results with those presented in Fig. 3.2 $(a)$, we find that the trends in terms of OP symmetries are similar. For small density, $s$- and extended $s$-wave OPs are finite while all other OPs remain zero. Near $n = 0.3$, $p_x + ip_y$ order emerges

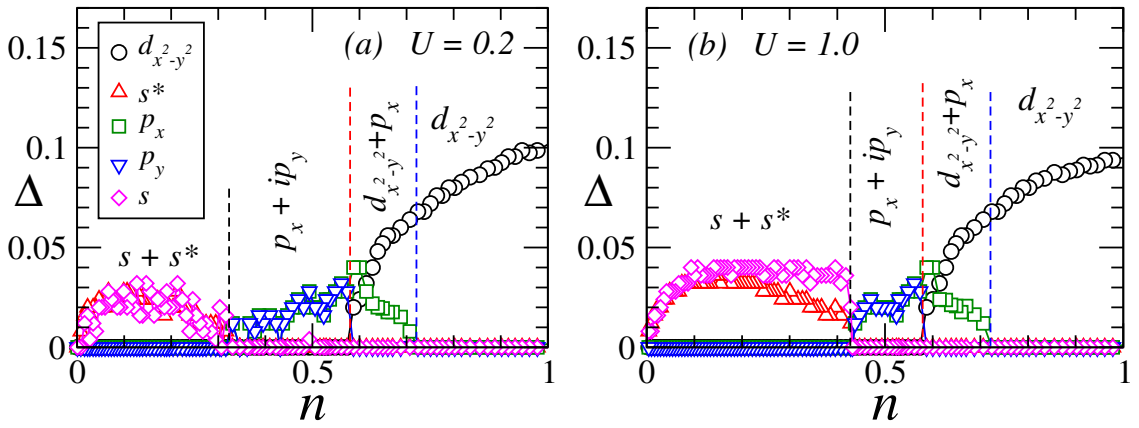


**Figure 3.7:** (Colour online) Order parameters as a function of density for $V = 1.5t$. Note that a pure $d_{x^2-y^2}$ symmetry of the order parameter is present close to half-filling for both $U = 0.2t$ and $U = t$. The results are obtained via explicit minimization on $32 \times 32$ **k**-point grid.

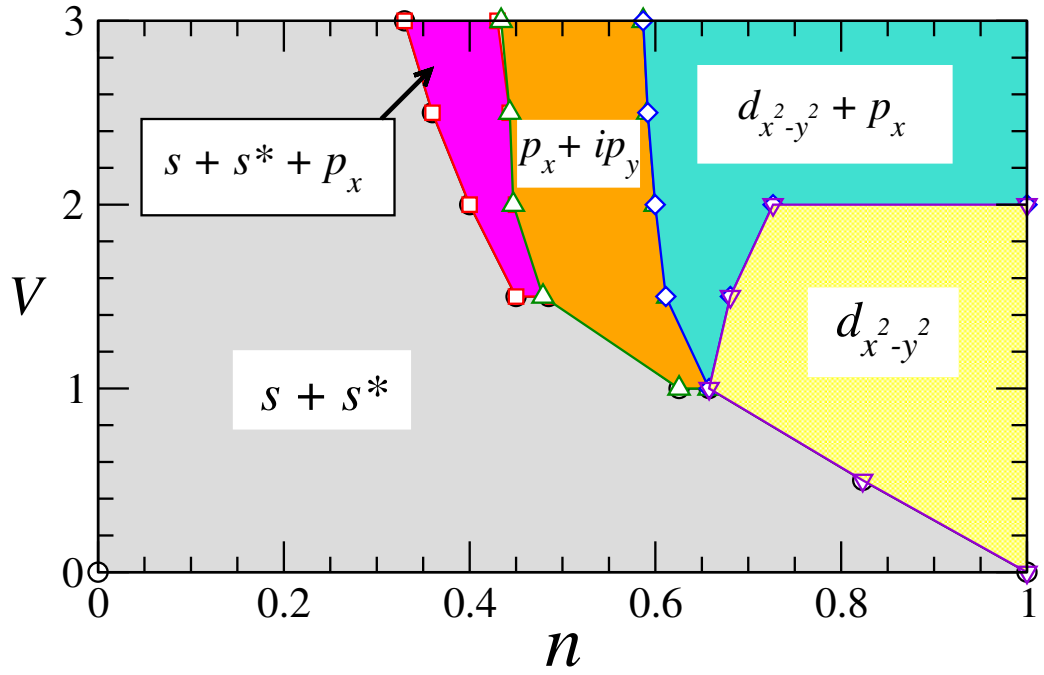


**Figure 3.8:** (Colour online) Phase diagram in the $V$-$n$ parameter space for on-site attraction strength $U = t$. The results are obtained via minimization using a $32 \times 32$ ($512 \times 512$) **k**-point grid for $V \geq 1.5$ ($V < 1.5$).

while $s + s^*$ disappears. This is followed by the appearance of $d_{x^2-y^2} + p_x$ order near $n = 0.55$ and finally pure $d$-wave order is present for $n \geq 0.7$. The trends for $U = 1.0$ (3.7 ($b$)) are similar to those just described. The key difference w.r.t. the results for $V = 4$ are the following: (i) The $s + s^* + p_x$ state is absent, and (ii) a pure $d_{x^2-y^2}$ state is present for $V = 1.5$.

For a comprehensive picture of the type of SC OPs present in the $U - V - n$ pa-

rameter space, we show $V - n$ phase diagram for $U = 1$. Most of the interesting superconducting states appearing in the EAHM are covered within the $U - n$ (Fig. 3.3) and $V - n$ (Fig. 3.8) phase diagrams. Given that we need to perform calculations on larger lattices for smaller $V$, we had to further restrict our OP choices for completing the $V - n$ phase diagram. For $V \geq 1.5$ we have used $N_s = 32^2$, and the minimization over the entire parameter space is performed. For smaller values of $V$ ($V \leq 1.5$), we specifically compute energy for the following phases: (i) $s + s^*$, (ii) $s + s^* + p_x$, (iii) $p_x + \mathrm{i}p_y$ and (iv) $d_{x^2-y^2} + p_x$. This variational set covers most of the non-trivial OPs found in the large $V$ regime. Additionally, all the OPs defined in Eq. (3.10) are allowed to exist in pure form without mixing with each other. Limiting the variational set of OPs allows us to perform calculations using $N_s = 512^2$, and therefore the results can be trusted for smaller values of $V$. A particularly interesting question is how a weak inter-site attraction effects the phase diagram of the on-site attractive model. In the purely on-site attractive model ($U \neq 0$, $V = 0$), $s$-wave SC order is present at all fillings except at $n = 1$ where a charge ordered state is degenerate with the $s$-wave SC state. Switching on inter-site attractive term $V$, we find that the extended $s$-wave order is induced leading to the $s + s^*$ SC phase. unconventional SC states begin to appear in the regime where the inter-site scale $V$ dominates over the on-site term $U$. In this regime, we recover SC states with $s + s^* + p_x$, $p_x + \mathrm{i}p_y$, $d_{x^2-y^2}$ and $d_{x^2-y^2} + p_x$ symmetries. Note that unlike the repulsive model where $U$ is the dominant energy scale over $V$, the hierarchy of these scales may be reversed in the attractive model. This is easy to see by recalling that the effective attractive couplings in the EAHM emerge as the sum of two contributions, the bare Coulombic repulsion and, say, the phonon-mediated attraction. If the spatial dependence of the phonon-mediated attraction happens to be weaker than $1/r$, then $|V| > |U|$ with both $U$ and $V$ being negative is a likely scenario. In fact, repulsive $U$-attractive $V$ model can be seen as an extreme case of reversed hierarchy of the EAHM where the phonon-mediated attraction can overcome the inter-site repulsion while it cannot overcome the on-site repulsion.

### 3.3.4 Finite temperature behaviour

It is interesting to also study the finite-temperature evolution of the ground-state phase diagram. The simplest scenario for the finite temperature behaviour in a mean-field scheme is that each of the superconducting phases have an associated $T_c$ and a normal state is obtained for $T > T_c$. However, within our approach we can perform the explicit minimization at finite $T$ and investigate into more general possibilities.

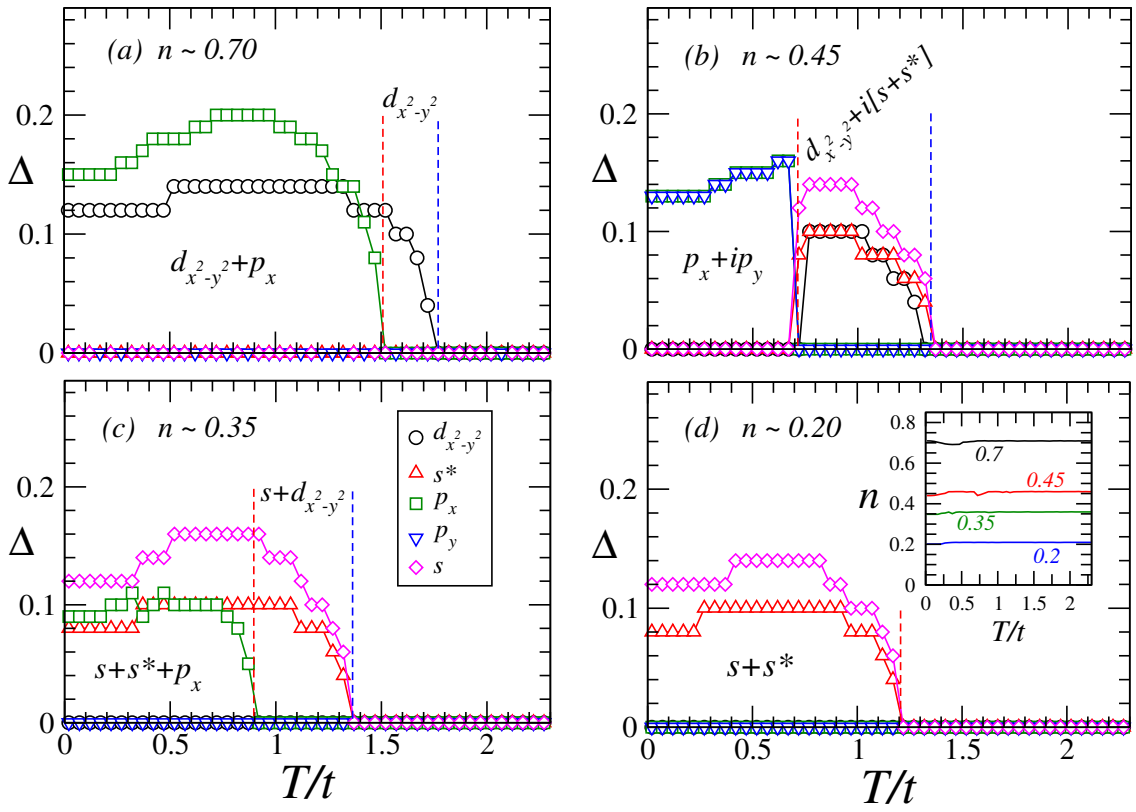


**Figure 3.9:** (Colour online) Superconducting order parameters as a function of temperature for $U = 2$ and $V = 4$ for some representative values of density.

Indeed, we uncover an interesting possibility of multiple phase transitions. We find that one superconducting order can disappear and another one can appear upon raising temperature before a normal non-superconducting state is finally obtained at high temperature. To demonstrate this, we plot the $T$-dependence of the SC OPs for a few representative average electronic densities for $V = 4t$ and $U = 2t$ (see Fig. 3.9).

We find that the $d_{x^2-y^2} + p_x$ state at $n \approx 0.7$ gives way to a pure $d_{x^2-y^2}$ state, and finally to a non-superconducting state upon increasing temperature (Fig. 3.9 $(a)$). Similarly, $p_x + ip_y$ state at $n \approx 0.45$ melts into a $d_{x^2-y^2} + s^* + p_x$ state at intermediate temperatures, before leading to a non-superconducting state (Fig. 3.9 $(b)$). Generally the $p$-wave order seems to disappear at lower temperatures leading to a different intermediate temperature state. The conventional scenario is found for $n \approx 0.2$ where $s + d_{x^2-y^2}$-wave ordering disappears at $T/t = 1.2$ and a non-superconducting state is directly obtained. Of course, the $T_C$ scales obtained within mean-field theory are not reliable. However, the feature that one superconducting order disappears and gives way to another is likely to be robust and can be tested in future studies involving more sophisticated methods such as the auxiliary field quantum Monte Carlo. Note that in

our calculations the chemical potential is adjusted to obtain a specific target density and the full minimization is performed at every trial value of chemical potential. There are still variations in density of the order of $\sim 0.01$ (see inset in panel $(d)$) which cause some fluctuations in the $T$-dependence of order parameters. The overall trends, however, are robust.

## 3.4 Conclusion

In conclusion, we have shown that the EAHM treated without imposing symmetry constraints presents an exciting possibility for hosting a variety of SC states with mixed OP symmetries. Our approach allowed for competition between SC orders of $s$- $p$- and $d$-wave type. The resulting phase diagram hosts some very interesting SC phases. Most notable of these are, (i) the chiral $p$-wave state, (ii) states with mixed $d$-wave and $p$-wave, and with $s$-wave, extended $s$-wave and $p_x$ symmetries, and (iii) a $d_{x^2-y^2} + \mathrm{i}[s + s^*]$ SC phase. To the best of our knowledge, the possibility of such mixed order-parameter phases has not been explored in the EAHM [111]. We should add that the SC phases obtained in this work are the broken-symmetry solutions of the mean-field Hamiltonian. Further work is required to test the stability of such exotic states in treatments of the model that go beyond mean-field. The comprehensive mean-field phase diagrams presented here should serve as a reference for such future studies. Some experiments on cuprates report the possibility of a mixed $s$ and $d$ wave order [51], while a possible mixing of a $p$-wave component with the $d$-wave order has been inferred via thermal transport measurements [112]. Experiments on $Sr_2RuO_4$ indicate a chiral $p_x + \mathrm{i}p_y$-wave order. Similarly, $p$-wave SC OP is consistent with experiments on Bechgaard salts $TMTSF_2PF_6$ and $TMTSF_2ClO_4$ [60–64, 113]. Although a microscopic theory of superconductivity in some of these systems is still awaited, our results suggest that EAHM can serve as the effective model for a number of such unconventional superconductors. It is particularly interesting to see the possibility of topologically non-trivial SC states being realized in the EAHM. One of the promising avenues for experimental realization of such states is in the ultracold Fermionic atoms trapped in optical lattices [114, 115]. Given the presence of various non-trivial SC phases, a number of interesting questions can be further asked for the EAHM. Indeed, the effect of non-magnetic and magnetic impurities, influence of Zeeman and Peierls's terms arising from an external magnetic field, effects of next-nearest hopping, etc. are some of the problems that can be readily addressed using the present model. The model can be made material specific by estimating the values of effective on-site and nn electron-electron attractions. Such model studies

can help in a microscopic characterization of various mixed-symmetry states and can be useful in improving our understanding of the rich experimental data available on unconventional superconductors.

# Chapter 4

# Effect of Zeeman coupling on superconducting phases with equal and opposite spin pairing

In the previous chapter we have shown the existence of unusual superconducting states in the extended attractive Hubbard model (EAHM). However, for simplicity we ignored equal spin pairing terms in our analysis. The present chapter is devoted to the study of the EAHM including the equal spin pairing terms. The physical motivation is to understand the influence of Zeeman coupling to an external magnetic field on the nature of superconducting order parameters.

## 4.1 Introduction

Superconducting wavefunctions with spin-singlet and spin-triplet pairing symmetry are well-known [15,33,43,116–118]. It is interesting to note that pairing between $\uparrow$ spin and $\downarrow$ spin electrons can lead to a more general scenario where mixed-parity states can also become stable. The functional form of the superconducting term $\Delta^{\uparrow\downarrow}(\mathbf{k})$ is such that, depending on the values of self-consistent pairing correlations ($\Delta_\delta^{+(-)}$) it can take either the form of a singlet pair, $\frac{1}{\sqrt{2}}(|\uparrow\downarrow\rangle - |\downarrow\uparrow\rangle)$, or that of a $|S_z = 0\rangle$ triplet pair, $\frac{1}{\sqrt{2}}(|\uparrow\downarrow\rangle + |\downarrow\uparrow\rangle)$ or even a mixed-parity state. On the other hand, superconducting terms $\Delta^{\uparrow\uparrow}(\mathbf{k})$ and $\Delta^{\downarrow\downarrow}(\mathbf{k})$ represent equal spin-pairing states (ESP) $|S_z = 1\rangle \equiv |\uparrow\uparrow\rangle$ and $|S_z = -1\rangle \equiv |\downarrow\downarrow\rangle$ respectively. The purpose of the present chapter is two-fold. Firstly, we validate the assumption of ignoring $\uparrow\uparrow$ and $\downarrow\downarrow$ pairing in the absence of a magnetic field. Secondly, we study the effect of an external magnetic field in the

form of Zeeman coupling on the stability of triplet superconducting phases.

## 4.2 Model and Method

The extended attractive Hubbard model (EAHM) was already described in chapter 2. We had studied a simplified version of EAHM in chapter 3. In the present chapter we take up the task of studying the full EAHM with Zeeman coupling to an external magnetic field. The model is described by the Hamiltonian:

$$\begin{aligned}\mathcal{H}_{MF} = &\sum_{\mathbf{k}} \left[\epsilon^{\uparrow}(\mathbf{k}) c^{\dagger}_{\mathbf{k}\uparrow} c_{\mathbf{k}\uparrow} + \epsilon^{\downarrow}(\mathbf{k}) c^{\dagger}_{\mathbf{k}\downarrow} c_{\mathbf{k}\downarrow}\right] \\ &+ \sum_{\mathbf{k}} \left[\Delta^{\uparrow\downarrow}(\mathbf{k}) c^{\dagger}_{\mathbf{k}\uparrow} c^{\dagger}_{-\mathbf{k}\downarrow} + H.c.\right] \\ &+ \sum_{\mathbf{k}} \left[\Delta^{\uparrow\uparrow}(\mathbf{k}) c^{\dagger}_{\mathbf{k}\uparrow} c^{\dagger}_{-\mathbf{k}\uparrow} + H.c.\right] \\ &+ \sum_{\mathbf{k}} \left[\Delta^{\downarrow\downarrow}(\mathbf{k}) c^{\dagger}_{\mathbf{k}\downarrow} c^{\dagger}_{-\mathbf{k}\downarrow} + H.c.\right] \\ &+ N_s U |\Delta|^2 \\ &+ N_s V \sum_{\delta} \left[|\Delta^{+}_{\delta}|^2 + |\Delta^{-}_{\delta}|^2 + |\Delta^{\uparrow}_{\delta}|^2 + |\Delta^{\downarrow}_{\delta}|^2\right] \end{aligned} \tag{4.1}$$

Where,

$$\begin{aligned}\epsilon^{\uparrow}(\mathbf{k}) &= -2t(\cos(k_x) + \cos(k_y)) - \mu - B_z \\ \epsilon^{\downarrow}(\mathbf{k}) &= -2t(\cos(k_x) + \cos(k_y)) - \mu + B_z \\ \Delta^{\uparrow\downarrow}(\mathbf{k}) &= -U\Delta - V \sum_{\delta} \left[\Delta^{+}_{\delta} e^{-i(\mathbf{k}\cdot\boldsymbol{\delta})} + \Delta^{-}_{\delta} e^{i(\mathbf{k}\cdot\boldsymbol{\delta})}\right] \\ \Delta^{\uparrow\uparrow}(\mathbf{k}) &= -V \sum_{\delta} \Delta^{\uparrow}_{\delta} e^{-i(\mathbf{k}\cdot\boldsymbol{\delta})} \\ \Delta^{\downarrow\downarrow}(\mathbf{k}) &= -V \sum_{\delta} \Delta^{\downarrow}_{\delta} e^{-i(\mathbf{k}\cdot\boldsymbol{\delta})} \end{aligned} \tag{4.2}$$

In the above, we continue to follow the standard notation introduced in the previous chapters. Following the standard mean-field decoupling scheme in the pairing channel discussed in the chapter 2, and imposing the spatial uniformity on the superconducting solutions, the mean field Hamiltonian $\mathcal{H}_{MF}$ (4.1) can be written in terms of Nambu spinors $\mathbf{\Psi_k}$ as:

$$\mathcal{H}_{MF} = \sum_{\mathbf{k}} \mathbf{\Psi}^{\dagger}_{\mathbf{k}} \mathcal{H}_{BdG}(\mathbf{k}) \mathbf{\Psi}_{\mathbf{k}} \tag{4.3}$$

Where, Nambu spinor $\mathbf{\Psi}_{\mathbf{k}}$ is a column vector of the form, $\mathbf{\Psi}_{\mathbf{k}} = (c_{\mathbf{k}\uparrow} \quad c^{\dagger}_{-\mathbf{k}\downarrow} \quad c_{\mathbf{k}\downarrow} \quad c^{\dagger}_{-\mathbf{k}\uparrow})$ and $\mathcal{H}_{BdG}(\mathbf{k})$ is a $4 \times 4$ Hamiltonian matrix of the form:

$$\mathcal{H}_{BdG}(\mathbf{k}) = \begin{pmatrix} \epsilon^{\uparrow}(\mathbf{k}) & \Delta^{\uparrow\downarrow}(\mathbf{k}) & 0 & \Delta_s^{\uparrow\uparrow}(\mathbf{k}) \\ (\Delta^{\uparrow\downarrow}(\mathbf{k}))^* & -\epsilon^{\downarrow}(-\mathbf{k}) & (\Delta_s^{\downarrow\downarrow}(\mathbf{k}))^* & 0 \\ 0 & \Delta_s^{\downarrow\downarrow}(\mathbf{k}) & \epsilon^{\downarrow}(\mathbf{k}) & -(\Delta^{\uparrow\downarrow}(-\mathbf{k})) \\ (\Delta_s^{\uparrow\uparrow}(\mathbf{k}))^* & 0 & -(\Delta^{\uparrow\downarrow}(-\mathbf{k}))^* & -\epsilon^{\uparrow}(-\mathbf{k}) \end{pmatrix} \tag{4.4}$$

$\mathcal{H}_{BdG}(\mathbf{k})$ is known as the mean field Bogoliubov-de Gennes Hamiltonian. We can diagonalize the BdG Hamiltonian via the canonical transformations:

$$\begin{aligned} c_{\mathbf{k}\uparrow} &= \sum_{\mathbf{k},\alpha} u^{\alpha}_{\mathbf{k}\uparrow} \gamma_{\mathbf{k}\alpha} + (v^{\alpha}_{\mathbf{k}\uparrow})^* \gamma^{\dagger}_{-\mathbf{k}\alpha} \\ c_{\mathbf{k}\downarrow} &= \sum_{\mathbf{k},\alpha} u^{\alpha}_{\mathbf{k}\downarrow} \gamma_{\mathbf{k}\alpha} + (v^{\alpha}_{\mathbf{k}\downarrow})^* \gamma^{\dagger}_{-\mathbf{k}\alpha} \end{aligned} \tag{4.5}$$

such that the BdG Hamiltonian acquires a diagonal form,

$$\mathcal{H}_{MF} = E_g + \sum_{\mathbf{k}\alpha} E_{\mathbf{k}\alpha} \gamma^{\dagger}_{\mathbf{k}\alpha} \gamma_{\mathbf{k}\alpha} \tag{4.6}$$

where $\{E_{\mathbf{k}\alpha}\}$ is the set of positive eigenvalues and $\gamma^{\dagger}_{\mathbf{k}\alpha}(\gamma_{\mathbf{k}\alpha})$ creates(annihilates) a Bogoliubov-quasiparticle with momentum $\mathbf{k}$ and pseudospin $\alpha$. The BdG quasiparticles describe elementary excitations of BCS condensate, $E_g$ being the ground state energy of the condensate.

## d-vector formalism

In equation (4.3), if we rearrange the structure of the Nambu spinors in the form: $\mathbf{\Psi_k} = (c_{\mathbf{k}\uparrow} \quad c_{\mathbf{k}\downarrow} \quad c^{\dagger}_{-\mathbf{k}\uparrow} \quad c^{\dagger}_{-\mathbf{k}\downarrow})$, the resulting BdG matrix becomes,

$$\mathcal{H}_{BdG}(\mathbf{k}) = \begin{pmatrix} \epsilon^{\uparrow}(\mathbf{k}) & 0 & \Delta_s^{\uparrow\uparrow}(\mathbf{k}) & \Delta^{\uparrow\downarrow}(\mathbf{k}) \\ 0 & \epsilon^{\downarrow}(\mathbf{k}) & \Delta^{\downarrow\uparrow}(\mathbf{k}) & \Delta_s^{\downarrow\downarrow}(\mathbf{k}) \\ (\Delta_s^{\uparrow\uparrow}(\mathbf{k}))^* & (\Delta^{\downarrow\uparrow}(\mathbf{k}))^* & -\epsilon^{\uparrow}(-\mathbf{k}) & 0 \\ (\Delta^{\uparrow\downarrow}(\mathbf{k}))^* & (\Delta_s^{\downarrow\downarrow}(\mathbf{k}))^* & 0 & -\epsilon^{\downarrow}(-\mathbf{k}) \end{pmatrix} \tag{4.7}$$

Where, we used the identity: $\Delta^{\downarrow\uparrow}(\mathbf{k}) = -\Delta^{\uparrow\downarrow}(-\mathbf{k})$. Now the $2 \times 2$ matrix of top right corner of the above $4 \times 4$ matrix describes the mean field gap function:

$$\hat{\Delta}_{\mathbf{k}} = \begin{bmatrix} \Delta_s^{\uparrow\uparrow}(\mathbf{k}) & \Delta^{\uparrow\downarrow}(\mathbf{k}) \\ \Delta^{\downarrow\uparrow}(\mathbf{k}) & \Delta_s^{\downarrow\downarrow}(\mathbf{k}) \end{bmatrix}. \tag{4.8}$$

The spin dependence of the pairing motivates the use of a general $2 \times 2$ matrix formalism for $\hat{\Delta}_{\mathbf{k}}$. The matrix elements correspond to the spin state of the electrons that constitute the Cooper pair. In this formalism, a singlet superconductor is described by setting $\Delta^{\uparrow\uparrow}(\mathbf{k}) = \Delta^{\downarrow\downarrow}(\mathbf{k}) = 0$ and $\Delta^{\uparrow\downarrow}(\mathbf{k}) = -\Delta^{\downarrow\uparrow}(\mathbf{k}) = \Delta_s$, while for the triplet case, $\Delta^{\uparrow\downarrow}(\mathbf{k}) = \Delta^{\downarrow\uparrow}(\mathbf{k}) = \Delta_0$. For singlet state $\hat{\Delta}_{\mathbf{k}}$ can be written as : $\hat{\Delta}_{\mathbf{k}} = d_0(\mathbf{k})\hat{\chi}_0$, where the quantity

$$\hat{\chi}_0 = i\hat{\sigma}_2 = \begin{pmatrix} 0 & 1 \\ -1 & 0 \end{pmatrix} \tag{4.9}$$

corresponds to the singlet wave function $\frac{1}{\sqrt{2}}[|\uparrow\rangle|\downarrow\rangle - |\downarrow\rangle|\uparrow\rangle]$. The factor $\hat{\chi}_0$ is antisymmetric upon interchanging spin variables of the order parameter while $d_0(\mathbf{k})$ is symmetric upon interchanging orbital variables of the order parameter, that is, $d_0(-\mathbf{k}) = d_0(\mathbf{k})$.

For the triplet pairing state, the total spin is $S = 1$ for the two paired electrons and accordingly there are three spin wavefunctions. Therefore, the pairing amplitude for each of these spin states can be different. The order parameter can then be written

in the form: $\hat{\Delta}_{\mathbf{k}} = \mathbf{d}(\mathbf{k}) \cdot \hat{\boldsymbol{\chi}}$. where the complex vector $\mathbf{d}$ measures the amplitude of the order parameter and the matrices

$$\hat{\chi}_1 = i\hat{\sigma}_1\hat{\sigma}_2 = \begin{pmatrix} -1 & 0 \\ 0 & 1 \end{pmatrix},$$
$$\hat{\chi}_2 = i\hat{\sigma}_2\hat{\sigma}_2 = \begin{pmatrix} i & 0 \\ 0 & i \end{pmatrix}, \text{and}$$
$$\hat{\chi}_3 = i\hat{\sigma}_3\hat{\sigma}_2 = \begin{pmatrix} 0 & 1 \\ 1 & 0 \end{pmatrix} \tag{4.10}$$

correspond to the following spin wavefunctions:

$$\hat{\chi}_1 \longrightarrow \frac{-1}{\sqrt{2}}[|\uparrow\rangle|\uparrow\rangle - |\downarrow\rangle|\downarrow\rangle]$$
$$\hat{\chi}_2 \longrightarrow \frac{-1}{\sqrt{2}}[|\uparrow\rangle|\uparrow\rangle + |\downarrow\rangle|\downarrow\rangle]$$
$$\hat{\chi}_3 \longrightarrow \frac{-1}{\sqrt{2}}[|\uparrow\rangle|\downarrow\rangle + |\downarrow\rangle|\uparrow\rangle] \tag{4.11}$$

Now all three of these wavefunctions are symmetric upon interchanging the spin indices. So we must have $\mathbf{d}(-\mathbf{k}) = -\mathbf{d}(\mathbf{k})$.

## 4.3 Determination of Relative Phase Angle between different Pairing Correlations

Before we discuss the competition among different superconducting states, we note the possibility of obtaining different triplet states from different combinations of pairing mean field parameters.

**Triplet combinations from $\Delta^{\uparrow\downarrow}(\mathbf{k})$:**

1. $p_x$ state: $\Delta_x^+ = -\Delta_x^- = C; \Delta_y^+ = \Delta_y^- = 0$ ($C$ is some complex number)

2. $p_x \pm ip_y$ state : $\Delta_x^+ = -\Delta_x^- = C; \Delta_y^+ = -\Delta_y^- = iC$

In general, $p_x$ and $p_y$ can be of the form: $p_x + e^{i\theta}p_y$. With the help of energetics and self-consistency we have checked that $\theta = \frac{\pi}{2}(-\frac{\pi}{2})$, i.e. it takes the form $p_x \pm ip_y$. So

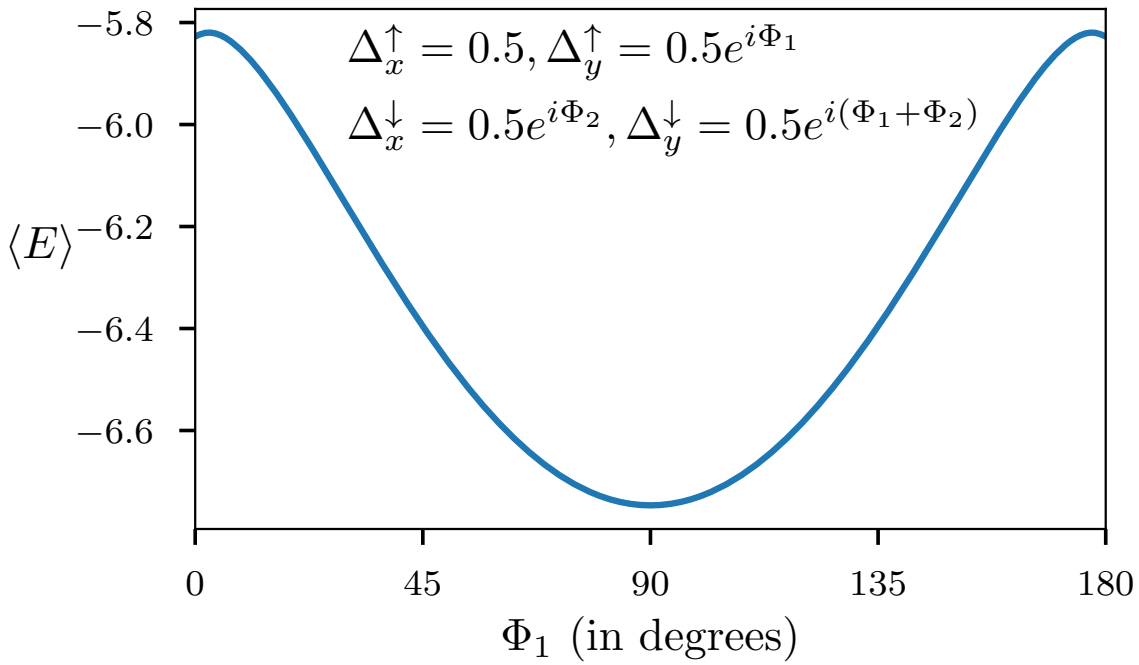


**Figure 4.1:** Variation of ground state average energy $\langle E \rangle$ with relative phase angle $\Phi_1$ at zero magnetic field for the parameter values $U = 1$,$V = 4$ and $\mu = 0$, where we chose $\Delta_x^{\uparrow} = 0.5, \Delta_y^{\uparrow} = 0.5e^{i\Phi_1}, \Delta_x^{\downarrow} = 0.5e^{i\Phi_2}$ and $\Delta_y^{\downarrow} = 0.5e^{i(\Phi_1+\Phi_2)}$. The variation shown here is independent of the choice of $\mu$, $t$ and $\mathbf{B}$.

the phase relations among $\Delta_x^+, \Delta_x^-, \Delta_y^+$ and $\Delta_y^-$ is fixed. This is ensured by energetics checked through numerical simulations.

**Triplet combinations from $\Delta^{\uparrow\uparrow}(\mathbf{k})$ and $\Delta^{\downarrow\downarrow}(\mathbf{k})$ :**

1. $\Delta^{\uparrow\uparrow} = 2iV\left[\Delta_x^{\uparrow}\sin(kx) + \Delta_y^{\uparrow}\sin(ky)\right]$

2. $\Delta^{\downarrow\downarrow} = 2iV\left[\Delta_x^{\downarrow}\sin(kx) + \Delta_y^{\downarrow}\sin(ky)\right]$

Again by comparing energies we find the phase relations between $\Delta_x^{\uparrow}$ and $\Delta_y^{\uparrow}$, $\Delta_y^{\uparrow} = e^{i\Phi_1}\Delta_x^{\uparrow}$, and $\Delta_y^{\downarrow} = e^{i\Phi_1}\Delta_x^{\downarrow}$. We find that $\Phi_1 = \frac{\pi}{2}$ gives us the solution corresponding to the minimum average energy $\langle E \rangle$ (Fig.4.1). These phase relations reduce our parameter space considerably. Though these relations are checked on the basis of mere energetics, we also checked the validity of these relations in self-consistent solutions. We do not find a similar phase relation between $\Delta^{\uparrow\uparrow}(\mathbf{k})$ and $\Delta^{\downarrow\downarrow}(\mathbf{k})$.

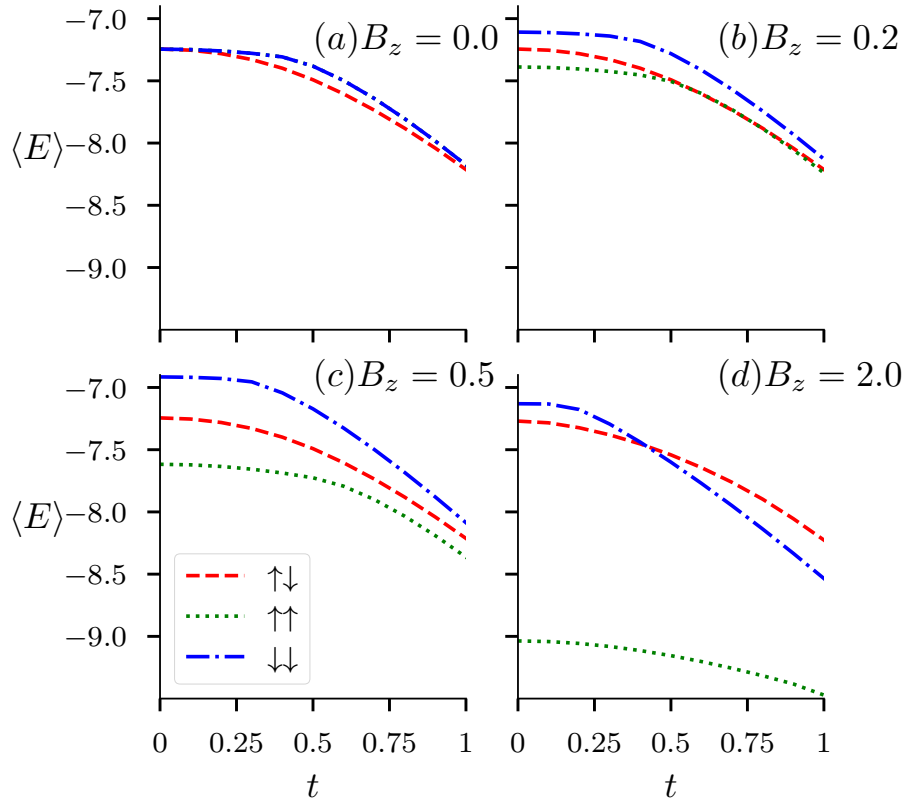


**Figure 4.2:** $(a)$-$(d)$ Variation of average energy $\langle E \rangle$ corresponding to three triplet states with hopping amplitude $t$ at zero temperature for different magnitudes of magnetic field $\mathbf{B}$ ($(a)$ $B_z = 0$, $(b)$ $B_z = 0.2$, $(c)$ $B_z = 0.5$ and $(d)$ $B_z = 2.0$).

.

## 4.4 Competition among the different triplet states

In this section we compare the energies of the three triplet states: $|S_z = 0\rangle \equiv \left(\frac{1}{\sqrt{2}}(|\uparrow\downarrow\rangle + |\downarrow\uparrow\rangle)\right)$, $|S_z = 1\rangle \equiv |\uparrow\uparrow\rangle$ and $|S_z = -1\rangle \equiv |\downarrow\downarrow\rangle$. The expectation is that all three states $|S_z = 0\rangle$,$|S_z = 1\rangle$ and $|S_z = -1\rangle$ are degenerate in the absence of magnetic field. Furthermore, equal spin pairing states (ESP) $|S_z = 1\rangle$ and $|S_z = -1\rangle$ will become lower in energy in the presence of a magnetic field. In our formulation singlet and $|S_z = 0\rangle$ triplet component enter into the hamiltonian through the superconducting pairing correlation $\Delta^{\uparrow\downarrow}(\mathbf{k})$ and $|S_z = 1\rangle$, $|S_z = -1\rangle$ triplet contributions enter through the triplet superconducting correlations $\Delta^{\uparrow\uparrow}(\mathbf{k})$ and $\Delta^{\downarrow\downarrow}(\mathbf{k})$.

We conclude this section with Fig.(4.2) and Fig.(4.3). In Fig.(4.2) we plot the variation of average system energy corresponding to all possible triplet states (both OSP and ESP) with increasing amplitude of nearest-neighbor hopping parameter $t$. As we focus on the energies of the triplet states, we pick a specific point in the parameter space ($U = 0$, $V = 1.8$, $\mu = -1.5$) where we found pure-triplet ($p_x \pm ip_y$

type) state being stabilized in our previous study. As the interaction strength $V$ is kept fixed while increasing nearest-neighbor hopping amplitude $t$, effectively we are moving from a strong-coupling (BEC) limit to a weak-coupling (BCS) limit.

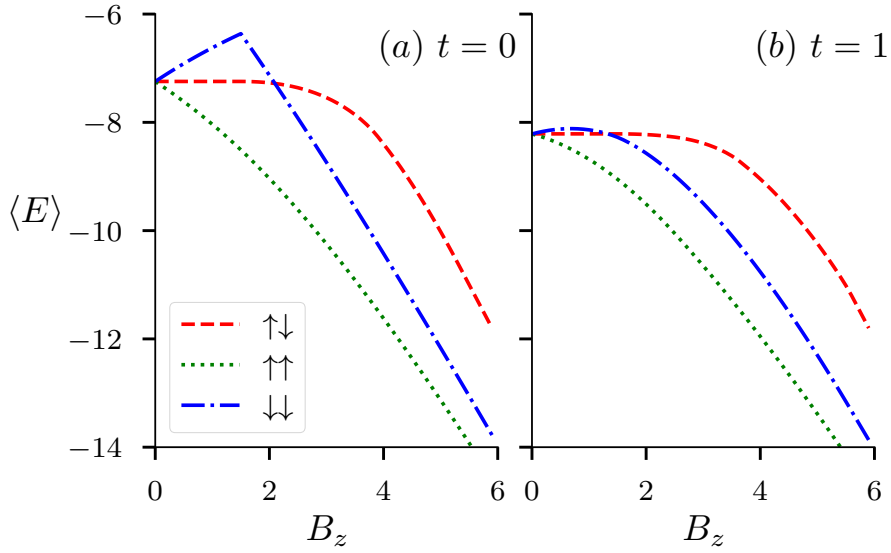


**Figure 4.3:** Variation of energy for the three triplet states with $B_z$, for $(a)$ $t = 0$ and $(b)$ $t = 1$.

In the strong-coupling limit, where the electron-pairs are tightly bound, we can appropriately apply the well-known physics of spin-singlet and spin-triplet pairing to the spin degrees of freedom associated with the electron-pairs. In this limit, absence of magnetic field leads to degenerate triplet states. In fact, absence of magnetic field provides the freedom to transform ESP states into specific OSP states, via a suitable choice of quantization axis. In the presence of a magnetic field this symmetry is broken and therefore the degeneracy is lifted. In weak-coupling limit the system gains energy via de-localization of electrons and characterization of different triplet states in terms of local spin operators is not valid. We use the phase-lock between different pairing correlations obtained in the previous section. This reduces the parameter space significantly and gives us the freedom to use only magnitudes of different $\Delta$s. In Fig.(4.2.$a$), at $t = 0$, we choose these magnitudes in a manner so that all the triplet states (both OSP and ESP) remain degenerate. With the increase of nn hopping amplitude $t$ we note that the OSP state ($\uparrow\downarrow$ in figure) becomes energetically favourable. At any finite value of Zeeman-coupling $\uparrow\uparrow$-type ESP state remain energetically favourable, while the energy of $\downarrow\downarrow$-type ESP state and OSP state behave differently in different coupling regimes. At moderate values of Zeeman-coupling system prefers OSP state to $\downarrow\downarrow$-type ESP state in both weak and strong coupling limits (Fig.4.2.($b$)-($c$)). At a larger value of Zeeman-coupling OSP state is completely disfavoured in the weak-coupling (BCS)

limit (Fig.4.2.($d$)). In fact, one should take a note of the fact that this particular observation is validated by self-consistent solutions we find in our next study. Fig.(4.3) completes this particular study, as it captures the variation of energy of the aforementioned triplet states with increasing values of Zeeman-coupling in the two limiting cases ($t = 0$ and $t = 1$). At strong-coupling ($t = 0$) limit, OSP state is of lower energy compared to $\downarrow\downarrow$-type ESP state below a critical Zeeman-coupling ($B_z \approx 2$). Beyond such critical value of Zeeman-coupling OSP state becomes completely disfavoured energetically with respect to the ESP states. On the other hand, at weak-coupling limit ($t = 1$), energy of OSP state remains comparable with $\downarrow\downarrow$-type ESP state at moderate values of Zeeman-coupling, and eventually becomes energetically disfavoured at higher values of Zeeman-coupling. On one hand this study provides us with the idea of how OSP and ESP states behave at two different coupling regimes. On the other hand, it provides us an insight into the nature of triplet states likely to be stabilized at different values of Zeeman-coupling.

## 4.5 Ground State Phase Diagrams

In the previous study we explored the possibility of stabilizing OSP superconducting solutions in the framework of Extended attractive Hubbard model defined on a square lattice in the absence of a magnetic field. The results of the previous study was based on the set of order parameters $\{\Delta\} = \{\ \Delta_s, \Delta_{s^*}, \Delta_{d_{x^2-y^2}} \Delta_{p_x}, \Delta_{p_y}\ \}$, which were obtained using standard definition of superconducting OPs, defined in literature, from the original set of pairing correlations $\{\ \Delta, \Delta_\delta^+, \Delta_\delta^-\ \}$. Note that $\delta$ index actually defines unit vectors $\boldsymbol{\delta} = \hat{x}, \hat{y}$ along two independent directions on a square lattice. So $\{\ \Delta, \Delta_\delta^+, \Delta_\delta^-\ \}$ is actually a shorthand notation for $\{\ \Delta, \Delta_x^+, \Delta_y^+, \Delta_x^-, \Delta_y^-\ \}$.

In this study we also include the possibility of the ESP-type superconducting solutions along with OSP-type solutions. Thus our new set of pairing correlations include four more terms, namely $\Delta_x^\uparrow$, $\Delta_y^\uparrow$, $\Delta_x^\downarrow$, and $\Delta_y^\downarrow$. So, our new set of order parameters becomes

$$\{\Delta\} = \overbrace{\{\Delta, \quad \Delta_\delta^+, \quad \Delta_\delta^-}^{\text{OSP}}, \quad \overbrace{\Delta_\delta^\uparrow, \quad \Delta_\delta^\downarrow}^{\text{ESP}}\}, \tag{4.12}$$

where, again we have used a shorthand notation as explained above. Note that, in Eq.(4.12), we have grouped the pairing correlations in two sets, namely OSP and ESP. The OSP group contains pairing correlations ($\Delta$,$\Delta_\delta^+$,$\Delta_\delta^-$) that allow the OSP-

type triplet states to exist, while the ESP group contains pairing correlations ($\Delta_\delta^\uparrow$,$\Delta_\delta^\downarrow$) that can give rise to ESP-type triplet states. We follow an unrestricted approach where OSP group of pairing correlations are allowed to take such forms where they can make the singlet or the OSP-type triplet or a mix of them to be stabilized in different parameter regimes. On the other hand, ESP group of pairing correlations allow only ESP-type triplet states to be stabilized.

Having defined our order parameters in the above manner, we set out to study the variation of magnitudes of these order parameters with varying chemical potential $\mu$. Average electron density per site, $\langle n \rangle$, is calculated for each value of $\mu$. Thus we try to plot magnitudes of the order parameters, defined in Eq.(4.12), with changing $\langle n \rangle$. In the self-consistent approach, if we start with different initial values of these $\{\Delta\}$, we find individual magnitudes of the converged solutions to be different for different initial configurations. This prevents us to plot a smooth variation of these OPs with $\langle n \rangle$. In the absence of Zeeman coupling this is quite expected. As in the absence of Zeeman coupling, there is no fixed quantization axis present in the system, possible OSP and ESP-type triplet states can form different linear combinations of corresponding pairing correlations, leaving us with a degenerate set of solutions for each value of $\mu$. In this case the *d-vector formalism*, defined in the section 4.2, comes to our rescue. We find magnitudes of $d_0(\mathbf{k})$ and $\mathbf{d}(\mathbf{k})$, averaged over the whole Brillouin zone, to be the best suited order parameters for the singlet and the triplet states in this scenario. Thus we define our singlet and triplet order parameters in the following way:

$$\Delta_{SP} = \frac{1}{N_s}\sum_{\mathbf{k}}|d_0(\mathbf{k})| \quad \text{and} \quad \Delta_{TP} = \frac{1}{N_s}\sum_{\mathbf{k}}|\mathbf{d}(\mathbf{k})| \tag{4.13}$$

Using the order parameters, the way it is defined in Eq.(4.13), we study the variation of these order parameters with average electron density per site $\langle n \rangle$. In Fig.(4.4) we plot the variation of singlet order parameter $\Delta_{SP}$ and triplet order parameter $\Delta_{TP}$ with $\langle n \rangle$ for different values of inter-site attraction $V$. We keep on-site attraction at a fixed value ($U = t$), as it is the inter-site attraction $V$ that plays an important role in stabilizing different unconventional superconducting orders. When inter-site attraction $V$ is small ($V = 0.4t$) compared to on-site attraction $U$, it is the singlet phase that occupies the whole density region (Fig.(4.4).($a$)). At $V = 1.6t$, singlet phase occurs both at lower density region and near half-filling (Fig.(4.4).($b$)). Though orbital information of the order parameter is kept hidden, it's easy to suggest that the singlet phase near half-filling is $d_{x^2-y^2}$ type, while the singlet phase near low-density region is

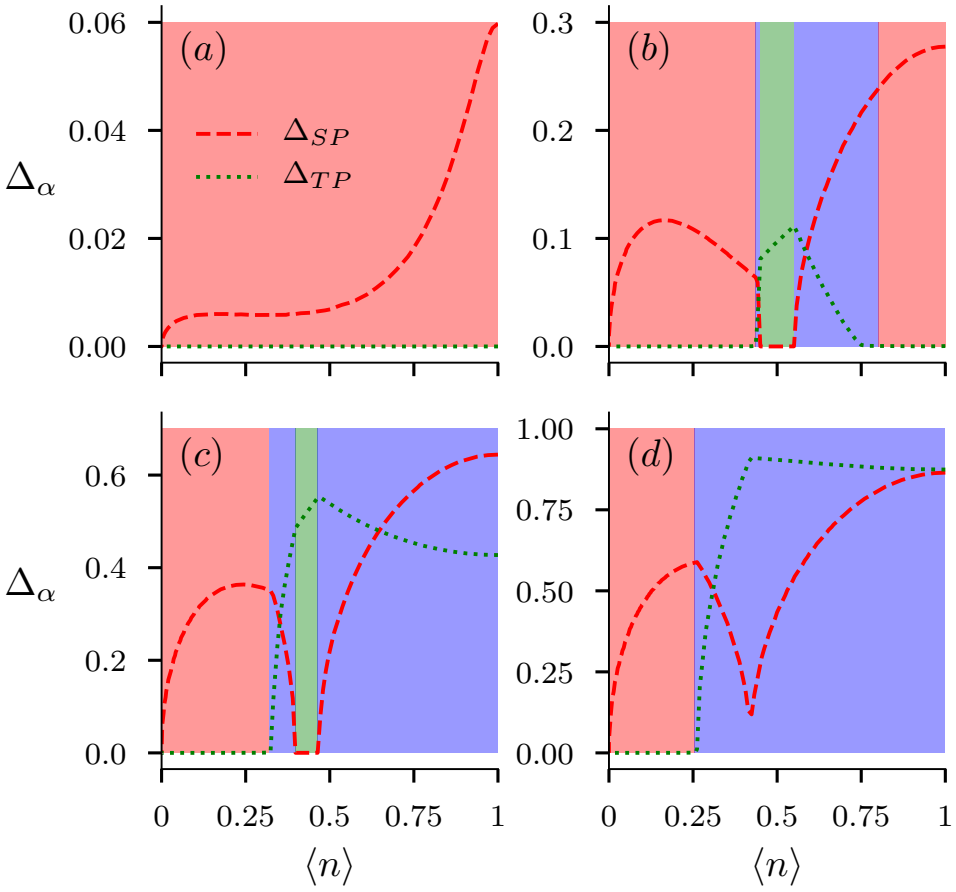


**Figure 4.4:** Variation of singlet ($\Delta_{SP}$) and triplet ($\Delta_{TP}$) OP magnitudes with electron density $\langle n \rangle$ at zero temperature for onsite interaction $U = 1$ and inter-site interaction strength: $(a)$ $V = 0.4t$, $(b)$ $V = 1.6t$, $(c)$ $V = 3.0t$ and $(d)$ $V = 4.0t$. The color in the background indicates the nature of the SC order as, red: pure-singlet, green: pure-triplet and blue: mixed parity.

of $s+s^*$ type. Pure triplet phase occurs near quarter-filling, while singlet-triplet mixed parity phase occurs between pure triplet phase and singlet phase of $d_{x^2-y^2}$ type. It is important to note that pure-$d_{x^2-y^2}$ type singlet phase occurs at low-$V$ region, when $V$ is still larger than on-site interaction $U$. At higher value of inter-site attraction ($V = 3t$), pure-$d_{x^2-y^2}$ type singlet phase vanishes (Fig.(4.4).$(c)$), while singlet-triplet mixed phase occupies the corresponding density region (near half-filling). At $V = 3t$ a small window of singlet-triplet mixed phase occurs between $s + s^*$ type singlet and pure triplet phase. If we increase $V$ further ($V = 4t$), most of the density region is occupied by dominant singlet-triplet mixed phase, while $s + s^*$ type singlet phase still occurs at low density region (Fig.(4.4).$(d)$).

This variation of order parameters with average electron density motivates us to draw a $V$-$\langle n \rangle$ ground state phase diagram in the absence of a magnetic field

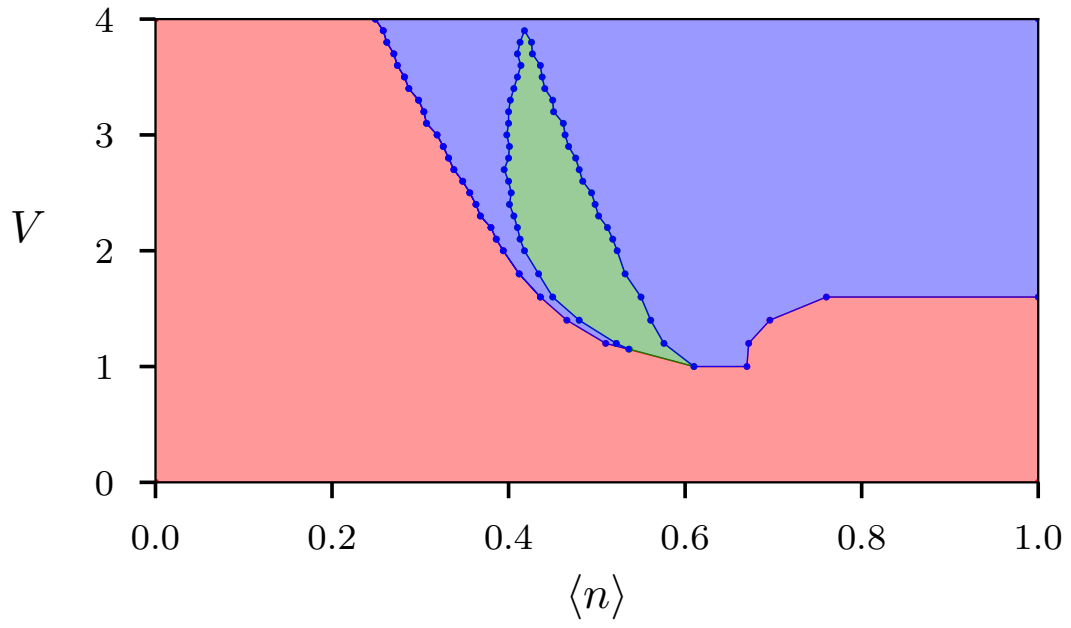


**Figure 4.5:** $V$-$n$ ground state phase diagram at $B_z = 0$, $U = t$, color coding is consistent with Fig.(4.4).

(Fig.(4.5)). We keep the on-site attractive interaction strength $U$ at a fixed value ($U = t$), for the reason mentioned before. We notice that when the inter-site interaction $V$ is less than the on-site interaction, i.e. $V < t$, the whole density region is occupied by the pure singlet phase (red in color). This is expected as a dominant on-site attraction is known to stabilize singlet $s$-wave SC order. While $U$ is stabilizing singlet $s$-wave SC order, $V$ is also playing an important role in stabilizing singlet $s^*$ and $d_{x^2-y^2}$ SC orders in this region along with $s$-wave. When the lower density region prefers singlet $s$ and $s^*$ SC orders to other phases, near half-filling it is the singlet $d_{x^2-y^2}$-wave that prevails. As inter-site interaction $V$ becomes larger compared to on-site interaction $U$, it not only stabilizes singlet $s^*$ and $d_{x^2-y^2}$ SC orders, it also helps pure triplet and mixed-parity phases to get stabilized at different density regimes. The pure triplet phase (green in color) occurs in a delta-shaped region near quarter filling ($0.4 \leq \langle n \rangle \leq 0.6$), when the inter-site attraction $V$ is higher than the on-site attraction $U$ but not as large as $V = 4t$. With $V$ getting larger, the mixed-parity (blue in color) phase becomes more stable, specially in the higher density region. It's interesting to note that $d_{x^2-y^2}$-type singlet phase is prone to get stabilized near half-filling region and pure triplet phase has a tendency to get stabilized near quarter-filling. But depending on the strength of inter-site interaction the system gains energy by stabilizing a new mixed-parity (possibly $d + p$-type) state, near the higher density region.

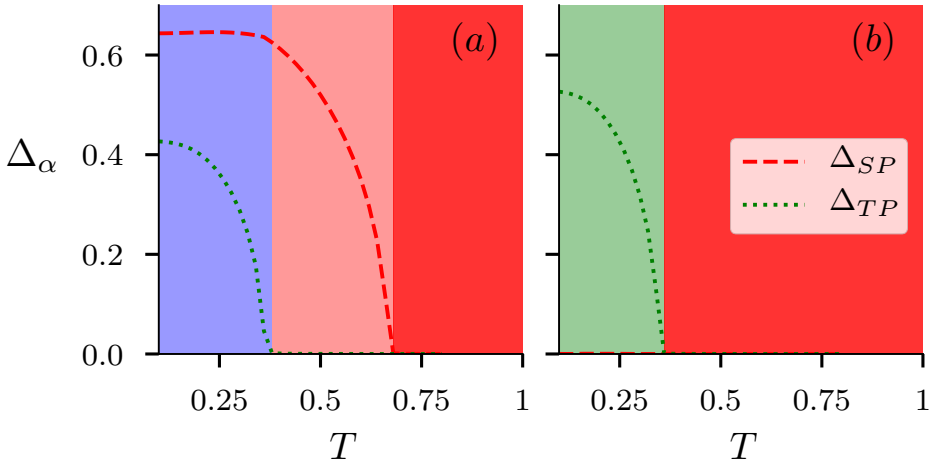


**Figure 4.6:** Variation of singlet ($\Delta_{SP}$) and triplet ($\Delta_{TP}$) OP magnitudes with temperature in the absence of Zeeman-coupling for on-site interaction $U = t$, inter-site interaction $V = 3t$, and average electron density: $(a)$ $\langle n \rangle = 1.0$ and $(b)$ $\langle n \rangle = 0.44$. Color coding in the background is consistent with Fig.(4.4). Dark red in the background represents non-superconducting region.

It's also important to note that, in the absence of a magnetic field OSP-type triplet states are likely to be stabilized. Presence of $d_{x^2-y^2}$-type SC order in mixed-parity state indicates that pairing between opposite spin still survives. This will not be the case, as we will see in section 4.7, when Zeeman-coupling to an external magnetic field will be considered.

## 4.6 Finite Temperature Study

After exploring the stability of singlet, triplet and mixed-parity states in the ground state of the EAHM on a square lattice, we intend to study the behavior of the corresponding SC states at finite temperatures. General consensus is that thermal excitations destroy superconductivity. So the expectation is that the magnitudes of the superconducting order parameters, defined in our system, will decrease and eventually vanish when temperature is increased beyond a critical value. It is well-known that beyond this critical temperature, $T_c$, superconductors make a transition from superconducting state to the normal state. As we limit ourselves to the framework of mean-field theory, it is not our aim to infer about the specific values of $T_c$ we obtain in our calculations. We rather intend to study how different SC orders react to the onset of finite temperature.

In Fig.(4.6) we plot the variation of singlet ($\Delta_{SP}$) and triplet ($\Delta_{TP}$) order parameter with temperature for two different points in parameter space taken from the

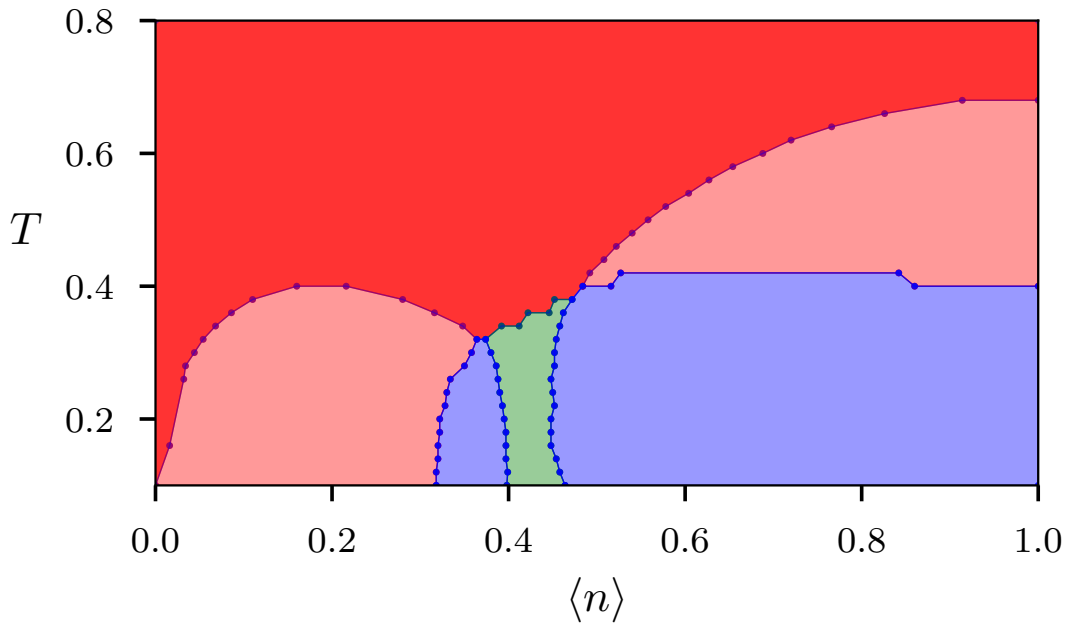


**Figure 4.7:** $T$-$\langle n\rangle$ phase diagram, in the absence of a magnetic field, at $U = t$ and $V = 3t$. Dark red represents non-superconducting region, while the rest of the color coding is consistent with Fig.(4.4).

ground state $V$-$\langle n\rangle$ phase diagram. In Fig.(4.6.($a$)) we start with a mixed-parity state exactly at half-filling ($\langle n\rangle = 1$). While the red dashed line represents the singlet order parameter ($\Delta_{SP}$), the green dotted line represents triplet order parameter ($\Delta_{TP}$). As temperature is increased, the triplet order parameter starts to fall off and around $T \approx 0.38$ it vanishes completely. Most interestingly, the singlet order parameter $\Delta_{SP}$ remains almost constant while $\Delta_{TP}$ falls off. It seems the $d_{x^2-y^2}$ type singlet remains protected as long as the triplet order parameter is finite. At $T \approx 0.38$ the system makes a transition from a mixed-parity SC state to a pure $d_{x^2-y^2}$ type singlet superconducting state. If temperature is increased further $\Delta_{SP}$ starts to fall off and it completely vanishes at $T \approx 0.68$. Thus Fig.(4.6.($a$)) depicts how interestingly the system makes a transition from a mixed-parity superconducting state to a pure singlet superconducting state before making a transition to a non-superconducting state. In Fig.(4.6.($b$)), we start with a different point of the parameter space, again taken from the ground state $V$-$\langle n\rangle$ phase diagram. In this case our zero temperature initial choice is at density $\langle n\rangle = 0.44$, where we find pure triplet state being stable. Notably with the increase of temperature the triplet order parameter $\Delta_{TP}$ falls off exactly the way it did for the previous case and the temperature where $\Delta_{TP}$ completely vanishes is exactly same as the previous case, i.e., $T \approx 0.38$. But in this

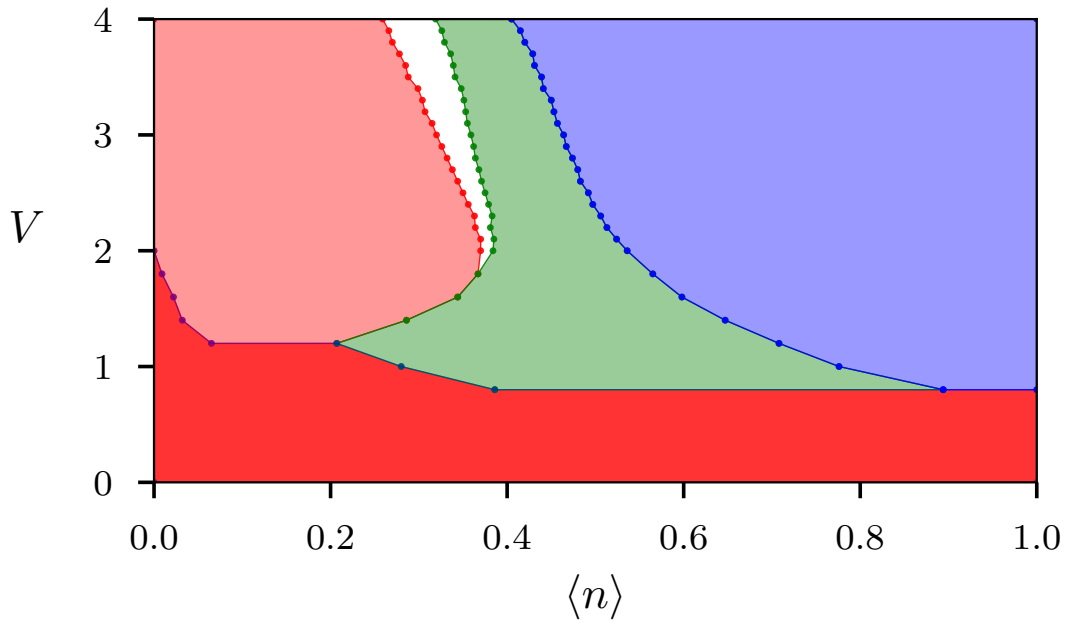


**Figure 4.8:** $V$-$n$ ground state phase diagram at finite magnetic field,$B_z = 0.1t$ and $U = t$. Dark red represents the non-superconducting region and the white represents phase separation as inferred from $\langle n \rangle$ vs. $\mu$ plots in Fig.(4.9).

case the triplet SC state makes a direct transition to non-superconducting state. In order to summarize these results we draw a $T$-$\langle n \rangle$ phase diagram to complete the picture of the finite temperature effects (Fig.(4.7)). In the $T$-$\langle n \rangle$ phase diagram we find, in general, every superconducting phases at zero temperature ($x$-axis) makes a transition from superconducting to non-superconducting phase when temperature is increased. While the transition temperature for singlet phase takes a dome-shaped feature as a function of density, for triplet and mixed-parity states the transition temperature does not have such sharp feature with varying density. As discussed earlier, we find four different sectors of such transition. In three sectors the system makes a direct transition from superconducting state to non-superconducting state retaining the specific form of pairing symmetry, while the mixed-parity state in the density region $0.5 \leq \langle n \rangle \leq 1.0$ makes a transition to singlet superconducting state before making a transition to non-superconducting state.

## 4.7 Effect of Zeeman Coupling

After validating our results for zero temperature and finite temperature in the absence of a magnetic field, we intend to study the effect of a magnetic field on the

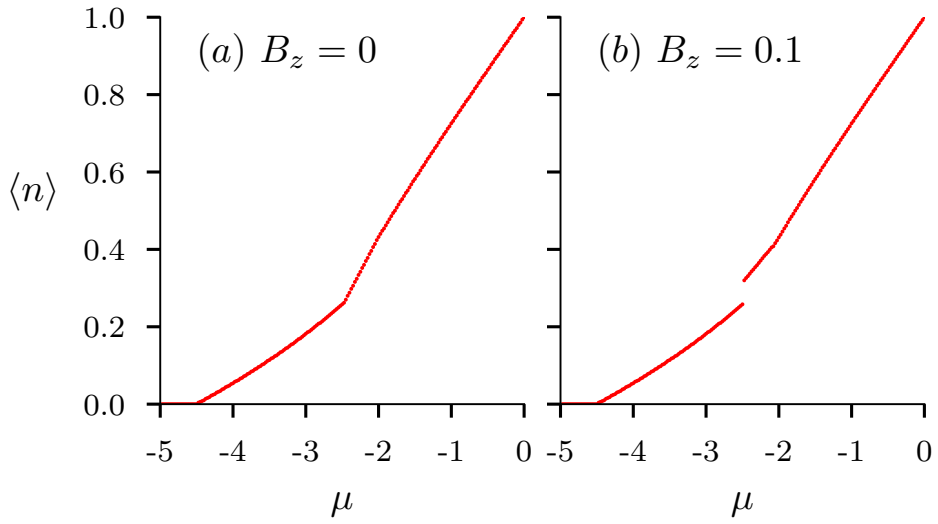


**Figure 4.9:** Variation of average electron density $\langle n \rangle$ with chemical potential $\mu$ for, $(a)$ $B_z = 0$ and $B_z = 0.1t$. Note the discontinuity in $(b)$ signifies the phase separation.

superconducting phases we found in different regimes of the parameter space. We limit our study to the effect of Zeeman-coupling to an external magnetic field. Thus we ignore the effect of an external magnetic field on orbital degrees of freedom and confine ourselves to study the effect of a magnetic field on the spin degrees of freedom only. An in-plane magnetic field serves our purpose. Motivated by the zero temperature $V$-$\langle n \rangle$ phase diagram (Fig.(4.5)), we drew in the absence of a magnetic field, we take interest in knowing how that $V$-$\langle n \rangle$ phase diagram changes with the onset of a Zeeman field. In Fig.(4.8) we draw a similar phase diagram, but in the presence of a magnetic field, $B_z = 0.1t$. The first thing we notice is the appearance of a non-superconducting region (dark red in color) in the phase diagram, which is quite expected.

From the ground state $V$-$\langle n \rangle$ phase diagram in the absence of a magnetic field (Fig.(4.5)), we notice that when inter-site interaction is less than the on-site interaction the whole density region is occupied by singlet superconducting phase. When the Zeeman field is switched on and the strength of the Zeeman field is maintained at $B_z = 0.1t$, it is strong enough to destroy superconductivity when $V$ is approximately less than $0.8t$. So any superconducting phase occuring below $V \approx 0.8t$ is destroyed by a Zeeman field of strength $B_z = 0.1t$. In the absence of a magnetic field, there is a pure $d_{x^2-y^2}$ type singlet phase, which is stable near half-filling. It appears that presence of an external magnetic field of strength $B_z = 0.1t$, destroys such pure $d_{x^2-y^2}$ type superconducting phase, as for any strength of $V$ (within the scale provided in

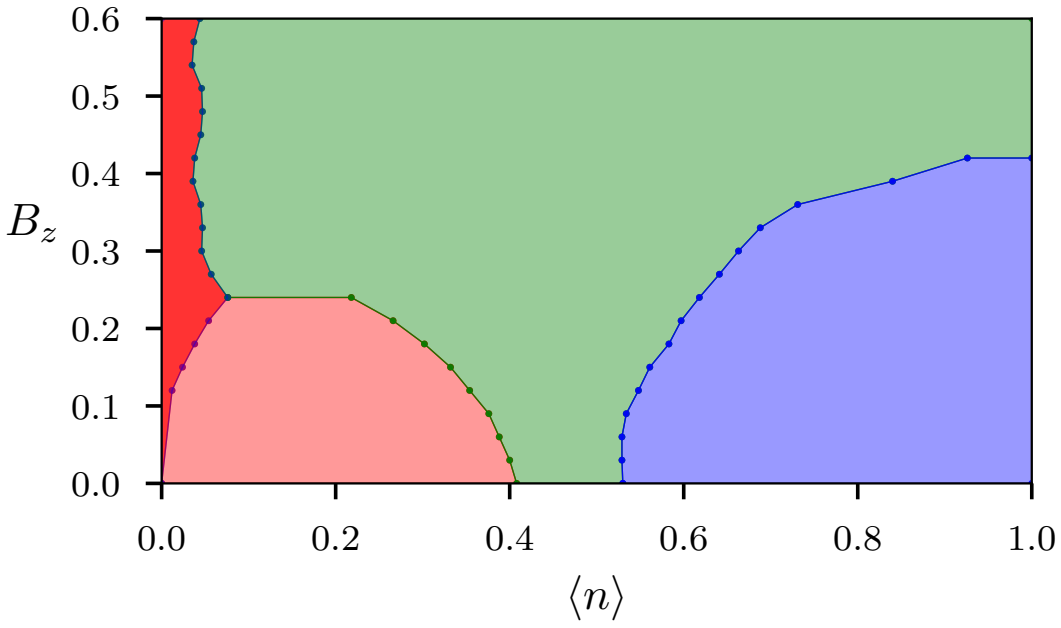


**Figure 4.10:** $B_z$-$n$ Phase Diagram at zero temperature, $V = 2t$, $U = t$,light red defines the singlet region,light violet defines the singlet-triplet mixed phase, the light green defines the pure triplet phase, dark red defines the non-superconducting region.

Fig.(4.8)) only mixed-parity state gets stabilized. Most interestingly, the pure triplet superconducting phase appears to be enhanced by the onset of a magnetic field. The region, where pure triplet superconducting phase is stabilized in $V$-$\langle n \rangle$ phase diagram, gets larger in presence of the Zeeman-coupling. Another important aspect we notice is that there is a region of phase separation appearing between the pure singlet phase and the pure triplet phase when $V$ is appropriately greater than $2t$.

To prove this aspect of phase separation, we draw a variation of average electron density per site, $\langle n \rangle$, with the chemical potential $\mu$ at two values of Zeeman-coupling,$(a)$ $B_z = 0$ and $(b)$ $B_z = 0.1t$ (Fig.(4.9)). For the purpose of the above-mentioned illustration we keep the on-site interaction at $U = t$, while the inter-site interaction is kept fixed at $V = 4t$. While in the absence of a Zeeman-coupling we see a continuous variation of $\langle n \rangle$ with $\mu$, in the presence of a Zeeman-coupling we definitely notice a jump in the electron density at $\mu \approx -2.5$.The jump in the density is of the order $\delta_{\langle n \rangle} \approx 0.1$, at $V = 4t$ (Fig.(4.8)).

To completely understand the effect of Zeeman-coupling on the superconducting phases, we further draw a zero temperature $B_z$-$\langle n \rangle$ phase diagram at $U = t$ and $V = 2t$ (Fig.(4.10)). At $B_z = 0$, $U = t$ and $V = 2t$, singlet, triplet and mixed-parity

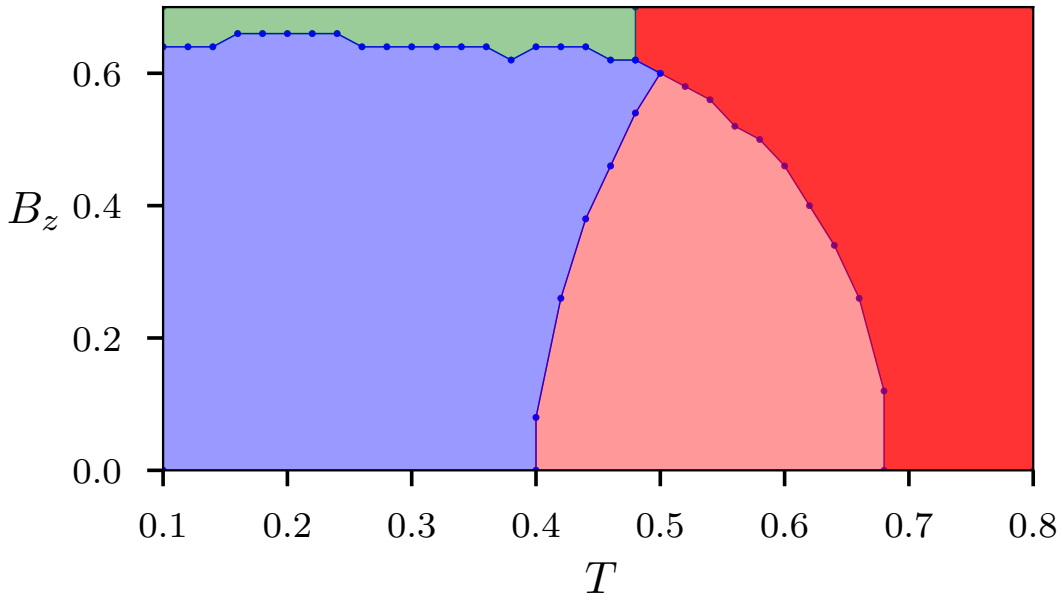


**Figure 4.11:** $B_z$-$T$ Phase Diagram at $U = t$ and $V = 3t$. Dark red represents non-superconducting region, while the rest of the color coding is consistent with Fig.(4.4).

superconducting phases occupy different sectors of density region, as observed in the ground state $V$-$\langle n \rangle$ phase diagram in the absence of the Zeeman-coupling to an external magnetic field. As the strength of the magnetic field is increased it appears that the pure triplet superconducting state becomes favourable. In fact, the pure singlet superconducting phase disappears from the whole density region when the strength of the magnetic field becomes approximately greater than $0.23t$, while the mixed-parity state completely disappears from the whole density region when $B_z$ becomes approximately larger than $0.4t$. Eventually at $B_z > 0.4t$ (approximately) only pure triplet superconducting phase survives throughout the whole density region. Though we must take a note of the fact that a non-superconducting region (dark red in color) prevails over the other phases at very low electron densities. The information we gather from this study is of two-fold nature. Firstly, it is clear that Zeeman-coupling to an external magnetic field at low strength favours pure triplet superconductivity. Secondly, the disappearance of pure singlet and mixed-parity state indicates the possibility of disappearance of OSP type superconducting states and appearance of ESP type superconducting states beyond certain strength of the external magnetic field. As OSP type states give rise to singlet states like $s$,$s^*$ and $d_{x^2-y^2}$ etc., and ESP type states give rise to pure triplet superconducting phases, the above-mentioned behavior

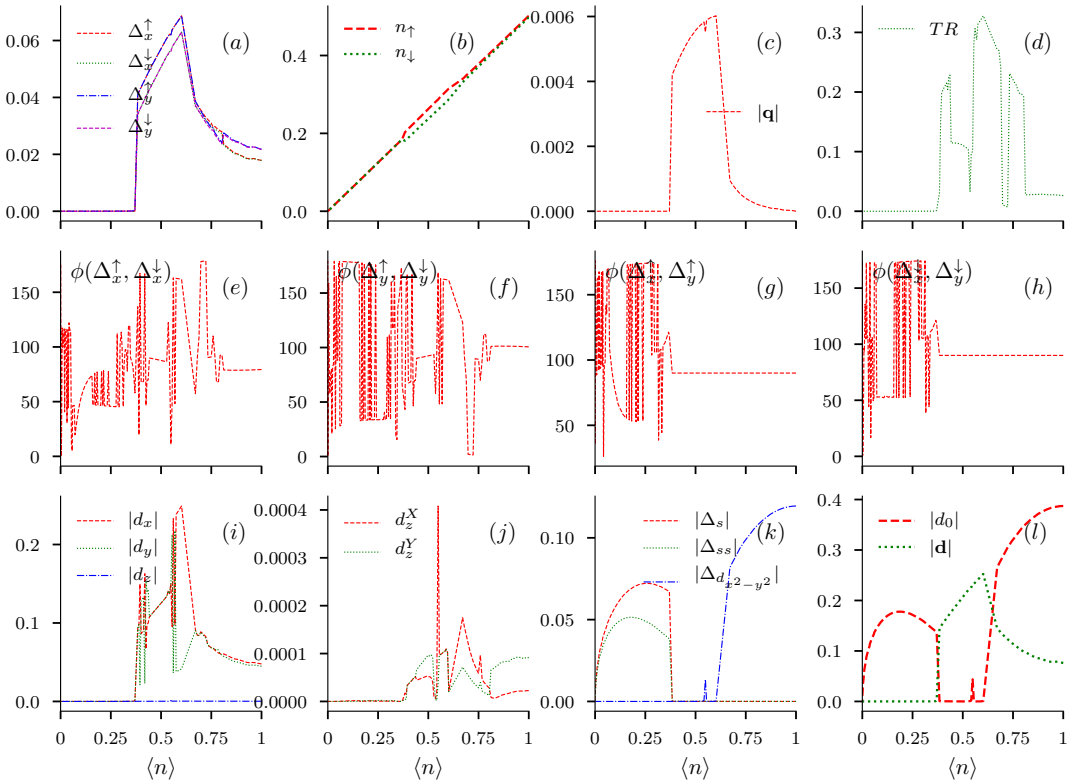


**Figure 4.12:** Variation of different quantities related to OPs or **d**-vector formalism, with average electron density per site $\langle n \rangle$ to characterize different superconducting phases. The entities on different plots are: $(a)$ ESP pairing correlations $\Delta_\delta^\uparrow$ and $\Delta_\delta^\uparrow$, $(b)$ $n_\uparrow$ and $n_\downarrow$, $(c)$ magnitude of non-unitarity of phases ($|\mathbf{q}|$), $(d)$ magnitude of broken time reversal symmetry (TR), $(e)$ relative phase angle between $\Delta_x^\uparrow$ and $\Delta_x^\downarrow$, $(f)$ relative phase angle between $\Delta_y^\uparrow$ and $\Delta_y^\downarrow$, $(g)$ relative phase angle between $\Delta_x^\uparrow$ and $\Delta_y^\uparrow$, $(h)$ relative phase angle between $\Delta_x^\downarrow$ and $\Delta_y^\downarrow$, $(i)$ three components of **d**-vector, $(j)$ $x$ and $y$ components of OSP pairing correlations, $(k)$ magnitude of singlet order parameters in terms of $s$, $s^*$ and $d_{x^2-y^2}$-wave components, and $(l)$ singlet and triplet order parameters in terms of $|d_0|$ and $|\mathbf{d}|$ averaged over the whole Brillouin zone.

is well-explained. We conclude our study of the effect of Zeeman-coupling on different superconducting orders by looking at the effect of Zeeman-coupling at finite temperatures. We plot a $B_z$-$T$ phase diagram to describe these effects at a specific point of the parameter space, namely $U = 1$, $V = 3$ and $\mu = 0$ (Fig.(4.11)).

## 4.8 Characterization of Phases

The motivation of this chapter has been the study of different superconducting order parameters in the presence of Zeeman coupling to an external magnetic field. So far we have classified our superconducting states in terms opposite spin pairing and

equal spin pairing states, giving rise to pure singlet, pure triplet and mixed-parity superconducting states in the form of stabilized solutions. While, the main classification is done based on the nature of the spin state of the system we do mention different pairing symmetries like $s$-wave, $s^*$-wave, $p_x + ip_y$-wave and $d_{x^2-y^2}$-wave to define the nature of the orbital part of the gap function. In case of pure singlet or pure triplet phase the nature of the orbital part can be easily understood, while for mixed-parity states such separation does not exist. In Fig.(4.12) we make an effort to study different entities related to the superconducting order parameters at zero temperature with varying average electron density per site $\langle n \rangle$. All the entities are plotted for the following set of parameter values: $B_z = 0.1t$, $U = t$ and $V = 2t$. In Fig.(4.12.($l$)) we plot the singlet and triplet order parameters as defined previously in this chapter. Clearly we observe three different sectors in the whole density profile, pure singlet at lower density region, pure triplet near quarter filling, and mixed-parity solution around half filling. In Fig.(4.12.($k$)) we plot the magnitudes of different components of singlet order parameter in terms of $s$, $s^*$ or $s^{ss}$ and $d_{x^2-y^2}$-wave pairing symmetries, which describes the orbital part of the gap function. This plot confirms the existence of $s$ and $s^*$ type singlet superconducting state at lower densities, while $d_{x^2-y^2}$ type singlet state occurs near half filling. Though in this case, it is a mixed parity state with $d_{x^2-y^2}$ component singlet. Fig.(4.12.($a$)) describes the variation of ESP type pairing correlations with average electron density. We observe that in the pure triplet state $\Delta_x^{\uparrow}$ and $\Delta_y^{\uparrow}$ become equal in magnitude. Similarly magnitudes of $\Delta_x^{\downarrow}$ and $\Delta_y^{\downarrow}$ also become equal, while $\Delta_\delta^{\uparrow}$ and $\Delta_\delta^{\downarrow}$ acquire different values due to the Zeeman coupling. This relation among the triplet ESP correlations appears to be different in the presence of dominant $d_{x^2-y^2}$ singlet component near half filling. In Fig.(4.12.($b$)) spin-resolved average electron densities are plotted. In the pure triplet region we observe the possibility of the formation of an effective magnetic moment. Fig.(4.12.($c$)) tells us that the gap function is non-unitary in nature when the triplet order parameter is finite. Fig.(4.12.($c$)) describes the amount of non-unitarity of the gap function. Time reversal symmetry is broken for the same state (Fig.(4.12.($d$))). $2^{\text{nd}}$ row of plots describes the relative phase angle between different pairing correlation as discussed in section 4.3. And these results from self-consistent calculations proves the prediction we made via energetics in section 4.3.

## 4.9 Conclusion

In this chapter we have studied the stability of spatially homogeneous superconducting solutions of the extended attractive Hubbard model including the possibility of

equal spin pairing correlations. Inclusion of equal spin pairing terms along with the opposite spin pairing terms allowed us to treat the problem in the presence of an external magnetic field coupled via Zeeman term. We found pure singlet, pure triplet and unconventional mixed-parity superconducting solutions being stabilized at different parameter regimes. We studied the effect of finite temperature on the stabilized superconducting orders. We observed different inter-state transitions driven by temperature and Zeeman coupling. Finally we characterized the different ESP and OSP type superconducting solutions in terms of relevant entities obtained via **d**-vector formalism. Most importantly we observe the effect of broken parity and time reversal symmetry on superconducting solutions at different parameter regimes. This study opens up many important directions to investigate superconducting orders in a lattice model like extended attractive Hubbard model.

# Chapter 5

# Thesis summary and future directions

In this thesis we study the possibility of stabilizing different unconventional superconducting phases in an extended attractive Hubbard model defined on a square lattice. Discoveries of different unconventional superconductors in recent decades motivated scientists to look for new unconventional pairing mechanisms. The conventional BCS theory certainly fails to explain high critical temperatures and various other properties of these unconventional superconductors. Search for different pairing mechanisms has been crucial to the understanding of these new family of superconductors. While finding new pairing mechanisms has not been an easy tasks for scientists, it drove physicists to study different pairing symmetries of the energy gap. In modern days experiments like NMR, angle-resolved photo-emission spectroscopy (ARPES), microwave resonator penetration depth measurements, Josephson interferometry experiments, etc., are capable of finding the angular dependence of energy gaps in momentum space and verify whether there is a nodal structure to it. Motivated by these lines of thoughts, it seems very crucial to study unconventional pairing symmetries in an effective lattice Hamiltonian.

In chapter 1 we introduce superconductivity from a historical point of view. We discuss the relevant properties of a superconductor. We elaborate on the relevant theories of superconductivity and discuss about our choice of framework to study superconductivity. It is important to understand the motivation behind the term *unconventional*. So we clarify the well-known differences between conventional and unconventional superconductors. We motivate the reason behind choosing extended attractive Hubbard model as the effective lattice Hamiltonian to study unconventional superconductivity. Attractive on-site Hubbard model has been a strong candidate to

explain conventional $s$-wave superconductivity. We explain how extended attractive Hubbard model helps us to look for different unconventional pairing symmetries in a lattice Hamiltonian.

In chapter 2 we discuss our model of choice, i.e., extended attractive Hubbard model in greater detail. We discuss the general mean field decoupling scheme we use, which allows us to study the possibilities of stabilizing pure singlet, pure triplet and even mixed-parity superconducting states. We discuss the minimization method and the self-consistent approach we chose to find different superconducting solutions.

In chapter 3, for simplicity of the calculation, we ignore equal spin pairing correlations in our model Hamiltonian. Absence of an external magnetic field justifies our choice. We study the system in the framework of a grand canonical ensembe. We find different superconducting phases with unconventional pairing symmetries being stabilized in our system. We draw different phase diagrams with average electron density being a variational parameter and study characteristics of different superconducting phases, which get stabilized at different density region.

In chapter 4 we study the effect of the Zeeman coupling to a planar magnetic field. Presence of magnetic field motivated us to incorporate both opposite spin pairing and equal spin pairing. We justify our choice in this chapter using energy minimization. We draw different phase diagrams to validate our results in the absence of a magnetic field. Then We study the effect of both temperature and magnetic field on the superconducting phases we find being stable in our system.

This work also motivated an MS thesis that focused on topological transitions driven by the proximity effect. This work has recently been accepted for publication in Physical Review B [45]. Using a prototype model for proximity-induced superconductivity on a bilayer square lattice, we show that interlayer tunnelling can drive change in the topology of the Bogoliubov quasiparticle bands. Starting with topologically trivial superconductors, transitions to a nontrivial $p_x + ip_y$ state and back to another trivial state are discovered. We characterize these phases in terms of edge-state spectra and Chern indices. We show that these transitions can also be controlled by experimentally viable control parameters, the bandwidth of the metallic layer, and the gate potential. Insights from our results on a simple model for proximity-induced superconductivity may open up a new route to discover topological superconductors.

It is important to note that the possibility of different modulated phases is not considered in this study. The possibility of charge density wave coexisting with superconducting order at half-filling for the on-site attraction case is well known. And so is the possibility of the existence of unconventional superconducting order in the vicinity of the anti-ferromagnetic order. There has also been the indication of super-

conducting modulated phase (Fulde-Ferrell-Larkin-Obchinikov phase) in the presence of a magnetic field. Possibility of all these modulated phases, although very interesting, if incorporated, increases the complexity of the "ground state finding process" exponentially, even at the mean-field level. There has been a lot of study in the literature relating to the competition between superconducting phases and other phases, including charge order and different magnetic orders already. However, that is not the case when the competition between different superconducting orders are concerned. Thus our focus remains to study an effective Hamiltonian which reveals the possible competition between different exotic superconducting orders with uniform charge and spin distribution. On the other hand, it is very promising to look for the possibility of stable modulated phases, which is on the list of our future endeavours. So is the aim to incorporate thermal fluctuations, using auxiliary field Monte Carlo, to study the effect of finite temperature more accurately.

# Bibliography


[1] H. K. Onnes, Koninklijke Nederlandse Akademie von Wetenschappen, Proceedings **11**, 168 (1908).

[2] P. L. Kapitza, Proceedings of the Royal Society of London. Series A-Mathematical and Physical Sciences **147**, 189 (1934).

[3] W. Meissner and R. Ochsenfeld, Naturwissenschaften **21**, 787 (1933).

[4] F. London and H. London, Proceedings of the Royal Society of London. Series A-Mathematical and Physical Sciences **149**, 71 (1935).

[5] M. Tinkham, *Introduction to superconductivity* (Courier Corporation, 2004).

[6] L. N. Cooper, Physical Review **104**, 1189 (1956).

[7] P.-G. De Gennes, *Superconductivity of metals and alloys* (CRC Press, 2018).

[8] N. N. Bogolûbov, *A new method in the theory of superconductivity* (Chapman & Hall, 1959).

[9] J. Carbotte and F. Marsiglio, *The Physics of Superconductors* (Springer, 2003), pp. 233–345.

[10] B. White, J. Thompson, and M. Maple, Physica C: Superconductivity and its Applications **514**, 246 (2015).

[11] F. Steglich *et al.*, Physical Review Letters **43**, 1892 (1979).

[12] J. G. Bednorz and K. A. Müller, Zeitschrift für Physik B Condensed Matter **64**, 189 (1986).

[13] M. Sigrist and T. Rice, Zeitschrift für Physik B Condensed Matter **68**, 9 (1987).

[14] J. F. Annett, Advances in Physics **39**, 83 (1990).

[15] M. Sigrist and M. E. Zhitomirsky, Journal of the Physical Society of Japan **65**, 3452 (1996).

[16] J. Hubbard, Proceedings of the Royal Society of London. Series A. Mathematical and Physical Sciences **276**, 238 (1963).

[17] M. C. Gutzwiller, Physical Review Letters **10**, 159 (1963).

[18] J. Kanamori, Progress of Theoretical Physics **30**, 275 (1963).

[19] J. Hubbard, Proceedings of the Royal Society of London. Series A. Mathematical and Physical Sciences **277**, 237 (1964).

[20] J. Hubbard, Proceedings of the Royal Society of London. Series A. Mathematical and Physical Sciences **281**, 401 (1964).

[21] J. Hubbard, Proceedings of the Royal Society of London. Series A. Mathematical and Physical Sciences **285**, 542 (1965).

[22] J. Hubbard, Proceedings of the Royal Society of London. Series A. Mathematical and Physical Sciences **296**, 82 (1967).

[23] S. Raghu, S. Kivelson, and D. Scalapino, Physical Review B **81**, 224505 (2010).

[24] R. Scalettar *et al.*, Physical review letters **62**, 1407 (1989).

[25] F. Patrik, *Lecture notes on electron correlation and magnetism* (World scientific, 1999), Vol. 5.

[26] C. Tsuei and J. Kirtley, Reviews of Modern Physics **72**, 969 (2000).

[27] J. Bardeen, L. N. Cooper, and J. R. Schrieffer, Physical review **108**, 1175 (1957).

[28] J. Bardeen, L. N. Cooper, and J. R. Schrieffer, Physical Review **106**, 162 (1957).

[29] R. Micnas *et al.*, Physical Review B **52**, 16223 (1995).

[30] A. Toschi, P. Barone, M. Capone, and C. Castellani, New Journal of Physics **7**, 7 (2005).

[31] J. Singer *et al.*, Physical Review B **54**, 1286 (1996).

[32] K. Aryanpour *et al.*, Physical Review B **73**, 104518 (2006).

[33] K. Aryanpour, T. Paiva, W. E. Pickett, and R. T. Scalettar, Physical Review B **76**, 184521 (2007).

[34] A. Moreo and D. Scalapino, Physical review letters **66**, 946 (1991).

[35] R. Micnas, J. Ranninger, and S. Robaszkiewicz, Journal of Physics C: Solid State Physics **21**, L145 (1988).

[36] P. Monthoux, A. Balatsky, and D. Pines, Physical review letters **67**, 3448 (1991).

[37] A. Hosseini *et al.*, Physical review letters **93**, 107003 (2004).

[38] A. Lichtenstein and M. Katsnelson, Physical Review B **62**, R9283 (2000).

[39] D. Sénéchal, P.-L. Lavertu, M.-A. Marois, and A.-M. Tremblay, Physical review letters **94**, 156404 (2005).

[40] L. P. Gor'kov and E. I. Rashba, Physical Review Letters **87**, 037004 (2001).

[41] S. Nayak and S. Kumar, Journal of Physics: Condensed Matter **30**, 135601 (2018).

[42] D. J. Scalapino, Physics Reports **250**, 329 (1995).

[43] B. Powell, J. F. Annett, and B. Györffy, Journal of Physics A: Mathematical and General **36**, 9289 (2003).

[44] R. Balian and N. Werthamer, Physical review **131**, 1553 (1963).

[45] N. Batra, S. Nayak, and S. Kumar, Phys. Rev. B **100**, 214517 (2019).

[46] J. Valatin, Il Nuovo Cimento (1955-1965) **7**, 843 (1958).

[47] C. C. Tsuei and J. R. Kirtley, Rev. Mod. Phys. **72**, 969 (2000).

[48] A. Mathai *et al.*, Phys. Rev. Lett. **74**, 4523 (1995).

[49] Q. P. Li, B. E. C. Koltenbah, and R. Joynt, Phys. Rev. B **48**, 437 (1993).

[50] D. J. Van Harlingen, Rev. Mod. Phys. **67**, 515 (1995).

[51] K. A. Muller, Nature **377**, 133 (1995).

[52] J. Betouras and R. Joynt, Phys. C Supercond. **317-318**, 669 (1999).

[53] R. Khasanov *et al.*, Phys. Rev. Lett. **98**, 057007 (2007).

[54] N. P. Armitage, P. Fournier, and R. L. Greene, Rev. Mod. Phys. **82**, 2421 (2010).

[55] E. Razzoli *et al.*, (2012).

[56] C. Kallin, Reports Prog. Phys. **75**, 042501 (2012).

[57] C. Kallin and J. Berlinsky, Reports Prog. Phys. **79**, 054502 (2016).

[58] T. Scaffidi, J. C. Romers, and S. H. Simon, Phys. Rev. B **89**, 220510 (2014).

[59] G. M. Luke *et al.*, Nature **394**, 558 (1998).

[60] S. Belin and K. Behnia, Phys. Rev. Lett. **79**, 2125 (1997).

[61] I. J. Lee, M. J. Naughton, G. M. Danner, and P. M. Chaikin, Phys. Rev. Lett. **78**, 3555 (1997).

[62] I. J. Lee *et al.*, Phys. Rev. Lett. **88**, 017004 (2001).

[63] I. J. Lee *et al.*, Phys. Rev. B **68**, 092510 (2003).

[64] J. I. Oh and M. J. Naughton, Phys. Rev. Lett. **92**, 067001 (2004).

[65] A. Trenkwalder *et al.*, Nat. Phys. **12**, 826 (2016).

[66] L. P. Gor'kov and E. I. Rashba, Phys. Rev. Lett. **87**, 037004 (2001).

[67] I. A. Sergienko, Phys. Rev. B **69**, 174502 (2004).

[68] K. A. Musaelian, J. Betouras, A. V. Chubukov, and R. Joynt, Phys. Rev. B **53**, 3598 (1996).

[69] R. Micnas, J. Ranninger, and S. Robaszkiewicz, J. Phys. C Solid State Phys. **21**, L145 (1988).

[70] R. Micnas, J. Ranninger, and S. Robaszkiewicz, Rev. Mod. Phys. **62**, 113 (1990).

[71] M. Keller, W. Metzner, and U. Schollw?ck, Phys. Rev. Lett. **86**, 4612 (2001).

[72] T. Paiva, R. R. dos Santos, R. T. Scalettar, and P. J. H. Denteneer, Phys. Rev. B **69**, 184501 (2004).

[73] P. W. Anderson, Phys. Rev. Lett. **34**, 953 (1975).

[74] A. Montorsi and D. K. Campbell, Phys. Rev. B **53**, 5153 (1996).

[75] M. Capone, C. Castellani, and M. Grilli, Phys. Rev. Lett. **88**, 126403 (2002).

[76] R. R. P. Singh and R. T. Scalettar, Phys. Rev. Lett. **66**, 3203 (1991).

[77] B. L. Gyorffy, J. B. Staunton, and G. M. Stocks, Phys. Rev. B **44**, 5190 (1991).

[78] J. K. Freericks, Phys. Rev. B **48**, 3881 (1993).

[79] S. Allen and A.-M. S. Tremblay, Phys. Rev. B **64**, 075115 (2001).

[80] L. Arrachea and A. A. Aligia, Phys. Rev. B **59**, 1333 (1999).

[81] M. Mayr, G. Alvarez, A. Moreo, and E. Dagotto, Phys. Rev. B **73**, 014509 (2006).

[82] S. Maiti and P. J. Hirschfeld, Phys. Rev. B **92**, 094506 (2015).

[83] J. E. Hirsch and D. J. Scalapino, Phys. Rev. B **32**, 117 (1985).

[84] T. Meintrup, T. Schneider, and H. Beck, Europhys. Lett. **31**, 231 (1995).

[85] K. Kuroki, K. Kusakabe, and H. Aoki, Phys. Rev. B **50**, 575 (1994).

[86] D. J. Scalapino, Rev. Mod. Phys. **84**, 1383 (2012).

[87] W.-M. Huang, C.-Y. Lai, C. Shi, and S.-W. Tsai, Phys. Rev. B **88**, 054504 (2013).

[88] H. Mori, J. Phys. Soc. Japan **58**, 1394 (1989).

[89] S. Robaszkiewicz, R. Micnas, and K. Chao, Physical Review B **23**, 1447 (1981).

[90] M. Köhl *et al.*, Physical review letters **94**, 080403 (2005).

[91] J. K. Chin *et al.*, Nature **443**, 961 (2006).

[92] D. Mitra *et al.*, Nature Physics **14**, 173 (2018).

[93] R. Jördens *et al.*, Nature **455**, 204 (2008).

[94] W. Hofstetter *et al.*, Physical review letters **89**, 220407 (2002).

[95] A. Singha *et al.*, Science (80-. ). **332**, 1176 (2011).

[96] P.-G. DeGennes, *Superconductivity of metals and alloys* (Advanced Book Program, Perseus Books, 1999).

[97] S. Robaszkiewicz, R. Micnas, and K. Chao, Physical Review B **24**, 1579 (1981).

[98] J. Ferrer, M. González-Alvarez, and J. Sánchez-Cañizares, Physical Review B **57**, 7470 (1998).

[99] S. Onari, R. Arita, K. Kuroki, and H. Aoki, Phys. Rev. B **70**, 094523 (2004).

[100] S. Onari, R. Arita, K. Kuroki, and H. Aoki, J. Phys. Soc. Japan **74**, 2579 (2005).

[101] C. Huscroft and R. T. Scalettar, Phys. Rev. B **55**, 1185 (1997).

[102] S. Daul, D. Scalapino, and S. R. White, Physical review letters **84**, 4188 (2000).

[103] T. Xiang *et al.*, Physical Review B **79**, 014524 (2009).

[104] M. Abram, J. Kaczmarczyk, J. Jedrak, and J. Spałek, Physical Review B **88**, 094502 (2013).

[105] J. Spałek, M. Zegrodnik, and J. Kaczmarczyk, Physical Review B **95**, 024506 (2017).

[106] R. Micnas, J. Ranninger, and S. Robaszkiewicz, Physical Review B **39**, 11653 (1989).

[107] O. Fischer *et al.*, Rev. Mod. Phys. **79**, 353 (2007).

[108] A. V. Balatsky, I. Vekhter, and J.-X. Zhu, Rev. Mod. Phys. **78**, 373 (2006).

[109] Y.-m. Lu, T. Xiang, and D.-h. Lee, Nat. Phys. **10**, 1 (2014).

[110] E. Taylor and C. Kallin, Phys. Rev. Lett. **108**, 157001 (2012).

[111] P. Monthoux and G. G. Lonzarich, Phys. Rev. B **59**, 14598 (1999).

[112] R. Movshovich *et al.*, Phys. Rev. Lett. **80**, 1968 (1998).

[113] S. Brown, Phys. C Supercond. its Appl. **514**, 279 (2015).

[114] R. Jördens *et al.*, Nature **455**, 204 (2008).

[115] W. Hofstetter *et al.*, Phys. Rev. Lett. **89**, 220407 (2002).

[116] Q. Li, B. Koltenbah, and R. Joynt, Physical Review B **48**, 437 (1993).

[117] C. Kallin, Reports on Progress in Physics **75**, 042501 (2012).

[118] I. Sergienko, Physical Review B **69**, 174502 (2004).